

UNIVERSITA' DEGLI STUDI DI PAVIA

FACOLTA' DI INGEGNERIA
DIPARTIMENTO DI INGEGNERIA INDUSTRIALE E DELL'INFORMAZIONE

DOTTORATO DI RICERCA IN TECNOLOGIE PER LA SALUTE, BIOINGEGNERIA E BIOINFORMATICA
XXXIV CICLO - 2021

TEMPORAL DATA ANALYTICS FOR DIABETES MONITORING WITH APPLICATIONS ON PEDIATRIC AND ADULT PATIENTS

PhD Thesis by
PIETRO BOSONI

Advisor:
Prof. Lucia Sacchi

PhD Program Chair:
Prof. Silvana Quaglini



Abstract (Italiano)

L'attività di ricerca descritta in questa tesi è stata condotta all'interno del Laboratorio di Informatica Biomedica "Mario Stefanelli" dell'Università degli Studi di Pavia da ottobre 2018 a novembre 2021. È stata motivata dalla necessità di un'applicazione per la gestione dei pazienti diabetici che permettesse l'integrazione dei dati di monitoraggio ottenuti attraverso l'utilizzo di diversi sensori indossabili, fornendo strumenti di analisi temporale per estrarre conoscenza e migliorare la predizione di episodi acuti.

Il diabete mellito è una condizione cronica la cui prevalenza è in continuo aumento nel mondo, costituendo una delle sfide per la salute in più rapida ascesa nelle ultime decadi. La gestione del diabete mellito si basa principalmente sul mantenimento dei valori glicemici all'interno di un range di normalità, così da ridurre il rischio di serie complicanze a lungo termine, senza però causare un sostanziale crollo dei valori di glucosio presente nel sangue. I sistemi per l'automonitoraggio del glucosio ("self-monitoring of blood glucose" o SBGM) e quelli per il monitoraggio in continua ("continuous glucose monitoring" o CGM) sono essenziali per il raggiungimento e il mantenimento di un buon controllo glicemico nel tempo, in modo particolare nei soggetti sottoposti a terapia insulinica. In ogni caso, è di grande importanza considerare anche altri fattori per poter fornire un quadro glicemico più completo, dove ogni misura è contestualizzata nell'arco della giornata e in base all'attività svolta in quel preciso momento.

La piattaforma "Advanced Intelligent Distant – Glucose Monitoring" (AID-GM), sviluppata all'interno del Laboratorio di Informatica Biomedica dell'Università degli Studi di Pavia, consente l'integrazione dei dati di monitoraggio provenienti da fonti differenti, quali ad esempio un sistema di monitoraggio glicemico in continua, un fitness tracker, o un diario clinico redatto dal paziente stesso. Attraverso la piattaforma, dunque, i pazienti e il personale clinico hanno la possibilità di condividere e visualizzare i dati provenienti dai propri dispositivi di monitoraggio insieme alle informazioni relative allo stile di vita, alla qualità del sonno e al battito cardiaco.

In questa prospettiva, l'attività di ricerca si è focalizzata sullo sviluppo di strategie innovative e allo stato dell'arte per l'analisi dei dati temporali basati su differenti sorgenti, al fine di estrarre nuova conoscenza. Inoltre, il monitoraggio a distanza è stato supportato dall'implementazione degli algoritmi per l'analisi temporale all'interno della piattaforma AID-GM, trasformando i dati grezzi delle serie storiche in informazioni cliniche rilevanti, offrendo ai medici un quadro completo delle condizioni di ciascun paziente.

Abstract (English)

The research activity described in this thesis has been conducted within the Laboratory for Biomedical Informatics “Mario Stefanelli” of the University of Pavia, Italy, from October 2018 to November 2021. It was motivated by the need of a diabetes management application that allowed the integration of patient-generated health data (PGHD) from different wearable sensors, providing temporal data analytics functionalities to gain deeper insights in the data and to enhance critical events prediction.

Diabetes mellitus (DM) is a life-long condition that continues to rise in prevalence across the globe, representing one of the fastest growing health challenges of the last decades. DM management is mainly focused on maintain near-normal glycemic values for reducing the risk of long-term life-threatening complications, without causing substantial falls in circulating glucose. Self-monitoring of blood glucose (SMBG) and continuous glucose monitoring (CGM) systems are essential to achieve the goal of a safe and prolonged glycemic control, especially in subjects on insulin therapies. Anyway, it is important to consider also other factors for providing a complete glycemic profile contextualized within the day.

The Advanced Intelligent Distant – Glucose Monitoring (AID-GM) platform, developed at the Biomedical Informatics Laboratory of the University of Pavia, consents the integration of PGHD from multiple sources, such as CGM systems, personal fitness trackers (PFTs), and self-reported daily diaries. Therefore, patients and healthcare providers were allowed to share and visualize CGM measurements integrated by lifestyle, sleep, and HR information.

In this context, the research activity is focused on the development of novel and state of the art temporal data analytics strategies based on multivariate PGHD to discover new insights in the collected data. Moreover, the long-term remote monitoring has been supported by the implementation of the proposed temporal data analytics functionalities in the AID-GM platform, turning the time-series raw data into relevant clinical information and making available to clinicians a complete overview of each patient’s conditions as a decision support in their healthcare tasks.

Contents

1	Introduction	1
1.1.	<i>Motivation and objectives</i>	1
1.2.	<i>Overview of the thesis</i>	2
2	Background	5
2.1.	<i>Diabetes monitoring</i>	5
2.1.1.	Characteristics of diabetes mellitus.....	6
2.1.2.	Monitoring systems.....	8
2.1.2.1.	Continuous glucose monitoring.....	11
2.1.3.	Glycemic variability.....	15
2.2.	<i>Analysis of blood glucose time-series</i>	25
2.2.1.	Univariate models for glucose prediction.....	25
2.2.2.	Multivariate models for glucose prediction.....	28
2.3.	<i>The AID-GM platform</i>	31
2.3.1.	Data integration infrastructure.....	31
2.3.2.	Graphical user interface.....	32
3	Datasets description and temporal data analytics techniques	37
3.1.	<i>Datasets description</i>	37
3.1.1.	The pediatric dataset.....	38
3.1.2.	The adult dataset.....	40
3.2.	<i>Glucose data analytics</i>	40
3.2.1.	Linear mixed effects models for glycated hemoglobin and time in ranges relationship.....	41
3.2.2.	Correlation between self-monitoring frequency and glycemic metrics.....	44
3.3.	<i>Temporal data mining with temporal abstraction</i>	45
3.3.1.	Libraries for temporal abstraction.....	45
3.3.2.	Domain-specific pattern detection.....	50
3.3.3.	Analysis of hypoglycemia episodes.....	55
3.4.	<i>Generalized deep learning models</i>	56
3.4.1.	Time series preprocessing.....	58
3.4.2.	Model infrastructure.....	61
3.4.3.	Model evaluation.....	62
4	Applications on real-world data	65
4.1.	<i>Descriptive statistics on the datasets</i>	65
4.2.	<i>Glucose data analytics results</i>	71
4.2.1.	Glycated hemoglobin and time in ranges.....	71
4.2.2.	Self-monitoring frequency and glycemic metrics.....	79
4.3.	<i>Temporal data mining results</i>	83
4.3.1.	Pattern detection.....	83
4.3.2.	Hypoglycemia analysis.....	86
4.4.	<i>Generalized deep learning model results</i>	91
4.4.1.	Results on the pediatric dataset.....	91

4.4.2. Results on the adult dataset.....	93
5 Conclusions	95
Appendix A - Impaired glucose-insulin metabolism in Multisystem Inflammatory Syndrome related to SARS-CoV-2 in children	99
Appendix B - Temporal abstractions workflows	103
Appendix C - Descriptive statistics using Fitbit activities information ..	111
References.....	117
List of publications.....	135
List of abbreviations	137

Chapter 1

Introduction

1.1. Motivation and objectives

Diabetes Mellitus (DM) is a high-prevalence lifelong condition that is rapidly growing worldwide, characterized by an excessive amount of circulating glucose and metabolic disorders. Early diagnosis, access to medication, education and frequent monitoring are necessary for preventing acute complications and reducing the risk of long-term complications. Indeed, raised levels of circulating glucose through time can lead to disabling and life-threatening health complications such as retinopathy, nephropathy, peripheral neuropathy, and cardiovascular diseases.

The latest developments in wearable blood glucose (BG) technologies have provided a great support in diabetes management, which is mainly focused on maintaining a near-normal glycemic control. Different continuous glucose monitoring (CGM) systems are now available on the market, able to measure BG levels around the clock through disposable subcutaneous sensors. Anyway, also other factors may influence the BG profile over the day, including physical activity, quality of sleep, and heart rate (HR), which can be automatically monitored by activity trackers. Therefore, the integration between information from CGM systems and activity trackers has become essential to achieve a complete glycemic profile contextualized within the day.

In this background, the Advanced Intelligent Distant – Glucose Monitoring (AID-GM) platform has been developed at the Biomedical Informatics Laboratory of the University of Pavia, allowing patients and healthcare providers to share and visualize glucose measurements integrated by daily activity, sleep, and HR information. In particular, this application has been used by two different cohorts of patients with DM, such as a group of pediatric patients recruited from the Pediatric Endocrinology and Diabetology outpatient service of Fondazione IRCCS Policlinico San Matteo hospital, and a group of adult patients recruited from the Endocrinology and Diabetology outpatient service of the IRCCS Istituti Clinici Scientifici Maugeri in Pavia, Italy.

This research activity is focused on developing novel and state of the art temporal data analytics methodologies based on multivariate patient-generated health data (PGHD) to discover new insights in the collected datasets. In addition, the proposed algorithms for temporal data analytics have been integrated within the AID-GM application to turn the raw data coming from different sources into relevant clinical information, providing clinicians with composite and advanced overviews of each patient's condition as a support in their healthcare tasks, facilitating long-term remote monitoring.

1.2. Overview of the thesis

The dissertation is organized as in the following.

Chapter 2 provides the background of the thesis. Since this research activity focuses on temporal analytics for diabetes monitoring, Section 2.1 introduces definition and pathophysiology of DM, illustrating the most common symptoms and the diagnostic tests recommended by international guidelines for a definitive diagnosis of DM, and explaining the diabetes classification proposed by the World Health Organization (WHO) in 2019 [1]. Particularly, CGM systems and CGM-derived glycemic metrics are explored in detail as they allow to assess the quality of glycemic control, evaluating the magnitude and the frequency of intra- and inter-day glucose fluctuations. Then, Section 2.2 presents a literature review regarding glucose time-series analysis and forecasting, considering univariate and multivariate models developed through statistical, machine learning and deep learning approaches, since glucose profile over the day can be influenced by several variables. Finally, Section 2.3 describes the data integration infrastructure and the graphical user interface of the AID-GM platform.

Chapter 3 illustrates the considered datasets and explains the proposed analytical methodologies. Section 3.1 introduces the two datasets used in this research activity, one collected on pediatric patients and the other on adult patients, in both cases affected by a specific subclass of DM, called type 1 diabetes, and monitored in real-life conditions through the same devices. Afterwards, Section 3.2 presents glucose data analytics. An algorithm for descriptive statistics and glycemic metrics computation is implemented, so that healthcare providers can have an immediate overview of each patient's conditions. In addition, the relationship between glycated hemoglobin and time in ranges is investigated, along with the correlation between self-monitoring frequency through CGM devices and glycemic metrics. Section 3.3 explains the knowledge-based Temporal Abstraction (TA) techniques used to automatically detect time intervals in which time-series assume behaviors of interest. In particular, several domain-specific patterns have been formalized in collaboration with the diabetologists of the Pediatric Endocrinology and Diabetology outpatient service of Fondazione IRCCS Policlinico San Matteo hospital, and of the Endocrinology and Diabetology

outpatient service of the IRCCS Istituti Clinici Scientifici Maugeri. Finally, Section 3.4 presents the proposed deep learning architecture for developing multi-patient and multivariate models for glucose prediction.

Chapter 4 exposes the outcomes of temporal analytics methods applied on real-world data, exploring the differences between the results obtained on pediatric and adult datasets and comparing the findings with the literature.

Finally, **Chapter 5** outlines and discusses the main conclusions of this research activity.

As a complement to the main research work of this thesis, **Appendix A** reports on the application of TA techniques to evaluate the presence of glucose disorders in young patients affected by multisystem inflammatory syndrome in children (MIS-C), a critical health condition associated with the severe acute respiratory syndrome coronavirus 2 (SARS-CoV-2). The data for this study have been provided by the Vittore Buzzi Children's Hospital in Milan, Italy, during the coronavirus disease 2019 (COVID-19) pandemic.

Chapter 2

Background

This chapter provides the background material and the literature review for technical and analytical diabetes monitoring solutions. Section 2.1 explains the clinical problem, first introducing the characteristics of DM, then presenting glucose monitoring systems and metrics used for glycemic assessment. Section 2.2 describes relevant works for BG time-series forecasting, considering statistical, machine learning and deep learning approaches in univariate and multivariate models. Finally, Section 2.3 illustrates the AID-GM platform.

2.1. Diabetes monitoring

DM is a lifelong condition that is rising worldwide, representing one of the fastest growing health challenges of the last decades. Within fifteen years, according to the 9th edition of the International Diabetes Federation (IDF) Diabetes Atlas [2], the number of adults with DM has risen from 151 million in 2000 to 415 million in 2015. In 2019 it was estimated that one in eleven adults had DM, and there was over one million of children and adolescents with a specific subclass of diabetes, called type 1 diabetes [2]. Nowadays, the trend is still upward: the overall projection of adults with DM in 2030 is 578 million, and 700 million in 2045 [2].

Globally, 11.3% of deaths in the 20-79 years age group are due to DM, mainly as a consequence of its complications, and almost half of these deaths are in adults aged under 60 years [2]. In this context, early diagnosis, access to medication, education and regular monitoring is essential in preventing acute complications and reducing the risk of long-term complications [3].

2.1.1. Characteristics of diabetes mellitus

DM in an umbrella term for a group of metabolic disorders characterized by hyperglycemia, i.e. an excessive amount of circulating glucose, together with disturbances in carbohydrate, fat, and protein metabolism [1], [4]. A prolonged exposure to hyperglycemia causes microvascular complications, including retinopathy, nephropathy, and peripheral neuropathy. DM is also associated to an increased risk of macrovascular complications, such as atherosclerosis, and some infectious diseases [1], [4].

The most common signs and symptoms of DM are thirst, polyuria, blurring of vision, and weight loss; genital yeast infection can also occur [1]. There are also severe clinical manifestations, such as ketoacidosis or a non-ketotic hyperosmolar state that may lead to dehydration, coma, and death [1], [4]. Anyway, a definitive diagnosis of DM has to be established through one of the four diagnostic tests recommended by international guidelines like the WHO “Classification of diabetes mellitus 2019” [1] and the American Diabetes Association (ADA) “Standards of Medical Care in Diabetes 2021” [5], as reported in Table 2.1.

Table 2.1: Criteria for the diagnosis of diabetes adapted from the American Diabetes Association guidelines [5].

FPG \geq 126 mg/dL (7.0 mmol/L) fasting is defined as no caloric intake for at least 8 hours *
OR
2-hours PG \geq 200 mg/dL (11.1 mmol/L) during OGGT performed as described by WHO, using a glucose load containing the equivalent of 75 grams of anhydrous glucose dissolved in water *
OR
HbA1c \geq 48 mmol/mol (6.5%) performed in a laboratory using a method that is NGSP certified and standardized to the DCCT assay
OR
Random plasma \geq 200 mg/dL (11.1 mmol/L) in an individual with DM characteristic symptoms

* In the absence of unequivocal hyperglycemia, diagnosis requires two abnormal test results from the same sample or in two separate test samples.

FPG: fasting plasma glucose; PG: plasma glucose; OGGT: oral glucose tolerance test; WHO: World Health Organization; HbA1c: glycated hemoglobin; NGSP: National Glycohemoglobin Standardization Program; DCCT: Diabetes Control and Complications Trial; DM: diabetes mellitus.

Although origin and etiology are heterogenous, defective pancreatic β -cells account for almost all forms of DM [6]. A dysfunction or destruction of β -cells can happen due to various mechanisms, including genetic predisposition and abnormalities, epigenetic processes, insulin resistance,

auto-immunity, concurrent illnesses, inflammation, and environmental factors [1], [5]. Sited in the islets of Langerhans throughout the endocrine pancreas, β -cells can detect variations in the circulating concentrations of nutrients, hormones, neurotransmitters, and neuropeptides, in a complex interaction with the autonomic nervous and the gastrointestinal systems [7]. β -cells respond to increasing levels of nutrients by releasing the polypeptide hormone insulin to enable the uptake and metabolism or storage of the nutrients in liver, muscles, and adipose tissues, preventing hyperglycemia. Insulin secretion is switched off when the consequent decrease in circulating nutrients is detected, preventing hypoglycemia [7].

Hypoglycemia in DM is fundamentally iatrogenic as a consequence of therapeutic hyperinsulinemia [8]. It produces recurrent morbidity and some mortality and weakens the physiologic defensive mechanism against successive hypoglycemic episodes [9]. Hypoglycemia can also be asymptomatic and cause brain fuel deprivation that, if unchecked, may lead to functional brain failure or sudden death. The so-called death-in-bed syndrome, indeed, refers to sudden death in young DM patients without any history of long-term complications [10], [11].

According to the WHO guidelines [1], DM can be classified into the following categories:

- Type 1 DM (T1DM)
- Type 2 DM (T2DM)
- Hybrid forms of diabetes mellitus, including slowly evolving immune-mediated DM and ketosis-prone T2DM
- Other specific types of DM, including monogenic DM, monogenic defects of insulin action, diseases of the exocrine pancreas, endocrine disorders, drug- or chemical-induced DM, infection-related DM, uncommon specific forms of immune-mediated DM, and other genetic syndromes sometimes associated with DM
- Unclassified DM, a temporary category used whether there is not a clear diagnostic category, especially close to the time of diagnosis
- Hyperglycemia first detected during pregnancy, including DM defined by the same criteria as in non-pregnant persons but first recognized during pregnancy, and gestational DM, defined by lower glucose cut-off points than those in Table 2.1

T1DM and T2DM are the most prevalent form of DM, accounting respectively for 5-10% and 90-95% of DM cases [5]. T1DM results from an almost complete insulin loss due to a progressive cellular-mediated autoimmune destruction of the β -cells [5], [12]. The onset of T1DM is typically during childhood, but it can occur at any age [1], [4]. The complex etiology of T1DM involves genetic and several presumed environmental factors, such as maternal factors, viral infections, dietary, high birth weight

and growth rate, psychologic stress, dietary, and toxic substances [12]. Insulin replacement therapy is required to reproduce a normal physiologic insulin profile without inducing significant hypoglycemia [8]. A possible approach is represented by the multiple daily injection (MDI) insulin-therapy, which involves a long-acting insulin injection once or twice a day for basal insulin requirements, and a short-acting insulin injection at each meal time [8]. Alternatively, the continuous subcutaneous insulin infusion (CSII) therapy may be prescribed; it requires the use of an insulin pump to continuously deliver predetermined insulin rates for basal insulin requirements, and to infuse a bolus to cover meal-time insulin requirements [13].

T2DM, instead, is characterized by insulin resistance with relative insulin deficiency due to β -cell dysfunction [4]. Although specific etiologies are not known, an increased risk of developing T2DM is associated to several factors, including age, obesity, unhealthy lifestyles and prior gestational DM [1], [14]. For most individuals with T2DM, an insulin treatment is not required for survival but it may be needed, often after many years, to maintain a good glycemic control [1], [4].

2.1.2. Monitoring systems

Diabetes management is mainly focused on reducing the risk of long-term complications, maintaining near-normal glycemic values without causing significant hypoglycemia [15]. In current practice, the quality of glycemic control is typically assessed by glycated hemoglobin (HbA1c) test and regular glucose monitoring.

HbA1c is a retrospective indicator that reflects the average glucose concentrations over approximately the previous 2-3 months [16], [17]. According to the consensus statement on the standardization of HbA1c measurements [18], the International Federation of Clinical Chemistry (IFCC) reference method should be used by all manufacturers for calibration procedures. In addition, HbA1c results should be reported both in Système Internationale (SI) units, i.e. mmol/mol without decimals, and in derived National Glycohemoglobin Standardization Program (NGSP) units, i.e. % with one decimal [19], using the IFCC-NGSP master equation [16], [18].

Elevated HbA1c concentrations have been associated with long-term DM complications and identified as significant risk factor for cardiovascular diseases [20]. The ADA guidelines recommend an overall HbA1c target of <53 mmol/mol ($<7.0\%$), emphasizing the importance of individualized goals, as shown in Figure 2.1, particularly for children and adolescent, older adults, and pregnant woman [5]. As stated by the International Society for Pediatric and Adolescent Diabetes (ISPAD), a HbA1c target of <53 mmol/mol (7.0%) is recommended for children, adolescents and young adults aged less than 25 years with DM who have access to comprehensive care, but a more-stringent goal of <48 mmol/mol ($<6.5\%$) may be appropriate if achievable without significant hypoglycemia, negative impacts on quality

of life, or undue burden of care [21]. In addition, a less-stringent HbA1c goal of <59 mmol/mol ($<7.5\%$) may be applicable in case of inability to articulate hypoglycemia symptoms; hypoglycemia awareness or history of severe hypoglycemia; lack of access to analog insulins and/or advanced insulin delivery technology, ability to regularly check BG, and continuous glucose monitoring; individuals who are “high glycaters”, in whom an at-target HbA1c would reflect a significantly lower mean glucose than 155 mg/dL (8.6 mmol/L) [21]. Across all age-groups, indeed, adolescents are the farthest from accomplishing the HbA1c target of <53 mmol/mol ($<7.0\%$) [19].

The measurement of HbA1c should be performed at least twice a year in adults with T2DM and a stable glycemic control, while unstable or intensively managed adults should be tested every three months [17]. In children and adolescent with DM the measurement of HbA1c should be performed quarterly a year [21].

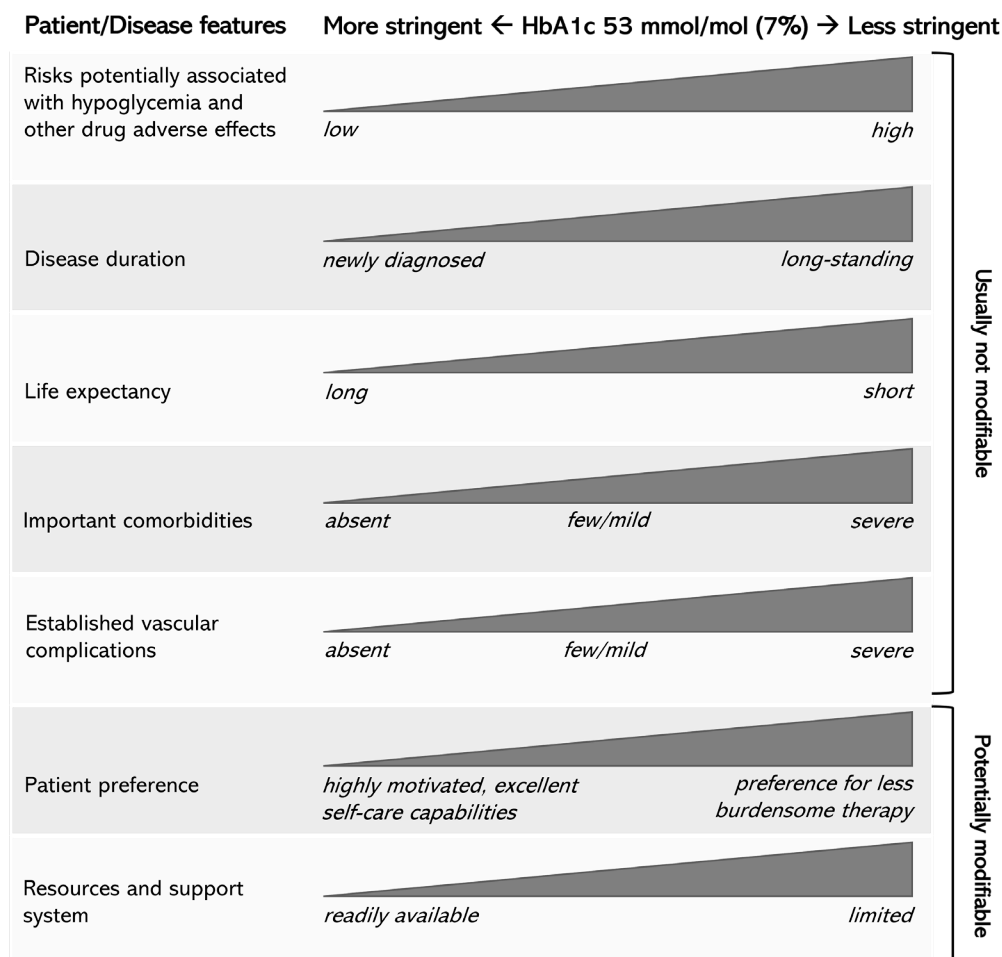


Figure 2.1: Approach for individualizing the glycated hemoglobin (HbA1c) target around the 53 mmol/mol (7%) recommendation, adapted from the American Diabetes Association guidelines [17].

The HbA1c test is used as the gold standard for long-term follow-up of glycemic control [22], but it cannot provide information about the day-to-day glycemic control and glycemic variability (GV), which refers to the oscillations in BG values over a given interval of time. Thus, the complementary use of glucose monitoring systems is essential to verify current glucose levels and eventually react to mitigate or prevent acute glycemic events, particularly for individuals with T1DM and insulin-treated individuals with T2DM [23].

Systems for BG monitoring can be divided into two major categories: self-monitoring of blood glucose (SMBG) devices, which measure glucose concentrations in capillary blood samples, and CGM devices, which measure glucose concentrations in interstitial fluid [24].

SMBG represent a standard of care for making therapeutic decisions such as insulin dosing [16], [17]. Although individual needs may vary, the American Association of Clinical Endocrinologists (AACE) guidelines recommend SMBG at least twice daily to all individuals using insulin and ideally before any insulin injection, so prior to meals and at bedtime [25]; ISPAD guidelines, instead, recommend SMBG six to ten times per day to children and adolescent with DM [21]. Anyway, additional checks are suggested in specific conditions for preventing the risk of hypoglycemia, e.g. before physical activity and critical tasks, or in the presence of hypoglycemic symptoms. Indeed, several studies in literature report that a higher SMBG frequency is correlated with lower HbA1c values in DM individuals on insulin therapies [26]–[28].

The most agreed upon standards for SMBG accuracy are the International Organization for Standardization (ISO) 15197:2013 [29] and the United States Food and Drug Administration (FDA) “Self-Monitoring Blood Glucose Test Systems for Over-the-Counter Use” [30]. Nevertheless, the accuracy of SMBG systems is dependent also to the end-user technique. As shown in Figure 2.2, the capillary blood sample should be obtained from the side of the finger pulp, applying the second drop of hanging blood to the test strip [16].



Figure 2.2: A self-monitoring of blood glucose (SMBG) device, which measures glycemia in capillary blood samples.

2.1.2.1. Continuous glucose monitoring

Unlike the SMBG episodic measurement process, CGM allow to gather glucose measurements on a continuous basis. In this way, it is possible to obtain a representative glycemic picture ideally without missing numerous hypoglycemic and hyperglycemic episodes, as indicated in Figure 2.3. Indeed, the adoption of a CGM system is recommended by the ADA guidelines for all individuals with DM on insulin therapy [31].

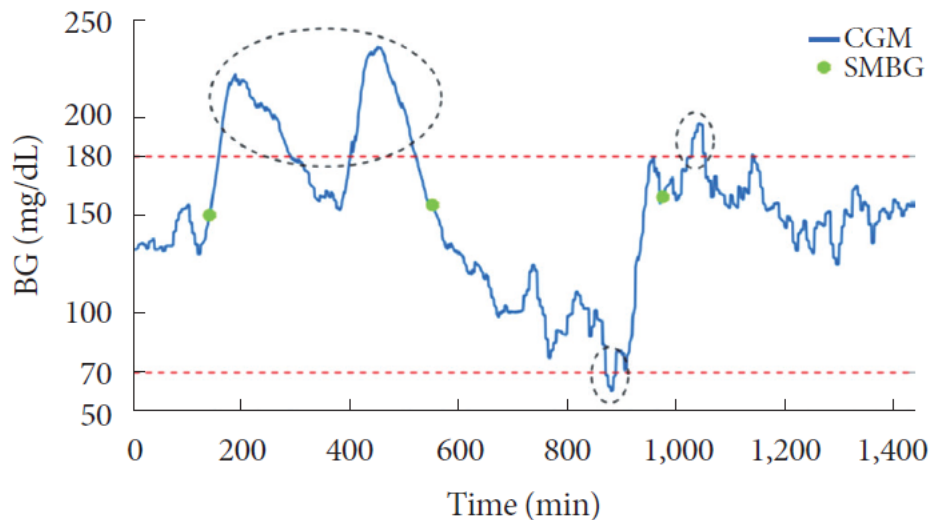


Figure 2.3: Illustration of glucose monitoring data obtained with self-monitoring of blood glucose (SMBG: in green) and continuous glucose monitoring (CGM: in blue). Dotted circles show hyperglycemic and hypoglycemic event that are not detectable using only SMBG measurements [32].



Figure 2.4: On the left a schema of continuous glucose monitoring (CGM) system [33], which measure glycemia in interstitial fluid, and on the right a CGM device in use.

As presented in Figure 2.4, CGM systems exploit a disposable subcutaneous sensor applied to the patient's abdomen or upper arm for

continuously measuring the interstitial glucose, which is strongly correlated with plasma glucose, although there could be a lag time between plasma and interstitial glucose concentrations during rapid BG changes [31], [33], [34]. Anyway, currently CGM algorithms tend to consider also this physiological delay in the estimation of plasma glucose values [33]. Attached to the sensor there is a transmitter that transfers glucose data to the user's cell phone or a dedicated receiver via a wireless connection. Finally, CGM systems are usually complemented with a proprietary software that allows to visualize glycemic reports like the ambulatory glucose profile (AGP).

Created by Mazze et al. [35] and further developed by the International Diabetes Center (IDC) [36], the AGP is an agreed upon dashboard characterized by a statistical summary section at the top, a daily view section at the bottom, and a central visual display section presenting a modal day in which all BG readings from multiple days are collapsed into a single 24-hours period, as shown in Figure 2.5.

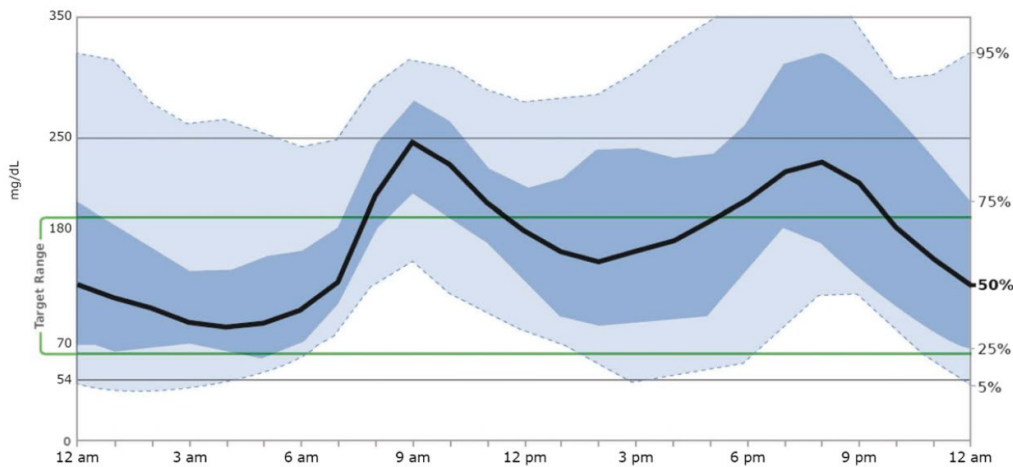


Figure 2.5: Example of the ambulatory glucose profile (AGP) visual display [23].

Since the approval of the first CGM device in 1999 [37] significant advancements have been made in terms of features, ease of use, and accuracy, which is commonly evaluated in mean absolute relative difference (MARD). Nowadays, according to the ADA guidelines [31], CGM systems can be divided into the following categories:

- Real-time CGM (rtCGM)
- Intermittently scanned CGM (isCGM)
- Professional CGM (pCGM)

The rtCGM systems are personal devices that passively transmit BG readings to the receiver and warn of imminent or occurring acute glycemic events. In the last decade several rtCGM devices have been approved by FDA, such as the Dexcom Platinum G4 Platinum and the Dexcom G5 Mobile

(Dexcom, San Diego, California), which were discontinued by Dexcom at the end of 2020 [38] in favor of the Dexcom G6 [39], the Medtronic Enlite Sensor [40] and the Medtronic Guardian Sensor 3 (Medtronic, Northridge, California) [41], whose characteristics are presented in Table 2.2. In 2018 FDA approved for adult patients the Senseonics Eversense (Senseonics, Germantown, Maryland) [42], which was the first long-term implantable rtCGM system able to provide glucose data for up to 90 days via an under-the-skin sensor, placed by a healthcare provider through a small incision, together with a removable and rechargeable smart transmitter. Contrary to the previous rtCGM systems, which use a glucose oxidase (GOD)-based glucose sensor, the Senseonics Eversense exploits a patented fluorescent glucose-indicating polymer technology to measure interstitial glucose.

Instead, the isCGM systems are personal devices that continuously measure interstitial glucose and display the measured values only when the sensor is scanned with the receiver. For this reason, these systems are also called flash glucose monitoring (FGM). The Abbott FreeStyle Libre (Abbott, Alameda, California) [43] was the first personal isCGM device on the market. In the United States it was approved by FDA only for adult patients, while in Europe and Australia it was approved both for adults and pediatric patients aged four years old and above. Moreover, a recent study across nine diabetes centers in the United Kingdom has demonstrated the accuracy, safety, and user acceptability of the FreeStyle Libre system specifically in the pediatric population [44]. As indicated in Table 2.2, the FreeStyle Libre system is characterized by more economic technology, factory calibration, and 14-days sensor life. The sensor measures interstitial glucose every minute and stores a reading (a weighted average value in a glucose range of 40–500 mg/dL) every 15 minutes in a rolling 8-hours memory. This means that if a patient swipes the reader over the sensor at least every eight hours, no information is lost and 96 automatic measurements per day are stored. The reader, instead, has a 90-days memory. In 2020 the FDA approved the Abbott FreeStyle Libre 2 [45] both for adults and pediatric patients aged four years old and above, provided with optional real-time alarms for acute glycemic events as the most recent rtCGM systems.

In addition, the FreeStyle Libre 2 isCGM and the Dexcom G6 rtCGM have been designated by FDA as integrated CGM (iCGM) devices [46], [47]. The iCGM is a higher standard for monitoring systems that can be used in an integrated mode alongside other diabetes management devices, including automatic insulin dosing systems and insulin pumps [31].

While rtCGM and isCGM systems are patient-owned devices, pCGM systems are clinic-based devices prescribed to patients for a short period of time, usually for one or two weeks [31], [48]. Upon return of the device to the healthcare provider's office, glucose monitoring data are downloaded and retrospectively analyzed to assess glycemic patterns. The pCGM systems offer a blinded mode, so that patients cannot verify current glucose levels and change behavior in response to real-time readings during the monitoring period [48], [49]. In this way, healthcare providers could have a more representative picture of patients' glycemic trends for making apposite

therapy adjustments [49]. Moreover, pCGM also offer to uncertain patients a trial opportunity before purchasing a personal CGM device [48]. Currently, a few pCGM devices are available on the market: the FreeStyle Libre Pro [50] and the Medtronic iPro2 [51] are blinded systems, while the Dexcom G6 Pro [52] is a rtCGM system available for professional use.

Table 2.2: Features of selected personal CGM systems approved by the Food and Drug Administration (FDA) and currently available on the market in the United States [53].

CGM sensor	Category	Life	Warm-up time	Calibration	Frequency of glucose readings
Dexcom G6	rtCGM	Up to 10 days	2 hours	Factory-calibrated	Every 5 minutes
Medtronic Enlite	rtCGM	Up to 6 days	2 hours	Every 12 hours	Every 5 minutes
Medtronic Guardian Sensor 3	rtCGM	Up to 7 days	2 hours	Every 12 hours	Every 5 minutes
Senseonics Eversense	rtCGM	Up to 90 days	24 hours	Every 10–14 hours	Every 5 minutes
Abbott Freestyle Libre	isCGM	Up to 14 days	1 hour	Factory-calibrated	Per scanning/stored every 15 minutes
Abbott Freestyle Libre 2	isCGM	Up to 14 days	1 hour	Factory-calibrated	Per scanning/stored every 15 minutes
Abbott FreeStyle Libre Pro	pCGM	Up to 14 days	1 hour	Factory-calibrated	Every 15 minutes
Dexcom G6 Pro	pCGM	Up to 10 days	2 hours	Factory-calibrated	Every 5 minutes
Medtronic iPro2 Enlite	pCGM	Up to 6 days	1 hour	Every 12 hours	Every 5 minutes

isCGM: intermittently scanned Continuous Glucose Monitoring; pCGM: professional Continuous Glucose Monitoring; rtCGM: real-time Continuous Glucose Monitoring.

Literature reports significant clinical benefits of CGM adoption in individuals with DM regardless of insulin delivery method, showing enhancements in glycemic control, management of hypoglycemic episodes,

and glycemic variability [23]. According to a randomized controlled trial (RCT) conducted by the Juvenile Diabetes Research Foundation (JDRF) CGM Study Group [54], the use of CGM compared to SMBG devices is associated with significant decrease in HbA1c levels in T1DM adult patients; a similar conclusion can be drawn from both the GOLD [55] and the DIAMOND [56] RCTs, which included only T1DM adult patients on MDI therapy. In addition, the REPLACE-BG RCT demonstrated that the use of CGM systems alone is as safe and effective as the adoption of CGM systems adjunctive to SMBG devices in adult patients with well-controlled T1DM on CSII therapy [57]. The HypoDE [58] RCT revealed that in T1DM adult patients on MDI therapy with hypoglycemia awareness the adoption of CGM devices could reduce the number of hypoglycemic events compared to SMBG, as observed also in the IN CONTROL [59] RCT, which included adult patients with T1DM on MDI or CSII therapy. Particularly, the RCT of Bolinder et al. indicated that the use of FGM systems reduced the time spent in hypoglycemia in adult patients with controlled T1DM [60]. Moreover, the RCT of Bergenstal et al. [61] showed that the integration of unblinded CGM systems within the insulin therapy resulted in lower HbA1c values in both adults and children with inadequately controlled T1DM [61].

Another RCT conducted by the DIAMOND study group reported that a high percentage of T2DM adult patients on MDI therapy improved their glycemic control using CGM systems [62]. Nevertheless, there are not significant evidences to determine whether CGM could improve such clinical outcomes also in T2DM individuals not on intensive insulin treatment [32].

2.1.3. Glycemic variability

Clinical evidences support that glucose fluctuations might play a negative role in the development of acute and chronic microvascular and macrovascular complications [63], [64]. Nevertheless, this dynamic cannot be reflected by the HbA1c test alone, but it need also the measurements of GV, which allow to investigate the magnitude and the frequency of intra- and inter-day glucose fluctuations [65].

Over the past years, the widespread diffusion of CGM systems has noticeably improved the evaluation of GV and numerous GV metrics have been proposed for the glycemic assessment. These metrics can be divided into two categories according to the length of time-interval under surveillance: long-term GV metrics are based on the variability between visit-to-visit HbA1c, fasting plasma glucose (FPG) or postprandial glucose (PPG) measurements, while short-term GV metrics consider BG changes within a day or between few days [65]. In the following, the short-term GV metrics that are most widely used in clinical practice are presented as belonging to four families of methods, such as traditional metrics, metrics based on absolute change in glucose levels, metrics based on risk of major glycemic excursions, and metrics based on time in ranges. In all equations,

BG_t represents the BG reading in mg/dL (which can be converted in mmol/L considering that $18 \text{ mg/dL} = 1 \text{ mmol/L}$) at time t , n is the total number of glucose readings, and N_{days} is the number of monitored days.

Traditional metrics

- Mean:

$$Mean = \frac{\sum_{t=1}^n BG_t}{n}$$

It is a simple measure of central tendency that has the best correlation with HbA1c levels; it can be influenced by outliers and it does not assign more importance to acute glycemic events [66].

- Overall standard deviation (SD):

$$SD = \sqrt{\frac{\sum_{t=1}^n (BG_t - Mean)^2}{n - 1}}$$

It combines information on variability from all days and all time points; it can be influenced by outliers and non-Gaussian skewed asymmetrical distribution of BG readings [66].

- Within-day standard deviation (SD_w):

$$SD_w = \frac{\sum_{i=1}^{N_{days}} SD(i)}{N_{days}}$$

It is the average over all days of intra-day SD values and it is consequently highly correlated with overall SD [67].

- Daily means standard deviation (SD_{dm}):

$$SD_{dm} = \sqrt{\frac{\sum_{i=1}^{N_{days}} \overline{mean(i) - Mean}}{N_{days} - 1}}$$

It is the SD of the BG readings daily means and it is correlated with overall SD [67].

- Percentage coefficient of variation ($\%CV$):

$$\%CV = 100 \cdot \frac{SD}{Mean}$$

It represents the extent of variability in relation to the Mean of BG readings, expressed as a percentage [66]. It is subject to the same

limitations as SD, but it is less influenced when comparing data with widely different Mean or HbA1c values. The recommended target for a good glycemic control is $\leq 36\%$, although some studies suggest that a lower target of $< 33\%$ provide additional protection against hypoglycemia for those receiving insulin or sulfonylureas [23].

- Median:

$$\text{Median} = BG_{50^{\text{th}}\text{percentile}}$$

It is a simple measures of central tendency with the advantage of being insensitive to outliers and unaffected by values that are outside the range of measurement; as the Mean, it does not assign more importance to acute glycemic events [66].

- Interquartile range (*IQR*):

$$\text{IQR} = BG_{75^{\text{th}}\text{percentile}} - BG_{25^{\text{th}}\text{percentile}}$$

It can handle non-Gaussian distributions and it has the advantage of being insensitive to outliers and unaffected by values that are outside the range of measurement [66].

- Range:

$$\text{Range} = \max(BG) - \min(BG)$$

It is the difference between the highest and the lowest BG reading; it is markedly sensitive to outliers or values that are outside the range of measurement [66].

Metrics based on absolute change in glucose levels

- M-value (M_{IGV}):

$$M_{IGV} = \frac{1}{n} \sum_{t=1}^n \left| 10 \cdot \log_{10} \left(\frac{BG_t}{IGV} \right) \right|^3$$

Also called Schlichtkrull's M-value [68], [69] it evaluates the glycemic control based on deviations from an arbitrary glycemic reference point, which represent healthy individuals, and it assigns more importance to hypoglycemia than hyperglycemia. IGV is the ideal glucose value that reflects the normal basal glycemia in healthy individuals, originally set at 120 mg/dL, then modified to 90 mg/dL when glucose is measured in the interstitial fluid or to 80 mg/dL when glucose is measured in capillary blood samples [70]. Alternatively, Tatoñ and Czec proposed to set IGV at 100 mg/dL [69]. According to Service and Nelson [71], considering a IGV equal to 90 mg/dL

healthy individuals generally present a M-value ≈ 1 , individuals with a well-controlled DM have a M-value ≈ 10 , while individuals with inadequately controlled DM present a M-value > 30 [71].

- Adjusted M-value ($M_{IGV,w}$):

$$M_{IGV,w} = M_{IGV} + M_w$$

$$\text{where } M_w = \frac{\max(BG) - \min(BG)}{20}$$

The amplitude correction factor M_w is added to the M-value formula if the number of BG readings n is less than 25 [70].

- J-index:

$$J - \text{index} = 0.001 \cdot (\text{Mean} + \text{SD})^2$$

The J-index was defined by Wójcicki [72], who combined Mean and SD through a mathematical formula. It is sensitive to hyperglycemia but relatively insensitive to hypoglycemia; compared to M-value, it has the advantage of being independent of any arbitrarily glycemic reference point, which can impede the comparison between studies that use different reference points. In addition, Wójcicki defined four categories for the assessment of glycemic control based on J-index values: ideal glycemic control if $10 \leq J \leq 20$, good glucose control if $20 < J \leq 30$, poor glucose control if $30 < J \leq 40$, and lack of glycemic control if $J > 40$ [72].

- Continuous Overlapping Net Glycemic Action at n-hour ($CONGA_n$):

$$CONGA_n = \sqrt{\frac{\sum_{t=t_1}^{t_{k^*}} (D_t - \bar{D})^2}{k^* - 1}}$$

where k^* is the number of observations with an observation $n \times 60$ minutes ago,

$$D_t = BG_t - BG_{t-m} \text{ with } m = n \times 60,$$

$$\text{and } \bar{D} = \frac{\sum_{t=t_1}^{t_{k^*}} D_t}{k^*}$$

It describes the within-day glycemic fluctuations by computing the SD of the differences between each current observation and the observation at n hours before [73]. High CONGA values indicate elevated glucose fluctuations, which are consistent to inadequate glycemic control.

- Mean of Daily Differences (*MODD*):

$$MODD = \sqrt{\frac{\sum_{t=t_1}^{t_k} (BG_t - BG_{t-1440})^2}{k}}$$

where k is the number of observation with an observation 24 hours ago

It describes the between-day glycaemic fluctuations by computing the mean difference between BG readings obtained at the same time of the day on two consecutive days [74].

Metrics based on risk of major glycaemic excursions

Risk-based metrics have been introduced to reduce the bias towards hyperglycemia due to the high asymmetry of the BG scale. As shown in part A of Figure 2.6, indeed, deviations towards hyperglycemia (above 180 mg/dL or 10 mmol/L [75]) occupy a wider space than deviations towards hypoglycemia (below 70 mg/dL or 3.9 mmol/L [75]) and euglycemia is not centered within the scale [76].

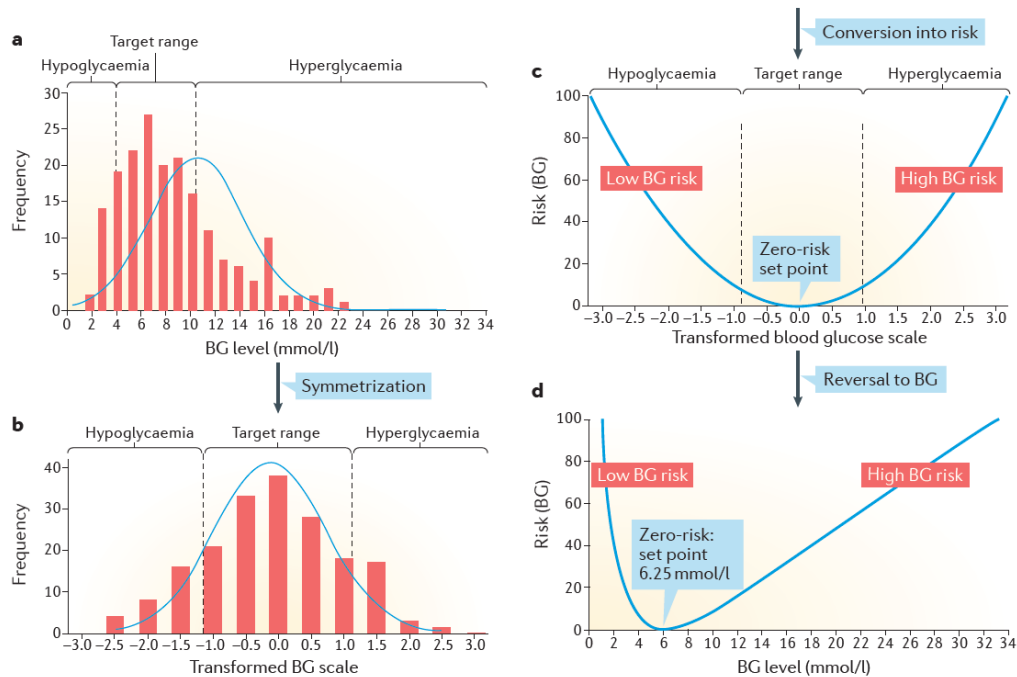


Figure 2.6: Risk analysis of blood glucose data proposed by Kovatchev et al. [76], [77]

- Low BG Index (*LBGI*) and High BG Index (*HBGI*):
Kovatchev et al. [77] first validated a numerical transformation of the BG scale to generate a symmetric BG distribution around zero, using

a continuous function defined in the range [20 mg/dL – 600 mg/dL] as displayed in part B of Figure 2.6:

$$f(BG) = \gamma * [(\ln(BG))^\alpha - \beta],$$

where $\alpha = 1.084$, $\beta = 5.381$, and $\gamma = 1.509$.

After the numerical transformation, a quadratic risk function is superimposed as shown in part C of Figure 2.6:

$$r(BG) = 10 \cdot f(BG_t)^2$$

defined in the range [0-100] with a minimum value around 113 mg/dL (6.25 mmol/L). The $r(BG)$ represents a measure of the risk associated to a specific BG reading; in particular, the left branch of the resulting parabola detects the risk of hypoglycemia, while the right branch identifies the risk of hyperglycemia [76]–[78]:

$$r(BG) = \begin{cases} rl(BG), & BG < 0 \\ rh(BG), & BG > 0 \end{cases}$$

Finally, once back to the original BG scale, part D of Figure 2.6 reveals that the risk of BG decreasing grows rapidly, while the risk of BG increasing has a more attenuated rise. Therefore, LBGI is a non-negative number that increases when the frequency and/or the extent of low BG readings increases, validated as a good predictor of severe hypoglycemia. Contrarily, HBGI is a measure of the frequency and extent of high BG readings, closely related to HbA1c and risk for hyperglycemia.

$$LBGI = \frac{1}{n} \sum_{t=1}^n rl(BG)$$

$$HBGI = \frac{1}{n} \sum_{t=1}^n rh(BG)$$

Based on the LBGI value, Kovatchev et al. [77] identified three risk categories for the development of severe hypoglycemic episodes: low risk if $LBGI \leq 2.5$, moderate risk if $2.5 < LBGI \leq 5$, and high risk if $LBGI > 5$. Similarly, based on the HBGI value, three risk categories for the development of hyperglycemia were defined: low risk if $HBGI \leq 4.5$, moderate risk if $4.5 < HBGI \leq 9$, and high risk if $HBGI > 9$.

- BG Risk Index (*BGRI*):

$$BGRI = LBGI + HBGI$$

It represents the overall risk of experiencing extreme glycemc values, ranging in the interval [0-100] [79].

- Average Daily Risk Range (*ADRR*):

$$ADRR = \frac{1}{N_{days}} \sum_{i=1}^{N_{days}} LR_i + HR_i$$

where for the i -th day

$$LR_i = \max(rl_i(BG))$$

$$HR_i = \max(rh_i(BG))$$

The ADRR is the average of the risk range per day, where rl and rh represent the same risk function defined by Kovatchev et al. [77] for the computation of LBGi and HBGI. Indeed, ADRR combines LBGi and HBGI in order to be equally predictive of extreme glycemic excursion towards to hypoglycemia and hyperglycemia [80]. ADRR values have been stratified by Kovatchev et al. [80] in three risk categories: low risk if $ADRR < 20$, moderate risk if $20 \leq ADRR \leq 40$, and high risk if $ADRR > 40$.

- Glycemic Risk Assessment Diabetes Equation (*GRADE*):

$$GRADE\ value_t = 425 \cdot \left\{ \log_{10} \left[\left(\log_{10} \left(\frac{BG_t}{18} \right) \right) + 0.16 \right] \right\}^2$$

$$GRADE\ score = \frac{\sum_{t=1}^n GRADE\ value_t}{n}$$

The GRADE score is the mean of all GRADE values. This formula was designed by Hill et al. [81] to operate for BG readings ranging in the interval [37 mg/dL - 630 mg/dL]; outside this range, a GRADE value of 50 is assigned by default. In addition, the relative risk contributions of hypoglycemia (below 70 mg/dL as defined by authors), euglycemia and hyperglycemia (above 140 mg/dL as defined by authors) to the GRADE risk score can be defined as in the following equations:

$$GRADE_{hypoglycemia} = \frac{\sum GRADE\ value_{only\ BG_t < 70\ mg/dL}}{\sum GRADE\ value_{all\ BG_t}} \cdot 100$$

$$GRADE_{euglycemia} = \frac{\sum GRADE\ value_{only\ 70\ mg/dL \leq BG_t \leq 180\ mg/dL}}{\sum GRADE\ value_{all\ BG_t}} \cdot 100$$

$$GRADE_{hyperglycemia} = \frac{\sum GRADE\ value_{only\ BG_t > 180\ mg/dL}}{\sum GRADE\ value_{all\ BG_t}} \cdot 100$$

A GRADE score > 5 indicate an inadequately controlled glycemic profile. The weighted risk contributions of $GRADE_{hypoglycemia}$,

GRADE_{euglycemia}, and GRADE_{hyperglycemia} are used in parenthesis alongside the overall risk score for specifying if the glycemic risk is more attributable to hypoglycemia or to hyperglycemia [81].

- Hypo Index and Hyper Index:

$$\text{Hypo Index} = \frac{\sum_{t=1}^n (LLTR - BG_t)^b}{n \cdot d}$$

for any $BG_t < LLTR$

$$\text{Hyper Index} = \frac{\sum_{t=1}^n (BG_t - ULTR)^a}{n \cdot c}$$

for any $BG_t > ULTR$

The Hypo Index represents a weighted average of hypoglycemic values, while the Hyper Index represents a weighted average of hyperglycemic values. These weights can be adjusted for mild, moderate, or severe hypoglycemia and hyperglycemia [82]. Generally, the exponents a and b range in the interval [1.0-2.0] and by default b=2.0 and a=1.1. The default values (d=30 and c=30) of the scaling factors were selected so that Hypo Index and Hyper Index could be approximately on the same range of numerical values as LBGI, HBGI, and GRADE. Finally, LLTR is the lower limit of target range, with a default value of 80 mg/dL, while ULTR is the upper limit of target range, with default value of 140 mg/dL.

- Index of Glycemic Control (*IGC*):

$$IGC = \text{Hypo index} + \text{Hyper Index}$$

It represents a flexible weighting for extreme glycemic values [82] that can be adjusted to mimic either BGRI or GRADE score.

- Mean Amplitude of Glycemic Excursions (*MAGE*):

$$MAGE = \sum_{k=1}^{N_{exc}} \frac{\lambda_k}{N_{exc}}, \text{ if } \lambda > SD$$

where N_{exc} is the number of upward or downward glycemic excursions that exceed one SD, and λ is the amplitude of the k -th excursion

The MAGE is the mean of the glycemic excursions from nadir to peak (or vice versa) that exceed one SD of BG readings [83]. The graphical estimation of MAGE based on the procedure described by Service [83] is time-consuming and may be subject to many sources of error. Nevertheless, there is a lack of agreement as to which automated

algorithm could constitute the gold standard to compute MAGE. Indeed, Czerwoniuk et al. [84], Hill et al. [85], Fritzsche et al. [86], and Baghurst [87] proposed different software programs for MAGE computation that show varying agreement, as discussed by Sechterberger et al. [88] and Rodbard [89].

Metrics based on time in ranges

The diffusion of CGM systems allowed the development of a new group of glycemic metrics based on the percentage of time spent in specific glucose ranges, such as within target range, below target range and above target range [90], [91].

- Time In Range (*TIR*):

$$TIR = \frac{N_{TIR}}{n} \cdot 100$$

where N_{TIR} is the number of glucose readings such that

$$70 \leq BG_t \leq 180 \text{ mg/dL}$$

- Time In Target Range (*TIT*):

$$TIT = \frac{N_{TIT}}{n} \cdot 100$$

where N_{TIT} is the number of glucose readings such that

$$70 \leq BG_t \leq 140 \text{ mg/dL}$$

- Time Below Range (*TBR*):

$$TBR = \frac{N_{TBR}}{n} \cdot 100$$

where N_{TBR} is the number of glucose readings such that

$$BG_t < 70 \text{ mg/dL}$$

It can be divided into Time slightly Below Range (*TBR_Lev1*) and Time severely Below Range (*TBR_Lev2*):

$$TBR_Lev1 = \frac{N_{TBR_Lev1}}{n} \cdot 100$$

$$TBR_Lev2 = \frac{N_{TBR_Lev2}}{n} \cdot 100$$

where N_{TBR_Lev1} is the number of glucose readings such that

$$54 \leq BG_t < 70 \text{ mg/dL}$$

and N_{TBR_Lev2} is the number of glucose readings such that
 $BG_t < 54 \text{ mg/dL}$

- Time Above Range (TAR):

$$TAR = \frac{N_{TAR}}{n} \cdot 100$$

where N_{TAR} is the number of glucose readings such that
 $BG_t > 180 \text{ mg/dL}$

It can be divided into Time slightly Above Range (TAR_Lev1) and Time severely Above Range (TAR_Lev2):

$$TAR_Lev1 = \frac{N_{TAR_Lev1}}{n} \cdot 100$$

$$TAR_Lev2 = \frac{N_{TAR_Lev2}}{n} \cdot 100$$

where N_{TAR_Lev1} is the number of glucose readings such that
 $180 < BG_t \leq 250 \text{ mg/dL}$

and N_{TAR_Lev2} is the number of glucose readings such that
 $BG_t > 250 \text{ mg/dL}$

In 2019, the Advanced Technologies and Treatments for Diabetes (ATTD) published consensus recommendations for the adoption of time in ranges clinical targets for glycemic assessment, as illustrated in Table 2.3 [23]. The importance of individualized goals was emphasized especially for pediatric patients with the advice that a lower TIR target of 60% may be considered in case of an higher HbA1c goal of 7.5% [23].

Table 2.3: Time in ranges targets for the glycemic assessment, adapted from the Advanced Technologies and Treatments for Diabetes (ATTD) consensus recommendations [23].

Group	TBR	TIR	TAR
T1DM/T2DM	<4%	>70%	<25%
Older or high risk T1DM/T2DM	<1%	>50%	<10%

TBR: Time Below Range; TIR: Time In Range; TAR: Time Above Range; T1DM: Type 1 Diabetes Mellitus; T2DM: Type 2 Diabetes Mellitus.

Among all the selected short-term GV metrics, TIR has been arising as a reference measurement. According to a study of Beck et al. [92], TIR can be considered as a valid end point for clinical trials because it is strongly associated with the risk of development or progression of microvascular complications. Furthermore, several studies in literature have demonstrated the relationship between TIR and HbA1c, which is the actual gold standard

for assessing the quality of glycemic control in the long period. Based on four RCT regarding adult patients with T1DM (JDRF CGM RCT [54], DIAMOND [56], REPLACE-BG [57], HypoDE [58]), Beck et al. [93] noticed that on average a TIR value of 70% corresponded with a HbA1c value of 7% (53 mmol/mol) at baseline and with a HbA1c value of 6.8% (51 mmol/mol) after six months of monitoring; in addition, it was observed that an increase in TIR of 10% corresponded to a decrease in HbA1c of 0.6%. A good correlation between HbA1c and TIR was evidenced through the analysis of 18 articles also by Vigersky and McMahon [94], who observed that an increase in TIR of 10% corresponded to a change in HbA1c of 0.8% (9 mmol/mol).

2.2. Analysis of blood glucose time-series

A time-series is a collection of observations made sequentially through time that can be expressed as:

$$x_{0:T} = x_1, x_2, \dots, x_T$$

Time-series can be divided into two categories: continuous time-series, when observations are recorded continuously through time, and discrete time-series, when observations are collected only at specific times, usually equally spaced [95], e.g., BG measurements provided by a isCGM device every 15 minutes. Qualitatively, time-series can be explored through the time-series plot, which is a univariate graph where the observations' values are plotted against the observations' times, generally displayed horizontally. A quantitative analysis, instead, focuses on providing plausible descriptions for observed data and predicting future values, modeling the underlying dynamics of the system.

Nowadays, CGM devices make available real-time snapshots of glycemic levels and allow using retrospective data to evaluate metabolic control between periodic clinical encounters, but an accurate forecasting of BG levels within a prediction horizon (PH) long enough to support decision-making still remains a challenge [96]. As reported in the review article of Oviedo et al. [97], several univariate models have been developed for glucose prediction, ranging from linear to machine learning and deep learning models. In addition, given that the BG profile over day is sensitive to multiple factors, e.g. insulin therapy, meals, sleep, physical activity, stress, and HR, also multivariate models have been considered [97].

2.2.1. Univariate models for glucose prediction

BG levels can be predicted with a great accuracy considering only historical BG values in univariate models. One of the first methodologies adopted for glucose prediction is based on the autoregressive (AR) process, which have

a simple and easily interpretable structure. Indeed, an AR model of order p predicts the variable of interest through a linear combination of the p previous values of the variable itself, e.g. the previous BG measurements, plus some noise term. Alternatively, a moving average (MA) model uses the previous q forecasting errors in a regression-like model, imposing a correlated noise structure beyond the traditional assumption of independent and identically distributed errors. In addition, both AR and MA models can be combined into a unique representation building a general autoregressive moving average model of orders p and q defined as ARMA(p , q). Reifman et al. [98] proposed a thirty-order AR model with fixed coefficients determined by the regularized least-squares technique. Resulting model was evaluated on 9 T1DM adult patients monitored for five days through the iSense rtCGM system (iSense Corporation, Portland, Oregon), which provides BG measurements every minute, obtaining adequate prediction performances on a 30-minutes PH as indicated by both the Clarke Error Grid (CEG) and the average root mean square error (RMSE) equal to 22.25 mg/dL (± 3.89 SD). Sparacino et al. [99], instead, presented a first-order AR model with time-varying parameters determined by the weighted least squares technique, exploiting a forgetting factor to regulate the weights of historical data used for glucose predictions. Resulting model was evaluated on a dataset of 28 T1DM patients monitored for 48 hours through the Menarini GlucoDay rtCGM system (Menarini Diagnostics, Florence, Italy), which provides BG measurements every 3 minutes [100]. Good average results in terms of mean square prediction error (MSPE), energy of the second-order differences (ESOD), and time delay demonstrated that acute glycemic events can be predicted with a sufficient margin for intervention. Moreover, Eren-Oruklu et al. [101] developed a second-order ARMA model with time-varying parameters determined by the weighted least squares algorithm integrated with a change detection method, which decreases the forgetting factor to a smaller value when a persistent change in model parameters is detected. Authors considered two different adult populations: one group consisted of 22 healthy individuals, 7 glucose-intolerant subjects and 11 T2DM patients hospitalized for 48 hours, while the other group consisted in 8 healthy individuals and 14 T2DM patients monitored at home for 48 hours, all wearing the Medtronic Gold rtCGM system that provides BG measurements every five minutes. Within a PH of 30 minutes, resulting model was able to predict glucose levels with a sum of squares of the glucose prediction error (SSGPE) of 6.14% and a relative absolute deviation (RAD) of 3.78 ($\pm 1.12\%$ SD) for T2DM patients.

Beyond autoregressive models a number of univariate machine learning approaches have been considered for glucose prediction, even if there is not a single methodology that can be identified as the most popular strategy. Hamdi et al. [102] developed a Support Vector Regression (SVR) model, using the differential evolution algorithm for hyperparameters selection. Resulting model was evaluated on a dataset of 12 T1DM patients monitored in real-life conditions through the Abbott Freestyle Navigator rtCGM system, which provides BG measurements every 15 minutes, obtaining an

average RMSE of 9.44 mg/dL on a PH of 15 minutes and an average RMSE of 10.78 on a PH of 30 minutes. Rodríguez-Rodríguez et al. [96], instead, compared the accuracy of SVR and Random Forest (RF) models for glucose prediction, varying the sampling frequency of BG measurements, the volume of historical data, and the PH. Model evaluation was performed on a dataset of 25 T1DM adult patients monitored in real-life conditions through the Abbott FreeStyle Libre isCGM system for up to 14 days. Authors reported the SVR models were less accurate than RF models, which allowed to obtain an average RMSE of 15.43 mg/dL on a 15-minutes PH with a 15-minutes sampling frequency, using 24 historical data points for each prediction.

Recently, given the considerable amount of data made available by CGM systems, deep learning models have been applied to glucose prediction. Pérez-Gandia et al. [103] developed a feed-forward neural network (NN) model with two layers, which consist of ten neurons and five neurons respectively, and an output layer with one neuron, considering for each prediction a 20-minutes sliding window and different PHs. Resulting models were evaluated on two different populations, both monitored in real-life conditions: 9 T1DM patients were monitored intermittently for 72 hours per week over a 4-week period through the Medtronic Guardian Real-time rtCGM system, which provides a BG measurements every five minutes, while 6 patients were monitored for around 72 hours through the Abbott FreeStyle Navigator rtCGM system, which provides a BG measurements every minute. Considering a PH of 15 minutes, the average RMSE was equal to 9.74 mg/dL (± 2.71 SD) for the first dataset and to 10.38 mg/dL (± 3.15 SD) for the second dataset; considering a PH of 30 minutes, instead, the average RMSE was equal to 17.45 mg/dL (± 5.44 SD) for the first dataset and to 19.51 mg/dL (± 5.53 SD) for the second dataset. In addition, authors also implemented a first-order AR model to compare the prediction performances, observing that the NN models were characterized by higher accuracies but also longer delays compared to the first-order AR model. Martinsson et al. [104] presented a NN model based on a first layer with 256 Long-Short Term Memory (LSTM) units followed by two hidden layers, which consisted of 512 and 256 neurons respectively, and an output layer with two neurons. Model evaluation was performed on 6 T1DM adult patients from the OhioT1DM dataset [105], monitored in real-life conditions for 8 weeks through the Medtronic Enlite rtCGM system that provides BG measurements every five minutes. The average RMSE was equal to 18.87 mg/dL (± 1.79 SD) on a 30-minutes PH and to 31.40 mg/dL (± 2.08 SD) on a 60-minutes PH. Moreover, Wang et al. [106] proposed a framework that integrates a fifth-order AR, extreme learning machine (EML), and SVR algorithms. Resulting model was evaluated on ten T1DM patients randomly selected from the RCT conducted by the JDRF CGM Study Group using the Medtronic Guardian and the Dexcom SEVEN rtCGM systems with a sampling frequency of five minutes and the Abbott FreeStyle Navigator rtCGM system with a sampling frequency of ten minutes [54]. Compared to single fifth-order AR, EML, and SVR models, the integrated framework

allowed to obtain the best prediction performance with an average RMSE of 19.0 mg/dL (± 0.3 SD).

2.2.2. Multivariate models for glucose prediction

As outlined in Figure 2.7, glucose prediction can be based on other input variables in addition to BG measurements, although it may be hard to formalize in mathematical terms and automatically extract useful signals from other source of information [97].

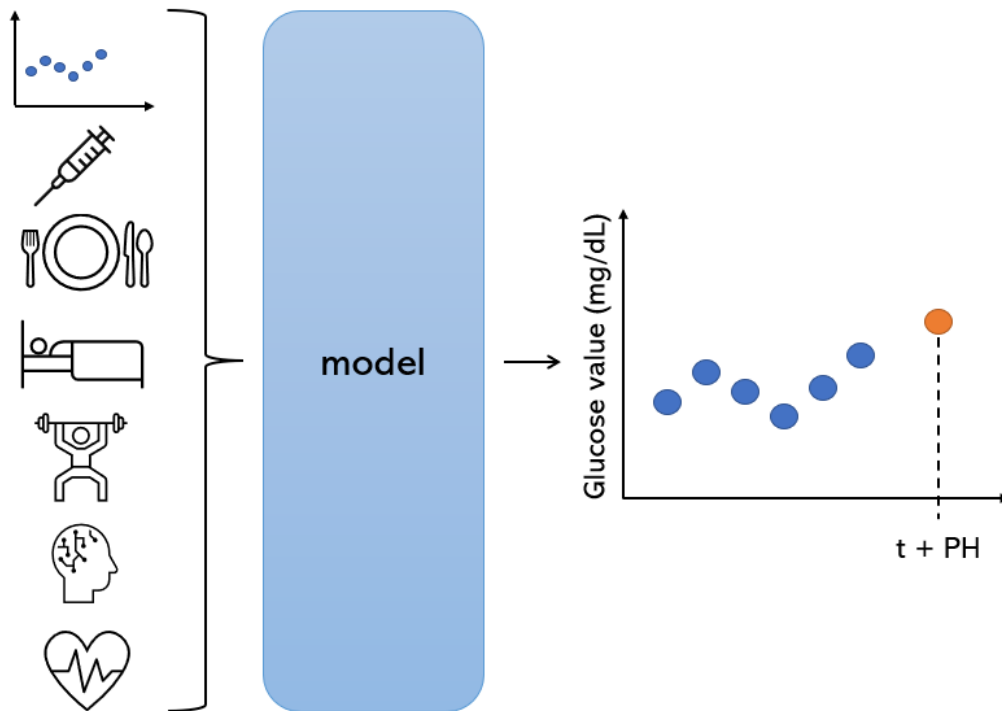


Figure 2.7: Conceptual schema of a multivariate model for glucose prediction at time $t + PH$ (prediction horizon) using several inputs, such as previous glucose measurements, insulin therapy, meals, sleep, physical activity, stress, and heart rate information, adapted from Zecchin et al. [107].

The autoregressive with exogenous inputs (ARX) models represent an extension of the AR models that allow to include one or more exogenous signals for glucose prediction. Finan et al. [108] compared a third-order time-invariant ARX model with a third-order time-variant ARX model considering in input CGM measurements, insulin pump records and patient-recorded estimates of meal carbohydrate (CHO) content. Data were collected from two datasets: the first dataset comprised 9 T1DM adult patients monitored for a period of 2-8 days in ambulatory conditions through the Medtronic MiniMed system, which consists of the MiniMed insulin pump and the Guardian rtCGM system with a 5-minutes sampling frequency, while the second dataset included 6 of the same monitored patients treated for 3

consecutive days with prednisone, a steroid medication. ARX models were evaluated on the second dataset studying the impact of a reduced insulin sensitivity due to prednisone on the prediction performances. Considering a 30-minutes PH, the time-variant approach produced slightly better predictions than the time-invariant approach (average RMSE ≈ 27 mg/dL), while on a 90-minutes PH the time-invariant ARX models with an average RMSE of 59 mg/dL was more accurate than the time-variant ARX models that showed an average RMSE of 61 mg/dL. Turksoy et al. [109] proposed a third-order autoregressive moving average with exogenous inputs (ARMAX) model for building a glucose prediction and alarm system, using a Savitzky-Golay filter and a Kalman filter to reduce noise in data. Model evaluation was performed on 14 T1DM adult patients monitored in real-life conditions through the Medtronic iPro rtCGM system, which provide BG measurements every five minutes, and the BodyMedia SenseWear Pro3 (BodyMedia Inc., Pittsburgh, Pennsylvania) armband device [110], which acquires body physiological signals every minutes. In particular, considering a 30-minutes PH for a specific patient, the ARMAX model based on BG measurements, energy expenditure, galvanic skin response, and insulin on board (amount of insulin that is accumulated in the body) showed a RMSE of 17.46 mg/dL and a SSGPE of 8.17%, while the univariate model had less accurate predictions with a RMSE of 41.16 mg/dL and a SSGPE of 19.26%.

Moreover, Zaho et al. [111] compared ARX and latent variable with exogenous input (LVX) prediction models, which were optimized through partial-least square algorithm and canonical correlation analysis, considering estimates of meal CHO content and recorded insulin boluses as exogenous variables. Models were evaluated on two datasets: ten in-silico adult patients, who were generated through the UVA/Padova Type-1 Diabetic simulator [112] with a 5-minutes sampling frequency and different scenarios (meal timing, meal amounts, and insulin-to-carbohydrate ratio) for three days, and seven adult patients monitored in ambulatory conditions through the Dexcom SEVEN Plus rtCGM system with 5-minutes sampling frequency. LVX models gave more accurate glucose predictions than ARX models for both datasets. In particular, considering the ambulatory dataset, LVX models provided an average RMSE of 11.1 mg/dL (± 2.4 SD) on a 15-minutes PH and 18.7 mg/dL (± 3.7 SD) on a 30-minutes PH, while ARX models provided an average RMSE of 11.3 mg/dL (± 2.5 SD) on a 15-minutes PH and 19.5 mg/dL (± 3.8 SD) on a 30-minutes PH.

Also machine and deep learning approaches have been adopted for developing multivariate models for glucose prediction. Georga et al. [113] proposed a SVR model with BG measurements, plasma insulin concentration, rate of appearance of meal-derived glucose into the systemic circulation (as described by the Lehmann and Deutsch model [114]), and cumulative amount of the energy expenditure during physical activities. Model evaluation was performed on 15 T1DM adult patients on MDI therapy enrolled in the METABO project [115], monitored in real-life conditions for a period of 5-22 days through the Guardian rtCGM system, which provide BG measurements every five minutes, and the BodyMedia SenseWear

armband device, which provides physiological signals every minute. Information regarding both insulin, i.e. doses, types, and injection times, and food intake, i.e. type of food, serving sizes, and times, were collected on a daily basis by patients using a paper diary. Overall, resulting model showed an average RMSE of 5.21 mg/dL on a 15-minutes PH and 6.03 mg/dL on a 30-minutes PH.

Zecchin et al. [116] proposed a NN model, which consisted of one hidden with eight neurons and an output layer with one neuron, considering BG measurements and estimates of meal CHO content in sliding windows of 15 minutes for each glucose prediction. Resulting model was evaluated on two datasets: five in-silico adult patients, who were generated through the UVa/Padova Type-1 Diabetic simulator with a 5-minutes sampling frequency for five days, and one patient monitored in real-life conditions through the Abbott FreeStyle Navigator with a 1-minute sampling frequency for seven days during the DIAdvisor project [117]. Considering a 30-minutes PH, the NN model obtained an average RMSE of 9.7 mg/dL (± 1.1 SD) on the simulated data and a RMSE of 28.2 mg/dL on the single real patient. Li et al. [118] developed a dilated convolutional neural network (CNN) framework called “GluNet”, which consisted of an input layer with 32 neurons, two hidden layers with 32 neurons, a hidden layer with 64 neurons and an output layer with 64 neurons, considering BG measurements, meals, and insulin information in sliding windows of 90 minutes for each glucose prediction. Authors collected both simulated and clinical data for model evaluation. On the one side, 20 T1DM adult and adolescent patients were generated through the UVa/Padova Type-1 Diabetic simulator with a 5-minutes sampling frequency for 180 days. On the other side, two clinical dataset were used: the ABC4D project dataset [119] included ten T1DM adult patients monitored in real-life conditions for six months through the Medtronic iPro rtCGM system with a 5-minutes sampling frequency, recording meals and insulin dosages in a dedicated app, while the OhioT1DM dataset [105] included six T1DM adult patients monitored in real-life conditions for eight weeks through the Medtronic Enlite rtCGM system with a 5-minutes sampling frequency. The resulting CNN model was compared with the NN model developed by Pérez-Gandia et al. [103], the LVX model developed by Zaho et al. [111], the third-order ARX model developed by Finan et al. [108], and the SVR model developed by Georga et al. [113]. Considering a 30-minutes PH, GluNet revealed the best prediction performances with an average RMSE of 8.88 mg/dL (± 0.77 SD) on the simulated data, an average RMSE of 19.19 mg/dL (± 2.74 SD) on the ABC4D data, and an average RMSE of 19.28 mg/dL (± 2.76 SD) on the OhioT1DM data. In addition, authors also trained a generalized CNN model on data corresponding to five ABC4D patients and tested it on the other patients one by one. The average RMSE of the generalized model was equal to 24.93 mg/dL, while the average RMSE of single personalized models was equal to 20.59 mg/dL. Also Aliberti et al. [120] proposed a generalized NN model, which consisted of a layer with 30 LSTM units and an output layer with six neurons for a 30-minutes PH and 12 neurons for a 60-minutes PH,

using several input variables in addition to BG measurements. Resulting model was evaluated on 451 T1DM patients (children, adolescents, and adults) from the JDRF CGM Study Group RCT, using the Medtronic Guardian and the Dexcom SEVEN rtCGM systems with a sampling frequency of five minutes and the Abbott FreeStyle Navigator rtCGM system with a sampling frequency of ten minutes. Considering monitoring data without filtering procedures, the RMSE was equal to 19.47 mg/dL on a 30-minutes PH and to 32.38 mg/dL on a 60-minutes PH.

2.3. The AID-GM platform

AID-GM is a web application developed at the Biomedical Informatics Laboratory of the University of Pavia, Italy, in collaboration with the Pediatric Endocrinology and Diabetology outpatient service of the Fondazione IRCCS Policlinico San Matteo Hospital and the Endocrinology and Diabetology outpatient service of the IRCCS Istituti Clinici Scientifici Maugeri, both located in Pavia [121]. This platform allows the integration of PGHD from multiple sources, such as CGM systems, personal fitness trackers (PFTs), and self-reported daily diaries. In this way, DM patients and their healthcare providers are enabled to share, visualize, and analyze the glycemic profiles integrated by HR, daily activity, and sleep information.

AID-GM is mainly developed in Java and integrated with JavaServer Faces (JSF) [122], Hibernate [123], and MySQL [124] technologies. JSF is a Java specification that simplifies the development of components in a web-based user interface, while Hibernate provides a framework for mapping Java objects manipulated by the AID-GM platform to relational databases. Finally, MySQL has been chosen as database management system because it is designed for web application, and it is open source.

2.3.1. Data integration infrastructure

The AID-GM data integration module has been designed to be independent of the specific PFT or CGM system. BG readings, insulin bolus, meals, and health-related issues can be periodically uploaded to the platform through a text file, which is downloadable by the patient from the CGM system application, or otherwise automatically retrieved from a proprietary cloud. Similarly, HR, daily activity, and sleep information are gathered from the cloud through an automatic night routine by the AID-GM platform.

Indeed, monitoring data can be synchronized to a cloud repository through a mobile application paired to the CGM system or the PFT worn by the patient. Afterwards, once new PGHD become available on the cloud, the downloader components in the data integration module exploit the Apache HttpClient library [125] for sending Hypertext Transfer Protocol (HTTP) requests to the PGHD source's server, which queries the cloud repository for data. The data integration module also includes the consent collectors

components, which are responsible to verify the consent status over time and, if expired, ask the patient to renew it, since a third application like AID-GM is allowed to access data within the cloud only in presence of the patient’s explicit permission.

Generally, PGHD sources provide documents in the JavaScript Object Notation (JSON) format, a lightweight data-interchange standard that is completely language independent [126]. Thus, the data integration module contains JSON parser components for extracting text elements and data converters components for translating such elements in the format requested by the MySQL relational database, provided by the Oracle Corporation [124]. Information on daily habits, instead, is collected directly through the AID-GM interface during registration and can be modified at any time.

In addition, the data integration module has the key task of contextualizing each BG and HR events within the patient’s day through two different tagging procedures. For each measurement, in fact, both the profile tag and the PFT tag that are assigned by the data taggers components are stored into the database using the data loaders components. The profile tag is assigned based on patient’s daily habits considering a set of possible values, such as awakening, after breakfast, before lunch, before dinner, after dinner, and night, which is attributed when the time of occurrence is between the bedtime and the awakening-time, as illustrated in Figure 2.8.

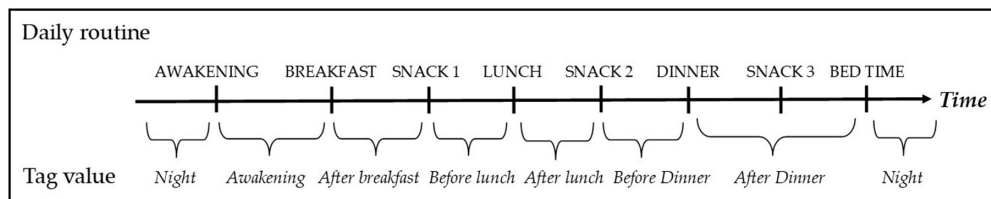


Figure 2.8: Procedure for assigning the profile tag value to blood glucose or heart rate measurements based on patient’s daily routine [127].

Contrarily, the PFT tag is assigned using the activity information provided by the patient’s tracker. In particular, workout and sleep values are attributed when an event occurs during a tracked workout or sleep session, respectively, while the routine value is used when patient is not sleeping and not training [121]. Finally, the not-available (NA) value is assigned to each BG measurement if the patient is not wearing the PFT at a specific time t_i , i.e. if there are not any HR measurements available in the interval $[t_{i-5\text{ minutes}}; t_{i+5\text{ minutes}}]$.

2.3.2. Graphical user interface

The AID-GM graphical user interface (GUI) has been developed to support the usability for both patients and healthcare providers, who have available different functionalities. As shown in Figure 2.9, the physician’s home page

presents a summary of patients' information and activities, like the last CGM data upload or the last PFT synchronization. Figure 2.10, instead, displays the form where patients are asked to provide their habitual time schedule regarding primary meals, snacks, and sleep, used for computing the profile tag.

Advanced Intelligent Distant
AID-GM
Glucose Monitoring

Home Data Analysis Therapy management Patients management Logout

Physician Home Page
Last login: 03/12/2019 07:11

Patients Custom Thresholds Enrollment Requests (3)

(1 of 2) 20

Patient	Patient Info	Clinical Info	Last glycaemia upload	Last Fitbit synchronization	Vocal messages	Physical activity	Available BG data trend during last 7 days	BG data Visualization Request
PAT-67			2018-10-13 18:59:00.0	2018-10-15 21:46:46.0				
PAT-68			2018-10-19 19:06:00.0	2018-10-20 00:44:11.0				No request
PAT-69			2018-10-20 01:04:00.0	2018-10-19 17:41:33.0				No request
PAT-75			2018-10-05 18:50:00.0	2018-10-14 23:21:31.0				No request
PAT-76			2018-10-12 17:58:00.0	2018-10-15 08:56:05.0				No request
PAT-77			2018-08-29 06:22:00.0	2018-10-21 05:55:08.0				No request

Figure 2.9: Physician' home page in the Advanced Intelligent Distant – Glucose Monitoring (AID-GM) platform [127].

Please input your daily habits.

Your daily habits									
	Awakening	Breakfast	Snack1	Lunch	Snack2	Dinner	Snack3	Bedtime	
Sunday	08:00	08:30		13:00		20:00		22:00	✓ Copy Paste
Monday	07:00	07:30		13:00		20:00		22:00	✓ Copy Paste
Tuesday	07:00	07:30		13:00		20:00		22:00	✓ Copy Paste
Wednesday	07:00	07:30		13:00		20:00		22:00	✓ Copy Paste
Thursday	07:00	07:30		13:00		20:00		22:00	✓ Copy Paste
Friday	07:00	07:30		13:00		20:00		23:00	✓ Copy Paste
Saturday	08:00	08:30		13:00		20:00		23:00	✓ Copy Paste

Figure 2.10: Patient's form to provide the time schedule of daily habits in the Advanced Intelligent Distant – Glucose Monitoring (AID-GM) platform [127].

Besides the consultation of general patient's information like demographics, contacts, DM onset date, weight, and personal thresholds for glycemic and HR alterations, the AID-GM GUI allows to visualize different kind of reports that integrate data from CGM system, PFT, and lifestyle.

Figure 2.11 shows an example of patient’s daily profile, where the HR profile is represented by the dark orange line and expressed in beats per minute (BPM), while the glycaemic profile is represented by the blue line and expressed in mg/dL. Particularly, the glycaemic profile presents both automatic and manual BG measurements, which are performed using the CGM system, respectively with blue and red dots. Finally, the icons on the timeline help to contextualize the BG and HR measurements within the day based on additional events such as sleep, workout, insulin injection, and meals, as explained in the legend of Figure 2.12.

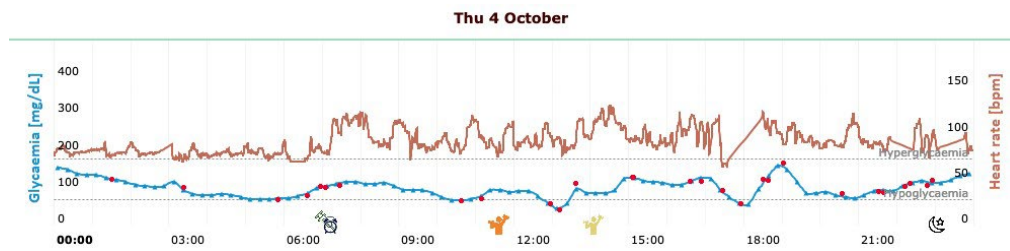


Figure 2.11: Visualization of a patient’s daily profile in the Advanced Intelligent Distant – Glucose Monitoring (AID-GM) platform [127].



Figure 2.12: Legend of the icons used in the Advanced Intelligent Distant – Glucose Monitoring (AID-GM) daily profile visualization [127].

Furthermore, AID-GM provides reports of patient’s lifestyle and physical activity. Figure 2.13 presents the lifestyle summary visualization, which gives an overview of patient’s activities over a user-defined time period. Figure 2.14, instead, shows the physical activity summary visualization, regarding HR measurements and workouts performed by patient in a specific time period [127]. Finally, all the available functionalities are indicated in Table 2.4, specifying if they are available for patients and/or clinicians.



Figure 2.13: Visualization of a patient's lifestyle summary in the Advanced Intelligent Distant – Glucose Monitoring (AID-GM) platform [127].



Figure 2.14: Visualization of a patient's physical activity summary in the Advanced Intelligent Distant – Glucose Monitoring (AID-GM) platform [127].

Table 2.4: Advanced Intelligent Distant – Glucose Monitoring (AID-GM) functionalities with the corresponding users, i.e., patient (P) or clinician (C), grouped by type of action [121].

Type of action	Functionality	User	
		P	C
Set up of the AID-GM account and access	Access through secure authentication	•	•
	Request to be enrolled in the clinical center	•	
	View and approval of enrollment request		•
	Set-up and update of daily habits	•	
	Set-up and update of patient-specific thresholds to identify glycemic alterations		•
	Set-up and update of patient-specific thresholds to identify HR alteration		•
Data upload	Upload of BG monitoring data	•	•
	Consent to download the PFT data	•	
	Visualization of patients list and recently uploaded data		•
	Visualization of patient’s information (e.g., demographics, contact information, onset date, weight, and thresholds for BG and HR)		•
	Visualization of BG overall time series, daily trends, and average glucose profile	•	•
	Visualization of a summary of the most recent hyperglycemic and hypoglycemic episodes	•	•
	Visualization of combined BG and HR daily profiles, complemented with information on sleep, workout, meal, and insulin intake	•	•
	Visualization of a summary of the physical activity in a selected period	•	•
	Visualization of a timeline that shows if the patient is regular in terms of sleep and activity	•	•
	Detection and visualization of patterns for one patient	•	•
	Detection and visualization of patterns for a group of patients		•
	Visualization of statistics related to pattern detection for a group of patients		•
	Drill-down to the BG and HR profiles related to the time intervals in which a selected pattern occurred	•	•
	Communication between patient and physician	Request for data visualization	•
Notification of data visualization request			•

Chapter 3

Datasets description and temporal data analytics techniques

This chapter describes the datasets considered in this research activity and methodologies proposed for the analyses, providing details on their implementations. Section 3.1 introduces the two considered datasets used in this research activity, collected in real-world conditions. Section 3.2 is dedicated to glucose data analytics, investigating the relationship between glycated hemoglobin and time in ranges along with the correlation between self-monitoring frequency and glycemic metrics. Section 3.3 presents temporal data mining techniques, considering temporal abstractions based on domain-specific pattern detection. Finally, Section 3.4 illustrates the architecture of the proposed deep learning model for glucose prediction.

3.1. Datasets description

Two different datasets have been considered in this research activity, one is collected on pediatric patients and the other on adult patients. In both cases all patients were affected by T1DM and monitored in real-life conditions through the same devices, as shown in Figure 3.1.

BG was measured through the Abbott FreeStyle Libre isCGM system (Abbott, Alameda, California), whose characteristics are described in Section 2.1.2, and all sensor readings were performed with the same version of the reader [43]. The FreeStyle Libre sensor provided BG measurements every 15 minutes, but it happened that the time interval between two consecutive readings was slightly different in terms of minutes, probably due to data processing made by the device algorithm. In addition to these automatic BG measurements patients could generate the so-called manual BG measurements, scanning the sensor whenever they wanted to check glycemic levels. On the other hand, HR, physical activity, and sleep were monitored using the Fitbit Charge 2 PFT (Fitbit, San Francisco, California) with a sampling frequency of one minute [128]. Activity information was used to assign the PFT tag (also called Fitbit tag) to BG and HR

measurements, distinguishing between workout, sleep, and routine intervals, as explained in Section 2.3.1. In particular, although Fitbit trackers' accuracy in the identification of specific stages within sleep occurrences has been debated, the accuracy of sleep detection is elevated and allows to reliably monitor patients' sleep quantity [129].

Additionally, both pediatric patients (or their caregivers) and adult patients provided personal and clinical information, like demographics, contacts, DM onset date, and a list of HbA1c tests.



Figure 3.1: On the left the Abbott FreeStyle Libre intermittently scanned Continuous Glucose Monitoring (isCGM) system, while on the right the Fitbit Charge 2 personal fitness tracker (PFT).

Data collection from these two wearable sensors required a limited active contribution by patients, who were asked to regularly recharge the devices, synchronize Fitbit data to the cloud, and upload glycemic text files produced by the Abbott software into the AID-GM platform. Specifically, the Freestyle Libre is characterized by an 8-hours rolling memory, which means that the oldest measurements are cyclically deleted from the sensor and lost if the patient does not swipe the reader over the sensor at least every eight hours, while the reader has a 90-days memory. The Fitbit tracker, instead, must be synchronized to the cloud at least once a week. In addition, patients were instructed to apply the FreeStyle sensor at the back of the upper arm and change it every 14 days.

This study was conducted according to the guidelines of the Declaration of Helsinki and the protocol was approved by the Institutional Review Board of the two hospitals. Children's caregivers (or subjects aged ≥ 18 years) provided written consent for inclusion in the study.

3.1.1. The pediatric dataset

A group of 30 T1DM children, adolescents and young adults on MDI therapy was recruited from the Pediatric Endocrinology and Diabetology outpatient service of Fondazione IRCCS Policlinico San Matteo hospital in Pavia, Italy. Exclusion criteria comprised retinopathy, nephropathy, established macrovascular disease, and therapies based on drugs likely to affect cardiac function or rhythm.

Out of the 30 recruited patients, three were discarded since they did not log into the AID-GM platform, nor did they upload data, therefore the

pediatric dataset used for the analyses effectively consisted of 27 patients. In addition, 10 patients did not use the Fitbit tracker. Table 3.1 summarizes the number (and percentages) of pediatric patients in specific pubertal stages monitored through the FreeStyle Libre system and the Fitbit tracker, grouped by sex. Pubertal stage was evaluated by clinicians using the Marshall and Tanner scale with the pre-pubertal characteristics corresponding to Tanner Stage 1 [130], [131].

Table 3.1: Number of pediatric patients in specific pubertal stages monitored through the FreeStyle Libre system and the Fitbit tracker, grouped by sex.

Patients	with FreeStyle	with Fitbit	Pubertal stage		
			<i>Pre-puberty</i>	<i>Puberty</i>	<i>Post-puberty</i>
Female	14 (52%)	9 (53%)	5	6	3
Male	13 (48%)	8 (47%)	7	2	4

Data were collected over a period of approximately 25 months between January 2018 and February 2020. A few patients did not use the monitoring devices in some periods, as outlined by the “Days without measurements” rows in Table 3.2, and Fitbit tracker was generally worn for a shorter time compared to the FreeStyle Libre device. Indeed, the average FreeStyle Libre follow-up was equal to 242.70 days (± 158.38 SD), computed as the difference between the last and the first FreeStyle Libre monitoring day, while the average Fitbit follow-up was equal to 98.18 days (± 118.96), computed as the difference between the last and the first Fitbit monitoring day.

Table 3.2: Characteristics of the pediatric dataset.

Characteristic		Summary statistics	
		Mean \pm SD	Median [25 th -75 th percentile]
Age (years)		11.33 \pm 4.98	11 [7.50-12.50]
Diabetes duration (years)		5.13 \pm 5.19	3.62 [1.93-6.95]
FreeStyle monitoring	Days of follow-up	242.70 \pm 158.38	180 [130-311]
	Days without measurements	56.44 \pm 119.47	3 [0-58.50]
Fitbit monitoring	Days of follow-up	98.18 \pm 118.96	47 [42-57]
	Days without measurements	33.88 \pm 90.82	0 [0-1]

3.1.2. The adult dataset

A group of 12 T1DM adult patients (3 females and 9 males) on MDI therapy was recruited from the Endocrinology and Diabetology outpatient service of the IRCCS Istituti Clinici Scientifici Maugeri in Pavia, Italy. Monitoring data were collected between November 2016 and July 2020. Patients wore the FreeStyle Libre system and the Fitbit tracker for a long time, as summarized in Table 3.3, but a number of patients temporarily suspended the use of monitoring devices in some periods.

Table 3.3: Characteristics of the adult dataset.

Characteristic		Summary statistics	
		Mean \pm SD	Median [25 th -75 th percentile]
Age (years)		35.84 \pm 9.93	37.84 [28.15- 42.93]
Diabetes duration (years)		17.37 \pm 7.72	15.80 [12.62- 20.58]
FreeStyle monitoring	Days of follow-up	467.83 \pm 267.49	410.50 [298-534.50]
	Days without measurements	95.83 \pm 103.34	79.50 [23-121.50]
Fitbit monitoring	Days of follow-up	533.17 \pm 490.38	372 [308.80-556.20]
	Days without measurements	138.58 \pm 280.57	52.50 [15.75- 100.25]

3.2. Glucose data analytics

An algorithm for descriptive statistics was implemented to provide clinicians with an immediate overview of each patient's situations. BG measurements were contextualized within the day and graphically related to physical activity and sleep periods, with a special attention to glucose values outside the euglycemic range (70-180 mg/dL). Several glycemic metrics introduced in Section 2.1.3 were computed for further considerations on glycemic control, considering all the monitoring period or specific monitoring windows for each patient, such as:

- Mean
- Overall standard deviation (SD)
- Within-day standard deviation (SD_w)
- Daily means standard deviation (SD_{dm})
- Percentage coefficient of variation (%CV)
- Median

- Interquartile range (IQR)
- Range
- M-value (M_{90})
- J-index
- Continuous Overlapping Net Glycemic Action at 1-hour ($CONGA_1$)
- Mean of Daily Differences (MODD)
- Low BG Index (LBGI)
- High BG Index (HBGI)
- BG Risk Index (BGRI)
- Average Daily Risk Range (ADRR)
- Glycemic Risk Assessment Diabetes Equation (GRADE)
- Hypo Index
- Hyper Index
- Index of Glycemic Control (IGC)
- Time In Range (TIR)
- Time In Target Range (TIT)
- Time Below Range (TBR)
- Time slightly Below Range (TBR_Lev1)
- Time severely Below Range (TBR_Lev2)
- Time Above Range (TAR)
- Time slightly Above Range (TAR_Lev1)
- Time severely Above Range (TAR_Lev2)

All the analyses and graphical representations related to glucose data analytics were performed using the R system for statistical computing, version 3.5.1 [132].

3.2.1. Linear mixed effects models for glycated hemoglobin and time in ranges relationship

As described in Section 2.1.2, HbA1c is the gold standard indirect measure of long-term glycemic control, and it estimates the glycemic exposure over the last 2-3 months before sampling. However, also glycemic metrics allow to monitor glycemic trends evaluating the magnitude and the frequency of intra- and inter-day glucose fluctuations. Particularly, metrics based on time in ranges like TIR have become reference measurements for glycemic control, as they have been associated with the risk of development or progression of microvascular complications [92]. In our real-world scenario, since both the pediatric and adult datasets had multiple distinct HbA1c measurements for each patient revealing clusters of not-independent observational units, the relationship between HbA1c and glycemic metrics was investigated through linear mixed effects (LME) models [133], which allowed to explore also the inter-subject variability.

LME models represent an extension of linear regression models that is particularly useful when the assumption of independent and identically distributed random variables is violated, as in case of repeated measurements made on the same statistical units or measurements made on clusters of related statistical units. Indeed, LME models incorporate both fixed effects, i.e. parameters that do not vary in the hypothesis that there are true regression lines in the population, and random effects, i.e. parameters that are themselves random variables.

A simple LME model with a single explanatory variable and a random intercept can be specified as:

$$Y_{ij} = \beta_{0j} + \beta_{1j}x_{ij} + \varepsilon_{ij}$$

where i indicates the level-one unit (e.g., individual measurement), j indicates the level-two unit (e.g., patient), Y_{ij} is the dependent variable to predict, x_{ij} is the explanatory variable at level one, ε_{ij} is the normally-distributed residual component, β_{1j} is a regression coefficient common to all groups, and β_{0j} is given by the sum between an average intercept γ_{00} and a group-dependent deviation U_{0j} .

In this scenario, given a j -th patient and a generic glycemic metric, the LME model equation for a i -th measurement can be reformulated as:

$$HbA1c_i = b_{pat_int} + b_{gly} \cdot glycemic_metric_i + \varepsilon_i$$

where the patient-specific intercept b_{pat_int} represents the random effect, since each patient may have a specific effect added to the average estimated intercept, while the glycemic metric coefficient b_{gly} is the fixed effect common to all patients, as in linear regression models. LME models were implemented with the function “lme” available in the R package called “nlme” [134].

Starting from each HbA1c exam date, glucose monitoring windows of past 30, 60, and 90 days were defined and considered valid if at least 70% of glucose measurements were available in those temporal intervals, in agreement with the ATTD consensus recommendations for CGM data usage [23]. For each monitoring windows width, the average percentages of time spent in different glucose ranges were displayed in a stacked boxplot colored according to the ATTD consensus recommendations for CGM data presentation [23], as shown in Figure 3.2. On the other hand, Afterwards, metrics based on time in ranges were computed in each valid window and separately used as explanatory variables (statistically significant if p -value<0.05) to explore the specific relationships with HbA1c, in particular the relationship between TIR and HbA1c [135].

For each LME model, the compliance of the prediction errors ε -distribution with the normality assumption is checked both by Shapiro-Wilk’s statistical test under the null hypothesis that the population is

normally distributed, using the function “shapiro.test” in the R package called “stats” [136] and setting the significance threshold to 0.05, and by visual inspection of quantile-quantile (q-q) plots. A q-q plot is graphical technique for determining if a set of data plausibly come from a theoretical distribution (e.g., the normal distribution): the quantiles of a given dataset is plotted against the quantiles calculated from a theoretical distribution and, if both sets of quantiles come from the same distribution, the resulting points should fall approximately along the 45-degrees reference line. Finally, the variance explained by the entire LME model is expressed by the conditional coefficient of determination R^2 on a 0–1 scale:

$$R^2 = \frac{\sigma_r^2 + \sigma_f^2}{\sigma_r^2 + \sigma_f^2 + \sigma_\varepsilon^2}$$

where σ_r is the random effects variance, σ_f is the fixed effect variance, and σ_ε is the observation-level variance [137], [138].

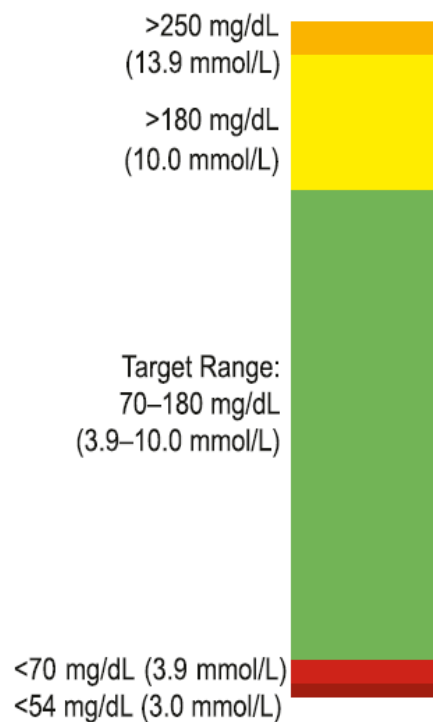


Figure 3.2: Stacked boxplot for continuous glucose monitoring (CGM) data presentation as suggested by the Advanced Technologies and Treatments for Diabetes (ATTD) consensus [23]. The two categories of Time Above Range (TAR) are displayed in yellow and orange, Time in Range (TIR) is represented in green, while the two categories of Time Below Range (TBR) are in light and dark red.

3.2.2. Correlation between self-monitoring frequency and glycemic metrics

Substantial clinical benefits from CGM systems adoption have been reported in literature for individuals with DM, including improvements in glycemic control and management of acute glycemic episodes, as discussed in Section 2.1.2. In our real-world scenario, the relationship between TIR and patient's self-monitoring frequency was analyzed both for exploring individual behaviors and examining if there was an overall enhancement in glycemic control related to an elevated manual scan frequency. Additionally, also the relationship between TIR and the other glycemic metrics was investigated.

Glucose data were divided into monitoring windows of 14 days, as the FreeStyle Libre sensors life. In order to make a comparison with other similar studies in other countries [139]–[142], each monitoring window was included in the analyses only if it had at least 480 automatically stored readings, which correspond to around 120 hours of monitoring. In every accepted windows several glycemic metric has been calculated, one for each of the four families of methods described in Section 2.1.3, such as traditional metrics, metrics based on absolute change in glucose levels, metrics based on risk of major glycemic excursions, and metrics based on time in ranges, considering SD, CONGA₁, ADRR, and TIR, respectively. The daily scan frequency was computed as the sum of the manual scans divided by the window length.

In the first analysis, all patients' monitoring windows were rank ordered by daily scan frequency and split into ten equally sized groups based on deciles. Average values of daily scan frequency and TIR were computed in each group, which contained 10% of the total monitoring windows data. A non-parametric Dunn's test was performed to verify if average TIR was significantly different among groups, using the function “dunnTest” in the R package called “FSA” [143] and setting the significance threshold to 0.05. Then, the correlation between TIR and daily scan frequency was investigated through the Spearman's correlation coefficient (ρ), computed with the function “rcorr” available in the R package called “Hmisc” [144].

Afterwards, monitoring windows were ranked ordered also by SD, CONGA₁, and ADRR in separate analyses and split into ten equally sized groups based on deciles. For each analysis, average values of TIR and the corresponding ranking variable were computed in every group. Similarly, Dunn's tests were executed to verify if average TIR was significantly different among groups and the Spearman's correlation coefficients were calculated to explore the relationship between TIR and the selected glycemic metrics.

3.3. Temporal data mining with temporal abstraction

In the analysis of temporal data it is useful to detect the occurrence of specific temporal patterns, i.e. time intervals in which one or more time-series assume a behavior of interest [145], especially in contexts where there is a combination of qualitative and quantitative variables with irregular sampling frequencies, such as in medical domains. Knowledge-based TA techniques, in particular, allow to automatically detect a sequence of qualitative time intervals corresponding to significant patterns from a time-point representation of quantitative data [146].

3.3.1. Libraries for temporal abstraction

The AID-GM application is integrated with the Java Time Series Abstractor (JTSA) library [147], which has been developed at the Bio-Medical Informatics Laboratory “Mario Stefanelli” of the University of Pavia and distributed as a jar file under general public license.

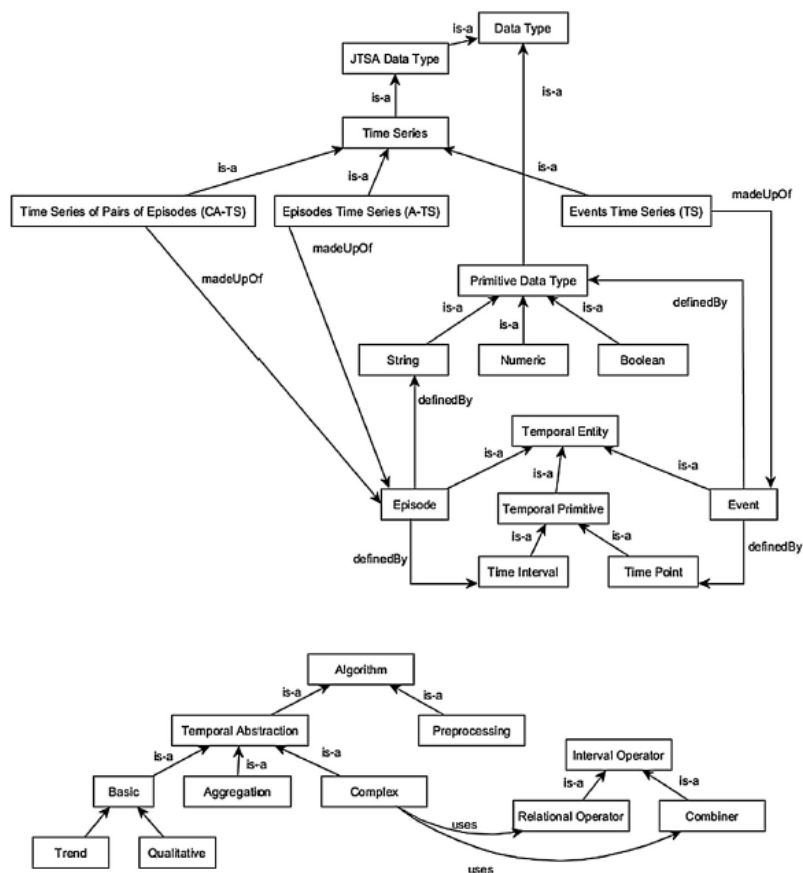


Figure 3.3: Methodological ontology of the Java Time Series Abstractor (JTSA) framework [147].

JTSA operates on the basis of two temporal primitives, the time point and the time interval, as illustrated in the methodological ontology of Figure 3.3, both represented according to a specific temporal resolution referred as granularity [145]. This makes possible to distinguish between events, which are characterized by a time point and a measurement value, and episodes, which are characterized by an interval of occurrence and a temporal pattern label. Events time-series (E-TS) are time-series of events, while episodes (abstractions) time-series (A-TS) are time-series of episodes. Additionally, JTSA allows to consider also complex abstractions time-series (CA-TS) with pairs of episodes [147].

JTSA algorithms can be divided into two categories: preprocessing algorithms like filtering, smoothing, normalization, and interpolation, which work only on E-TS producing E-TS as the output, and TA algorithms, which can work on both E-TS and A-TS producing A-TS as the output [147]. TA algorithms can be further split into three subcategories, such as basic (including qualitative and trend), aggregation, and complex algorithms, which differ on the input data type and on the number of inputs, as shown in Table 3.4.

Table 3.4: Input and output of the Java Time Series Abstractor (JTSA) algorithms [147].

Algorithm	Input	Output
Preprocessing	E-TS	E-TS
Basic	E-TS	A-TS
Aggregation	A-TS	A-TS
Complex	Pair of A-TS	A-TS

E-TS: events time-series; A-TS: abstractions time-series; CA-TS: complex abstractions time-series.

Qualitative TAs map a series of events onto a sequence of qualitative time intervals, while trend TAs detect increasing, decreasing, or stationarity patterns. Aggregation TAs accept A-TSs as the input and combine successive episodes having the same pattern label, considering parameters like “minLen”, i.e. the minimum length for an episode to be included in the output A-TS, and the “gap”, i.e. the maximum distance for two consecutive episodes to be aggregated in a single episode. Finally, complex TAs work on pairs of A-TS associated through the relational operators based on the Allen’s relationships (and their corresponding inverse relationships) [148], as presented in Table 3.5.

Table 3.5: List of Allen’s relationships [148]; X and Y are times intervals.

Relation	Description	Graphical representation
Before	X ends before Y	<p>X start X end Y start Y end</p>
Equal	X and Y are the same time intervals	<p>X start = Y start X end = Y end</p>
Meets	X ends where Y starts	<p>X start X end = Y start Y end</p>
Overlaps	X starts before Y and Y starts before the end of X and X ends before the end of Y	<p>X start Y start X end Y end</p>
During	X is fully contained within Y	<p>Y start X start X end Y end</p>
Starts	X shares the same start as Y and ends before the end of Y	<p>X start = Y start X end Y end</p>
Finishes	X shares the same end as Y and starts after the start of Y	<p>Y start Y end = X start X end</p>

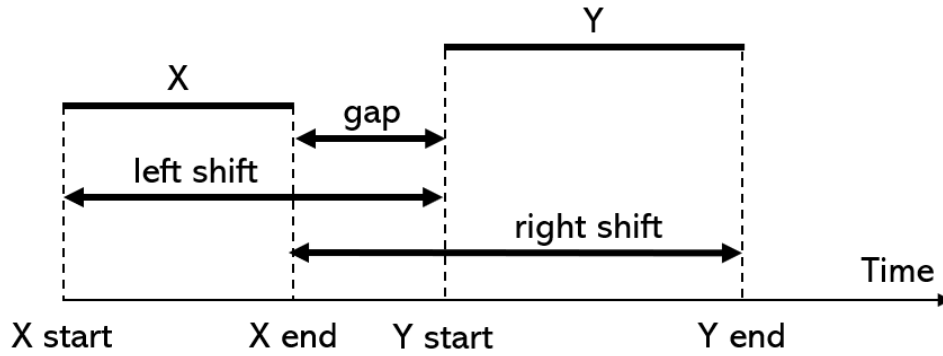


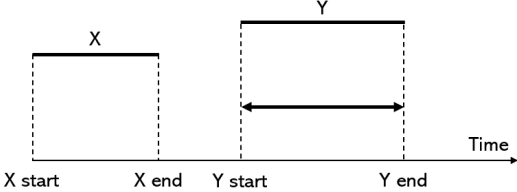
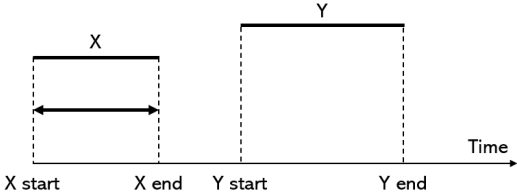
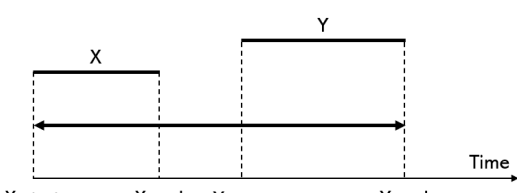
Figure 3.4: Parameters used to make the Allen's temporal relations more or less restrictive; X and Y are times intervals.

All the temporal patterns that use relational operators require the specification of one or more parameters to make the temporal relations more or less restrictive. As displayed in Figure 3.4, the “left shift” (LS) designates the maximum distance between the X-start point and the Y-start point, the right shift (RS) indicates the maximum distance between the X-end point and the Y-end point, while the “gap” reveals the maximum distance between the X-end point and the Y-start point.

In case of CA-TS, as shown in Table 3.6, complex TAs intervals in output are defined through the combiner operators, which specify how each pair of complex TAs intervals in input has to be processed, e.g., connecting the pair of time intervals with a union or an intersection.

Table 3.6: List of the combiners component provided by the Java Time Series Abstractor (JTSA) framework; X and Y are times intervals.

Combiner	Description	Graphical representation
Gap between starts	Time interval between the start of X and the start of Y	
Gap between ends	Time interval between the end of X and the end of Y	
Intersection	Time interval that X and Y share	

Longest	The longest time interval between X and Y	
Shortest	The shortest time interval between X and Y	
Union	Time interval including both X and Y, in addition to eventual intervals between them	

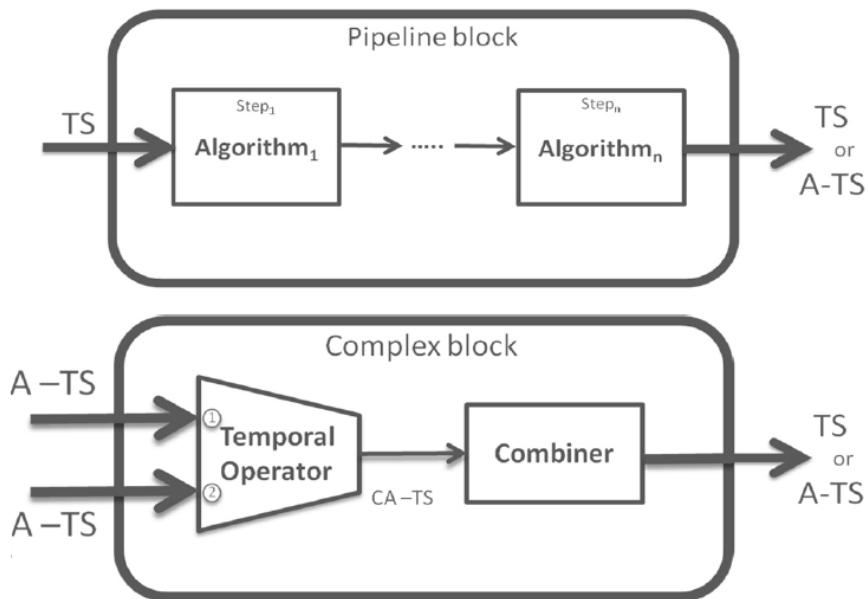


Figure 3.5: Pipeline and complex blocks used in Java Time Series Abstractor (JTSA) workflows [147].

Preprocessing and TA algorithms can be combined in user-defined workflows, which are extensible markup language (XML) documents made up of a set of blocks based on a JTSA-specific schema and executed by the JTSA engine. As illustrated in Figure 3.5, it is possible to distinguish between pipelines, which contain an ordered set of step components for implementing a single preprocessing, basic, or aggregation algorithm, and

complex blocks, which are used for obtaining complex TAs based on a single relational operator and combiner [147].

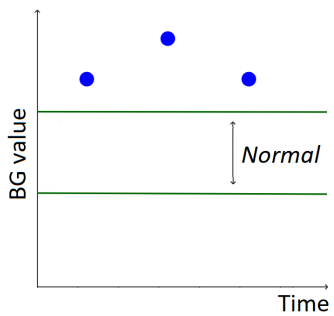
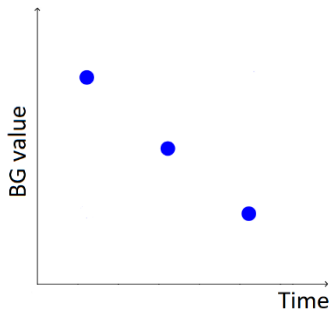
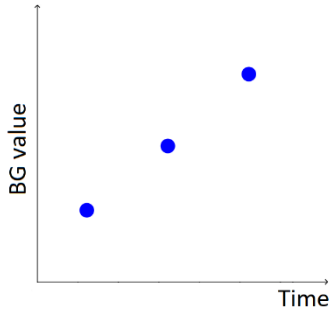
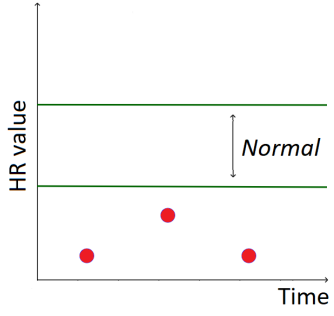
3.3.2. Domain-specific pattern detection

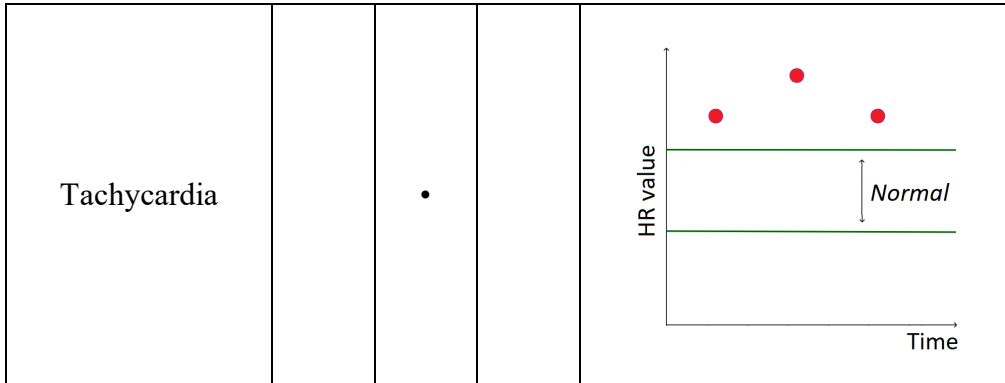
As a novel contribution in this thesis, several temporal patterns relevant for evaluating DM outcomes have been formalized in collaboration with the diabetologists of the Pediatric Endocrinology and Diabetology outpatient service of Fondazione IRCCS Policlinico San Matteo hospital, and the diabetologists of the Endocrinology and Diabetology outpatient service of the IRCCS Istituti Clinici Scientifici Maugeri.

Basic and aggregation TA algorithms were used to detect knowledge-based temporal patterns either considering all the BG monitoring data or contextualizing the search for glycemc patterns based on the Fitbit tag. Specifically, the suffix “S” was added to pattern labels when the search was restricted to sleep intervals, the suffix “W” was used when the search concerned only workout intervals, while the suffix “R” was adopted when the search excluded sleep and training periods. Moreover, the set of simple patterns was extended with the elaboration of univariate HR patterns. Table 3.7 presents an outline of the most relevant patterns based on basic and aggregation TA algorithms; in addition, all patterns and implementation details are provided in Appendix B.

Table 3.7: Some of the implemented patterns based on basic and aggregation temporal abstractions (TA) algorithms [127]. Red dots represent HR measurements, while blue dots represent BG measurements (normal glycemia refers to BG values between 70 mg/dL and 180 mg/dL).

Description	Input data			Graphical representation
	BG	HR	Sleep	
Hypoglycemia	•			

<p>Hyperglycemia</p>	<p>•</p>			 <p>The plot shows BG value on the y-axis and Time on the x-axis. Two horizontal green lines define a 'Normal' range. Three blue dots are plotted at different time points, all of which are above the upper green line, indicating hyperglycemia.</p>
<p>BG Decreasing</p>	<p>•</p>			 <p>The plot shows BG value on the y-axis and Time on the x-axis. Three blue dots are plotted at different time points, showing a clear downward trend in BG value over time.</p>
<p>BG Increasing</p>	<p>•</p>			 <p>The plot shows BG value on the y-axis and Time on the x-axis. Three blue dots are plotted at different time points, showing a clear upward trend in BG value over time.</p>
<p>Bradycardia</p>	<p>•</p>			 <p>The plot shows HR value on the y-axis and Time on the x-axis. Two horizontal green lines define a 'Normal' range. Three red dots are plotted at different time points, all of which are below the lower green line, indicating bradycardia.</p>



In a glucose monitoring application, Hypoglycemia and Hyperglycemia represent the core patterns. As a result of the integration between AID-GM platform and the JTSA library, it is possible to search such patterns considering either subject-specific or fixed thresholds (BG value <70 mg/dL for Hypoglycemia and BG value >180 mg/dL for Hyperglycemia). Figure 3.6 displays the pipeline block of the Hypoglycemia workflow that consists of a basic and an aggregation TA algorithm. As indicated also in the “type” and “subtype” parameters of the following XML code, the first step of the workflow is a basic qualitative algorithm, which discretizes the input events using a set of thresholds defined in the “qualitativeGlycemia” properties file. In this way, BG values lower than 70 mg/dL were labelled as “hypoglycemia” while BG values greater than 180 mg/dL as “hyperglycemia”, and all the other BG values were identified as “euglycemia” (in case of fixed thresholds). The second step of the workflow, instead, aggregates all the episodes with the “hypoglycemia” label which last at least 13 minutes ($\text{minLen}=13$), and whose distance is not greater than 60 minutes ($\text{gap}=60$), as specified in the “HighLevelAgg_Hypo” properties file. In this example, the search for hypoglycemic patterns is performed on all the available glucose data, but it is possible to restrict the analysis only to sleep, workout or routine periods modifying the “dataIn” parameter to “BGSleep”, “BGWorkout” or “BGRoutine”, with the definition of HypoglycemiaS, HypoglycemiaW, and HypoglycemiaR patterns, respectively.

Additionally, the hypoglycemic abstraction was further refined distinguishing between mild hypoglycemia (Hypoglycemia_Lev1: $54 \leq$ BG value <70 mg/dL) and severe hypoglycemia (Hypoglycemia_Lev2: BG value <54 mg/dL). Similarly, beyond the hyperglycemic abstraction, also mild hyperglycemic (Hyperglycemia_Lev1: $180 <$ BG value ≤ 250 mg/dL) and severe hyperglycemic (Hyperglycemia_Lev2: BG value >250 mg/dL) patterns were defined.

- Hypoglycemia.xml:

```

<workflow>
  <block>
    <pipeline id="Hypo" type="pipeline" note=""
      dataType="memory" dataIn="BG">
      <step order="1" title="hypo1"

```

```

        parameters="qualitativeGlycemia.properties"
        type="BASIC"
        subtype="BASIC_QUALITATIVE">
    </step>
    <step order="2" title="hypo2"
        parameters=" HighLevelAgg_Hypo.properties"
        type="AGGREGATION"
        subtype="AGGREGATION_HIGHLEVEL">
    </step>
</pipeline>
</block>
</workflow>

```

- qualitativeGlycemia.properties:

```

label=hypoglycemia,euglycemia,hyperglycemia
th=70,181

```

- HighLevelAgg_Hypo.properties:

```

gap=60
minLen=13
granularity=MINUTES
label=Hypoglycemia
levels=hypoglycemia

```

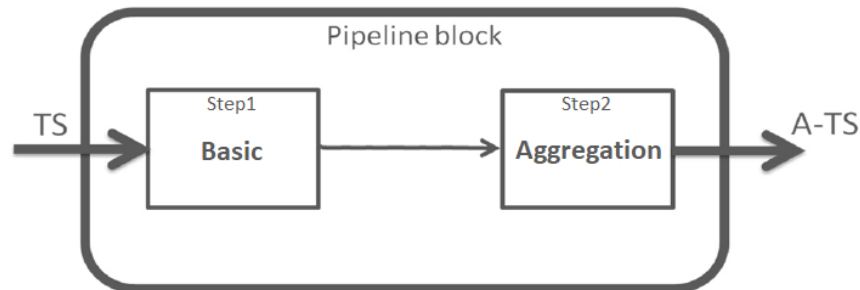
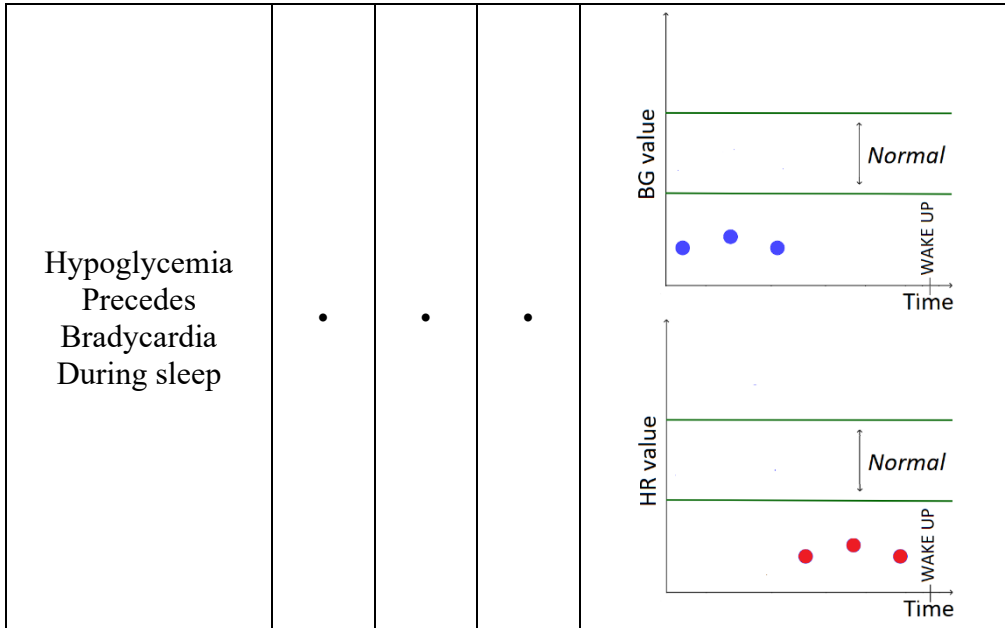


Figure 3.6: Pipeline block for hypoglycemia detection, based on basic and aggregation TA algorithms.

Furthermore, even complex TA were used to discover composite temporal patterns like the Dawn Effect, which refers to periodic episodes of hyperglycemia occurring in the early morning hours [149], as presented in Table 3.8. Additionally, multivariate patterns were explored combining BG, HR, and activity data, detecting for instance time intervals where Tachycardia precedes Hypoglycemia, or Hypoglycemia precedes Bradycardia during sleep periods; all the other complex patterns and their implementation details are provided in Appendix B.

Table 3.8: Some of the implemented patterns based on complex temporal abstractions (TA) algorithms [127]. Red dots represent HR measurements, while blue dots represent BG measurements (normal glycemia refers to BG values between 70 mg/dL and 180 mg/dL).

Description	Input data			Graphical representation
	BG	HR	Sleep	
Dawn Effect (Euglycemia at night followed by Hyperglycemia at wake up)	•		•	
Hypoglycemia Before Hyperglycemia	•			
Tachycardia Precedes Hypoglycemia (During sleep)	•	•	(•)	



3.3.3. Analysis of hypoglycemia episodes

Iatrogenic hypoglycemia is a limiting factor in DM management. Generally, a T1DM patient experiences a few episodes of symptomatic hypoglycemia per week but several episodes of asymptomatic hypoglycemia, which impair the physiologic defensive mechanism against subsequent hypoglycemia [9].

Thanks to the adoption of CGM systems, which allows detecting and investigating all hypoglycemic episodes, it was possible to provide clinicians with a qualitative and quantitative outline of each patient’s hypoglycemia situation. A summary table with the total number of hypoglycemic episodes was realized for every patient, distinguishing between severe and mild hypoglycemia, and contextualizing all the episodes within the day.

A particular attention, especially for the pediatric patients, was given to the analysis of hypoglycemia during sleep since it may be correlated with the “dead-in-bed” syndrome [10], [11], as discussed in Section 2.1.1, using the HypoglycemiaS, Hypoglycemia_Lev1S, and Hypoglycemia_Lev2S patterns. Also the profile tag was used to search for hypoglycemic patterns during sleep, considering the habitual bedtime and awakening-time for each patient, in order to make a comparison between the effective sleep periods as detected by the Fitbit trackers and those based on patients’ habits. Furthermore, HR time-series related to hypoglycemia during sleep were investigated for examining if there was a specific pattern that could improve the detection and prevention of such hypoglycemic episodes, considering children and adolescent, who were free of complications, since adult patients could have more evident HR alterations [150]. In the preprocessing phase, the first step consisted in a filter application to exclude all the sleep intervals that were preceded by hypoglycemic episodes in the previous two hours, since the succeeding BG and HR measurements could be altered. Consequently, only the HR measurements recorded in the remaining sleep

intervals were considered in the analysis. In addition, subjects with less than three overall hypoglycemia during sleep (HypoglycemiaS) patterns were excluded. For each remaining subject, three HR datasets were created: the before-hypoglycemia dataset included HR measurements recorded in the hour before HypoglycemiaS, the after-hypoglycemia dataset contained HR measurements collected in the hour after HypoglycemiaS, while the no-hypoglycemia dataset had HR measurements related to sleep intervals without hypoglycemic episodes, excluding the first hour after falling asleep and the last hour before waking up. Finally, HR measurements from each dataset were aggregated into separate five-minute time intervals to capture the average values [150].

For each subject, after a visual inspection through boxplots, the non-parametric Mann-Whitney U test was performed to compare both the before-hypoglycemia and no-hypoglycemia HR distributions, and the after-hypoglycemia and no-hypoglycemia HR distributions, using the function “wilcox.test” available in the R package called “stats” [151] and setting the significance threshold to 0.05.

3.4. Generalized deep learning models

A general glucose-prediction model built on a population of patients could be functional in real clinical scenarios, where the information for a new patient can be scarce at the beginning of the monitoring period. In our real-world scenario, given the considerable amount of time-series data from different sources, LSTMs were considered since they were particularly suitable for developing accurate multi-patient and multivariate models for glucose prediction.

LSTMs are a specific subclass of Recurrent Neural Network (RNN) introduced by Hochreiter and Schmidhuber [152] and designed for solving the vanishing or exploding gradients problems. First introduced by Bengio et al. [153] and further explored by Pascanu et al. [154], the exploding gradients problem during model training refers to a large increase of the long-term components, which grow exponentially more than short-term components, while the vanishing gradients problem concerns a significant decrease of the long-term components, which go exponentially fast to norm zero. Consequently, models can hardly learn correlation between temporally distant events. Instead, LSTMs can remember the previous data patterns over arbitrary time intervals, removing or adding information to a memory implemented as a cell state (C), without suffering from problems of long-term dependencies.

As illustrated in Figure 3.7, LSTM networks are characterized by a chain-like structure of repeating units, each one provided with three gates, such as the input layer, the output gate, and the forget layer, which regulate the flow of information into and out of the cell. Every gate is composed of a sigmoid layer that returns values in a [0-1] range, defining how much of each component should be let through, and an element-wise multiplication

operator. Figure 3.8 displays a zoom on a single conventional LSTM unit, showing that each block receives three inputs, such as the input at the current time step (X_t), the output from the previous unit (h_{t-1}), and the cell state of the previous unit (C_{t-1}), then updates the cell state of the current unit (C_t), and provides an output (h_t) [155], [156].

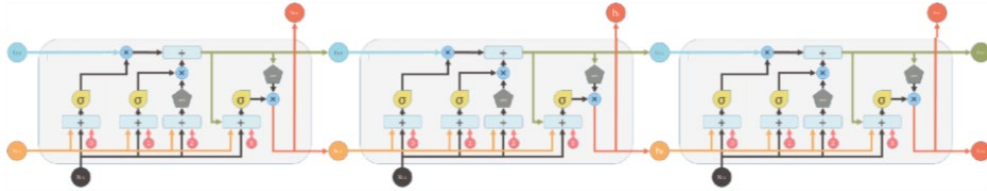


Figure 3.7: Sequential processing in Long Short-Term Memory (LSTM) neural networks, adapted from Yan [156].

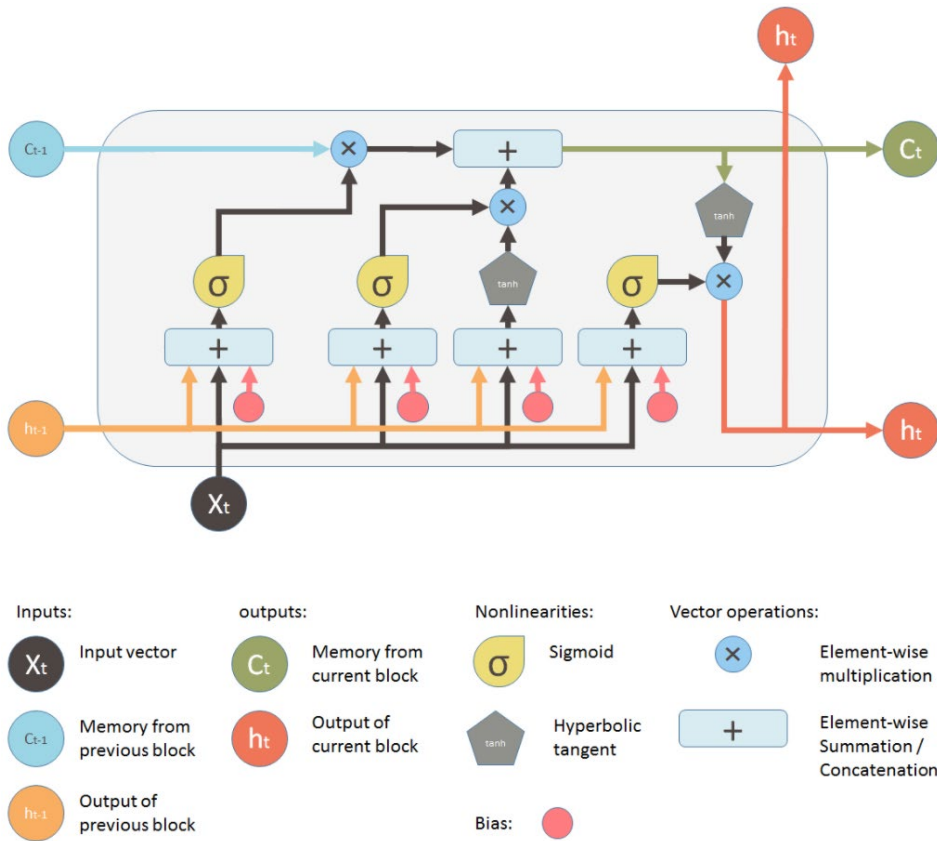


Figure 3.8: Schema of a Long Short-Term Memory (LSTM) neural network, adapted from Yan [156].

In the equations regarding the cell update process, W_q and U_q represent the weights matrices of the input and the recurrent connections, respectively, where the subscript q can be either referred to the input gate, the output gate, the forget gate or the cell state [152].

Considering the LSTM schema presented in Figure 3.8, the first sigmoid layer on the left corresponds to the so-called forget gate layer (f_t), which controls which information has to be eliminated from the cell state at step t . Indeed, based on the output of the previous unit and the input at the current time step, f_t provides a value ranging in the $[0-1]$ interval for all components in C_{t-1} , defined as:

$$f_t = \sigma(W_f \cdot X_t + U_f \cdot h_{t-1} + b_f)$$

Afterwards, new information can be stored in the cell state using two layers. The second sigmoid layer represents the so-called input gate layer (i_t) that decides the C_t components to update, while a vector of new cell candidates \tilde{C}_t is created through a hyperbolic tangent layer. Consequently, the cell state is updated multiplying the cell state of the previous unit by the forget gate vector, and adding the new cell candidates scaled by the input gate vector, according to the following equations:

$$i_t = \sigma(W_i \cdot X_t + U_i \cdot h_{t-1} + b_i)$$

$$\tilde{C}_t = \tanh(W_c \cdot X_t + U_c \cdot h_{t-1} + b_c)$$

$$C_t = f_t * C_{t-1} + i_t * \tilde{C}_t$$

Finally, the last sigmoid layer represents the so-called output gate layer (o_t), which determines the C_t components to return in output. The output vector is a filtered version of o_t , which is multiplied by C_t components pushed between -1 and 1 by the hyperbolic tangent layer, according to the following equations:

$$o_t = \sigma(W_o \cdot [h_{t-1}, X_t] + b_o)$$

$$h_t = o_t * \tanh(C_t)$$

All the analyses and graphical representations related to the development of deep learning models were performed using PyCharm version 2019.3 [157] as integrated development environment and the high-level NN application programming interface (API) Keras version 2.2.5 [158] with TensorFlow backend [159].

3.4.1. Time series preprocessing

The application of LSTMs to the specific problem of integrating BG monitoring data with Fitbit information is illustrated as a novel contribution of this work. Indeed, the Fitbit tracker and the FreeStyle Libre system provided readings with different sampling frequency, as introduced in Section 3.1: HR measurements are taken every minute, while BG measurements are recorded every 15 minutes, although it happened that the

time intervals between consecutive BG readings were slightly shorter or longer than the conventional sampling frequency.

Therefore, the first preprocessing step concerned the alignment of the HR time-series with the BG time-series. As shown in Figure 3.9, a weighted mean (*WeightHR*) was computed on the n HR measurements available in the interval $(t_{BG} - 1; t_{BG}]$ between two consecutive BG measurements, according to the following equation:

$$WeightHR = \frac{\sum_{i=1}^n HR_i \cdot w_i}{\sum_{i=1}^n w_i}$$

Increasing weights w were adopted so that the HR measurements closer to the corresponding BG measurement gave progressively higher contributions compared to the first HR measurements in the interval, similarly to the procedure adopted by FreeStyle Libre system, which measures interstitial glucose every minute and stores a weighted average value (using a proprietary algorithm) every 15 minutes. In case of a missing BG measurement, n is set to 14 and a weighted means is computed considering the HR measurements available in that time interval.

In addition, the corresponding Fitbit tag information was processed using a one-hot encoding strategy. Each Fitbit tag categorical value (sleep, workout, and routine) was converted into a new binary column with 1 or 0 values indicating the presence or the absence of that activity, respectively.

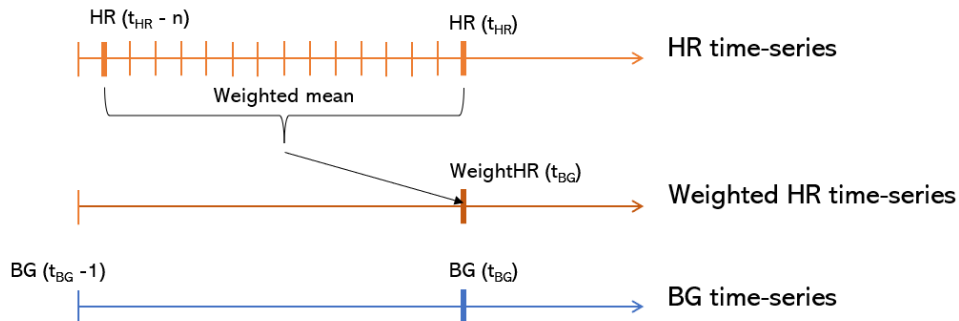


Figure 3.9: Preprocessing procedure for aligning heart-rate (HR: in orange) time-series to blood glucose (BG: in blue) time-series, computing a weighted mean (in dark orange) on the HR measurements between two consecutive BG measurements.

The second preprocessing step consisted in the missing data handling. BG and weighted HR time-series were split in subseries using frames of 96 timestamps (corresponding to 24 hours). The resulting subseries were discarded either if the percentage of missing data was greater than 20%, or if there were more than 8 consecutive missing values (corresponding to 2 hours). After the investigation of several interpolation algorithms, including linear, quadratic, spline, and cubic algorithms, the spline bidirectional

interpolation method was applied to deal with the remaining missing data for short gaps in BG and weighted HR time-series.

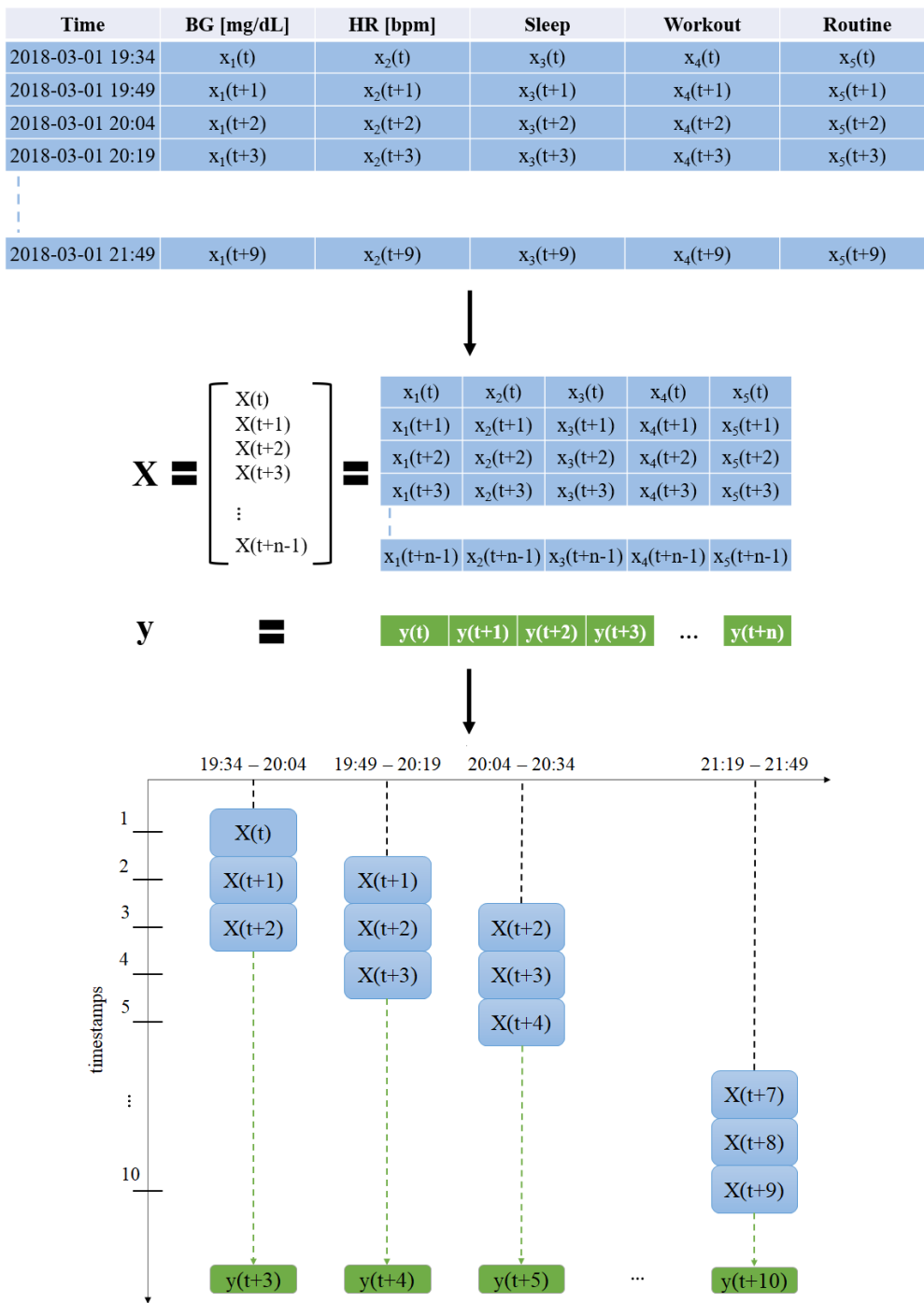


Figure 3.10: Preprocessing procedure for organizing data in a structure suitable for neural networks.

The last preprocessing step concerned the organization of time-series data in a structure suitable for deep learning, reframing the time-series forecasting task in a supervised learning problem. Past values are provided as features

and future values as labels, exploiting a sliding window of different lengths, such as 15, 30 and 45 minutes, for controlling the volume of historical value used for each prediction. As outlined in Figure 3.10, time-series data are exploded into a 2-D array of features called “X”, where the input data consist of overlapping lagged values at the desired number of timesteps, and a 1-D array of labels called “y”, containing the future values for each features row. The sliding window in the example has length=3, meaning that each sequence comprises 45 minutes of data at 15-minutes intervals and that $y(t)$, $y(t+1)$, $y(t+2)$ values at the beginning are excluded. Additionally, the resulting data matrix was reshaped using the “reshape” Python function in the “NumPy” library [160], since the NN input layer expected the input data in a specific 3D tensor format of sample size by lag time (sliding window length) by the number of input features.

3.4.2. Model infrastructure

The infrastructure of the proposed multi-patient and multivariate deep learning framework for short-term glucose prediction is presented in Figure 3.11. The input layer was designed to work in three different scenarios considering various features in input, such as:

- Univariate scenario with only BG time-series (sBG)
- Multivariate scenario with BG and HR time-series (sBG-HR)
- Multivariate scenario with a combination of BG, HR, and activities time-series (sBG-HR-Activity)

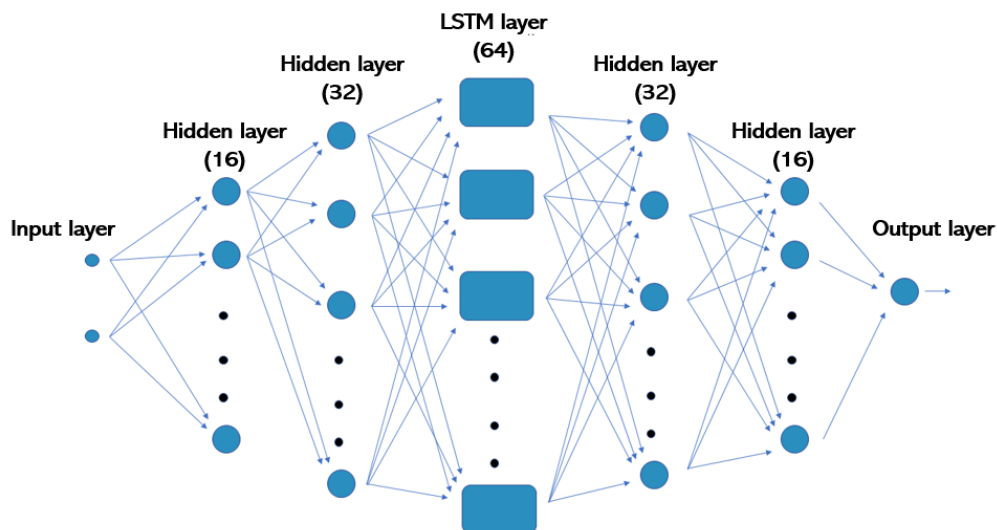


Figure 3.11: The architecture of the proposed Long-Short Term Memory (LSTM)-based neural network [161].

Besides the input layer, the architecture comprises other five intermediate layers and an output layer. The core of the model is represented by a LSTM layer with 64 units, surrounded by two hidden layers on the left with 16 and 32 neurons and two hidden layers on the right with 32 and 16 neurons, respectively.

A linear activation function was used in the output layer, while the hidden layers were characterized by a rectified linear unit (ReLU) activation function [162], which is defined as the positive part of its input argument and offers the advantages of an efficient computation, a better gradient propagation compared to sigmoidal activation functions, and a sparse activation, useful in a randomly initialized network since only about half of hidden units are activated [163]. Weight matrices and bias vectors, introduced in Section 3.4, were randomly initialized at the beginning of the training procedure, and then updated using the truncated Backward Propagation Through Time (BPTT) method [164].

Network hyperparameters were experimentally selected through a grid search. The Adam optimizer was adopted to minimize the Mean Absolute Error (MAE) as the loss function setting the learning rate, i.e. the step size at each iteration towards a minimum of the loss function, equal to 0.001 [165]. The number of epochs, i.e. the number of complete passes through the training dataset, was set to 250 to avoid underfitting, while the problem of overfitting was prevented by the use of the “EarlyStopping” [166], which is a Keras API callback for monitoring the performance of the model for every epoch on a validation set during the training, and for stopping the training when the monitored quantity, e.g. the loss function on the validation set (“val_loss”), has stopped improving. In particular, the “min_delta” parameter was set to 10^{-5} , meaning that an absolute change in the loss function of less than 10^{-5} was qualified as no improvement, the “patience” parameter was set to 50, meaning that with no improvements for more than 50 epochs the “model.stop_training” was marked as “true” and the training terminated, and the “restore_best_weights” was set to “true” for restoring model weights from the epoch with the best value of the monitored quantity. The batch size, i.e. the number of training samples to work through before the model’s internal parameters are updated, was set equal to the subseries length (96 points) less the lag time.

3.4.3. Model evaluation

The preprocessing procedure described in Section 3.4.1 was applied to the pediatric and adult datasets considering only those patients who simultaneously used the Fitbit tracker and the FreeStyle Libre system. The preprocessed pediatric dataset (consisting of 17 patients) was randomly divided into a training set of 12 patients, a validation set of one patient, and a test set of four patients, while the preprocessed adult dataset (consisting of ten patients) was randomly partitioned into a training set of eight patients, a validation set of one patient, and a test set of three patients. Additionally,

each feature in the training set was individually scaled in the [0-1] range using the “MinMaxScaler” function from the Scikit-learn Python library [157]. This process was repeated ten times varying the composition of training, validation, and test sets. At the end, an average of the prediction performances is computed for every scenario, both in analytical and clinical terms [161]. Moreover, multi-patient and multivariate models developed on the pediatric training sets were tested also on the adult test sets, considering the same adult patients used to test the adult models in each repetition. Similarly, models developed on the adult training sets were tested also on pediatric test sets for further examining the generalization capabilities.

The analytical assessment was realized through the RMSE, which is one of the most used evaluation metrics in literature, as evidenced in Section 2.2, and returns a quantitative measure of the prediction error on the same unit scale as the data, i.e. mg/dL. The RMSE is computed as the standard deviation of the residuals between the BG prediction \hat{y}_t and the corresponding BG actual value y_t , where T represents the time-series length:

$$RMSE = \sqrt{\sum_{t=1}^T \frac{(\hat{y}_t - y_t)^2}{T}}$$

Since RMSE does not provide any information about the consequences of prediction errors on treatments decisions, a clinical assessment through the Clarke Error Grid analysis (CEGA) was considered [167]. CEGA is a non-parametric graphical method to interpret the mapping between the BG reference measurements (on the x-axis) and the corresponding BG predictions (on the y-axis) in terms of severity of the potential harm caused by the prediction error.

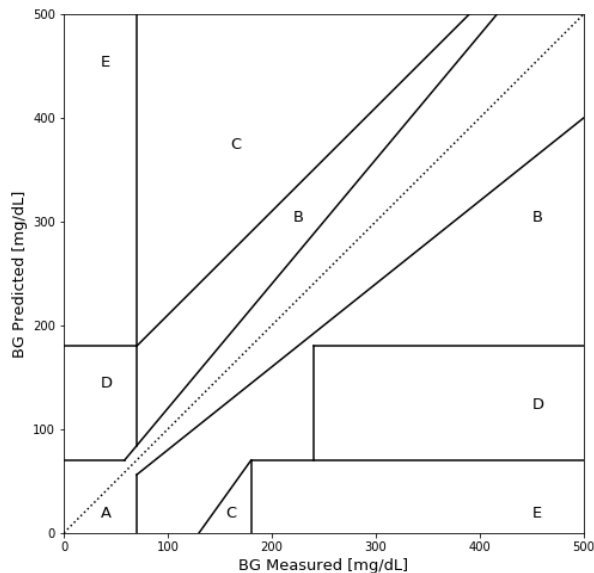


Figure 3.12: The Clarke Error Grid for clinically evaluating the accuracy of glucose predictions.

As shown in Figure 3.12, the grid is divided into five zones of accuracy, while the dotted diagonal line designates the perfect agreement between measured and predicted values. Points below the diagonal indicate an underestimation of the measured values, while points above the diagonal show an overestimation of the measured values. Specifically, zone A includes the area on both sides of the diagonal where the difference between measured and predicted BG values is less than 20%, leading to correct clinical decisions based on the prediction. In zone B, although this difference is greater than 20%, the resulting decision is at least clinically uncritical. Consequently, all the points that fall within zones A and B are clinically acceptable. In zone C, instead, BG prediction errors may prompt unnecessary corrections that could lead to a poor outcome, whereas in zone D the necessary corrections are not triggered, both in case of hypoglycemia and hyperglycemia. Prediction errors in zone E are the most dangerous because they lead to treat hypoglycemia instead of hyperglycemia and vice-versa [167].

Chapter 4

Applications on real-world data

This chapter presents the results obtained on the real-world described in Section 3.1. Section 4.1 outlines patients characteristics with descriptive statistics regarding the FreeStyle Libre glucose measurements and the Fitbit activity information. Section 4.2 involves glucose data analytics and shows the overall relationships observed between glycated hemoglobin and time in ranges, exploring also the inter-subject variability, and the significant correlations between self-monitoring frequency and glycemic metrics. Section 4.3 describes the temporal data mining results, analyzing the diabetes-specific patterns detection with a particular attention to the hypoglycemic episodes. Finally, Section 4.4 illustrates the outcomes of the multi-patient and multivariate deep learning model for glucose prediction on both the pediatric and the adult datasets.

4.1. Descriptive statistics on the datasets

Although monitored with the same procedures, the pediatric and adult datasets show some important differences. As outlined in Table 4.1, the adult dataset is characterized by a lower number of patients but longer time-series. Indeed, the average count of BG automatic measurements is twice the count of BG automatic measurements in the pediatric dataset, while the average number of BG manual measurements is comparable between the two datasets. In addition, the percentage of hypoglycemic events (<70 mg/dL) in the adult dataset is more than double the percentage of hyperglycemic events (>180 mg/dL) in the pediatric dataset, while the average percentage of hyperglycemic events in the pediatric dataset is greater than the adult dataset.

Figure 4.1 and Figure 4.2 graphically present the BG measurements that were automatically detected by the FreeStyle Libre system, while Figure 4.3 and Figure 4.4 show the BG measurements that were manually detected by each patient through the FreeStyle Libre reader, considering the pediatric

and adult datasets, respectively. Overall it is possible to notice that pediatric patients exhibit higher median values, in several cases also greater than 200 mg/dL, and a larger variability compared to adult patients, although there are a few exceptions like Patient 105 or Patient 108.

Table 4.1: Comparison between pediatric and adult datasets.

Measurements	Pediatric	Adult
Percentage of hypoglycemic events	3.47 ± 3.45	7.56 ± 3.47
Percentage of euglycemic events	41.80 ± 21.13	54.44 ± 10.79
Percentage of hyperglycemic events	54.76 ± 23.01	38.00 ± 13.21
Number of BG automatic measurements	$15,799.48 \pm 9,673.80$	$31,187.17 \pm 19,104.65$
Number of BG manual measurements	$2,016.74 \pm 1,584.84$	$2,809.33 \pm 1,948.52$
Number of HR measurements	$80,350.77 \pm 72,316.13$	$438,172.67 \pm 233,358.02$

BG: blood glucose; HR: heart rate. Hypoglycemic events: $BG < 70$ mg/dL; euglycemic events: $70 \text{ mg/dL} \leq BG \leq 180 \text{ mg/dL}$; hyperglycemic events: $BG > 180$ mg/dL.

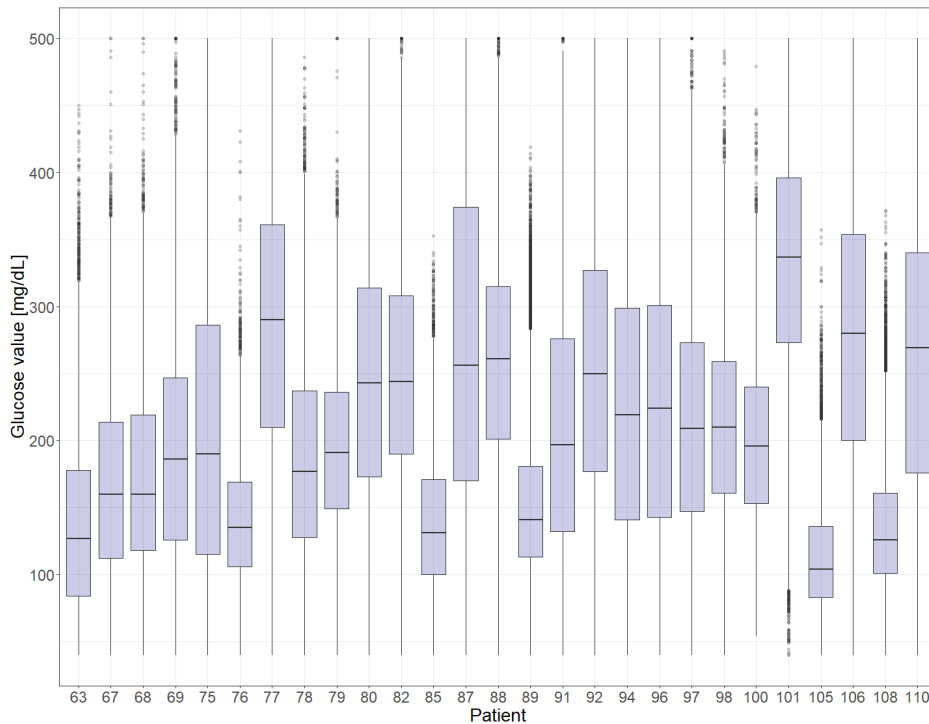


Figure 4.1: Boxplot representation of blood glucose (BG) automatic measurements per patient in the pediatric dataset.

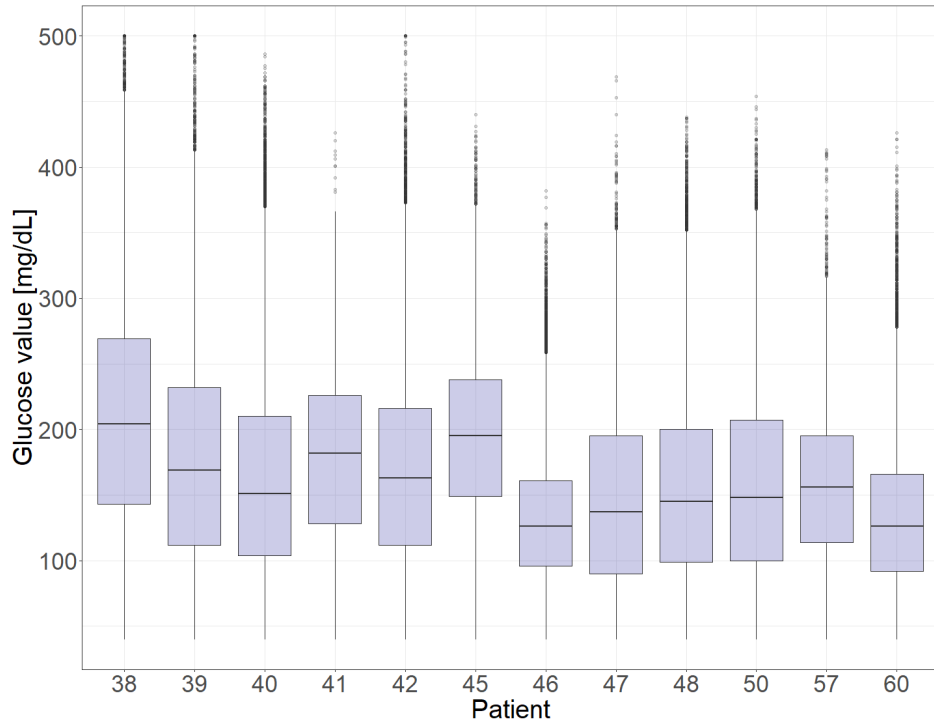


Figure 4.2: Boxplot representation of blood glucose (BG) automatic measurements per patient in the adult dataset.

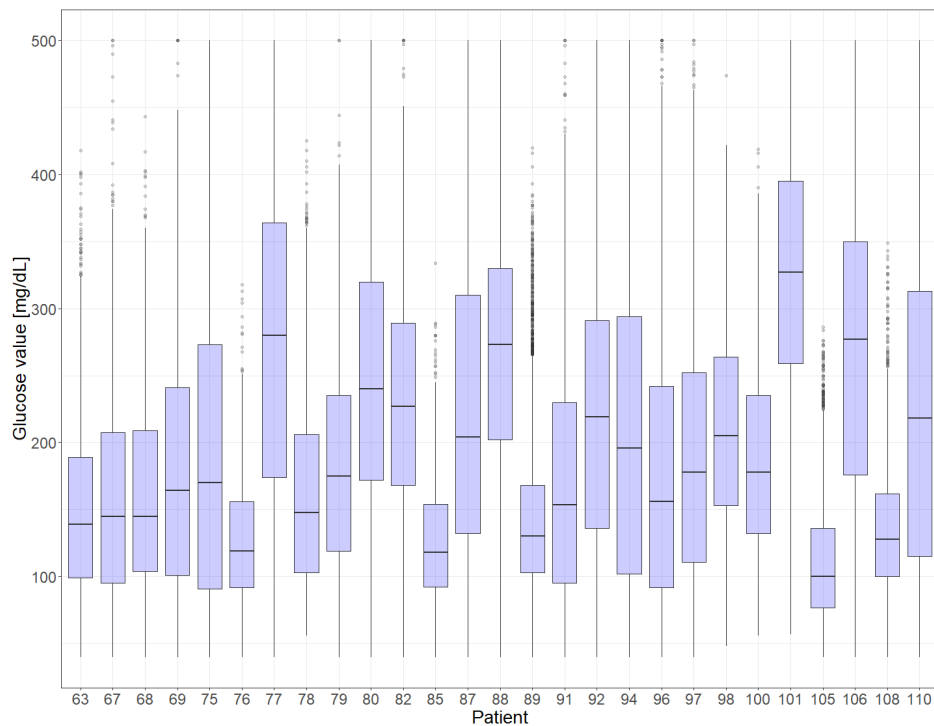


Figure 4.3: Boxplot representation of blood glucose (BG) manual measurements per patient in the pediatric dataset.

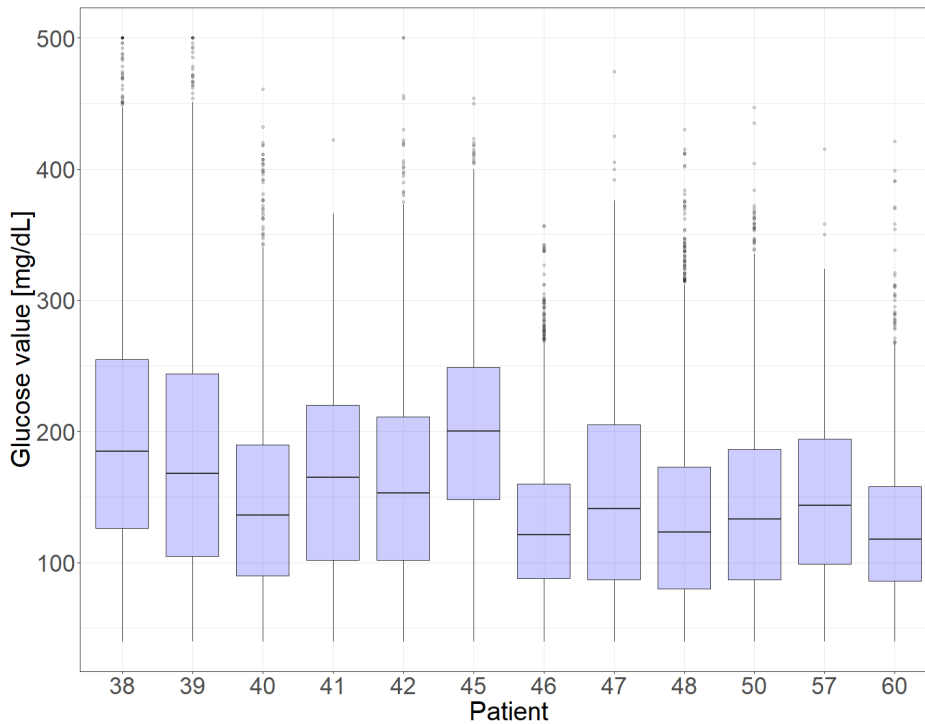


Figure 4.4: Boxplot representation of blood glucose (BG) manual measurements per patient in the adult dataset.

Going deep into manual scanning, Figure 4.5 and Figure 4.6 allow to understand when pediatric and adult patients mainly used the FreeStyle Libre reader during the day, revealing a higher variability in the behavior of children and adolescents. The day was discretized in four intervals, such as morning, afternoon, evening, and night, defined as in the following:

- $07:00:00 < \text{Morning} \leq 13:00:00$
- $13:00:00 < \text{Afternoon} \leq 18:00:00$
- $18:00:00 < \text{Evening} \leq 23:00:00$
- $23:00:00 < \text{Night} \leq 07:00:00$

Moreover, the stacked bar plots in Figure 4.7 and Figure 4.8 (part D) consent to understand in which condition each patient tended to increase the frequency of manual scans. Indeed, BG manual measurements are grouped based on the Fitbit tag, such as routine, sleep, and workout, and the distribution of the corresponding values is presented for each patient in the boxplots of part A, B, and C, respectively. In percentages, pediatric patients had more scans during sleep and workout intervals compared to adult patients, who concentrated BG manual measurements during routine activities. Other Fitbit information such as HR measurements distributions, daily activities, workouts per week, and sleep quality were used to provide clinicians with visual overviews of each patient's situation, as reported in Appendix C.

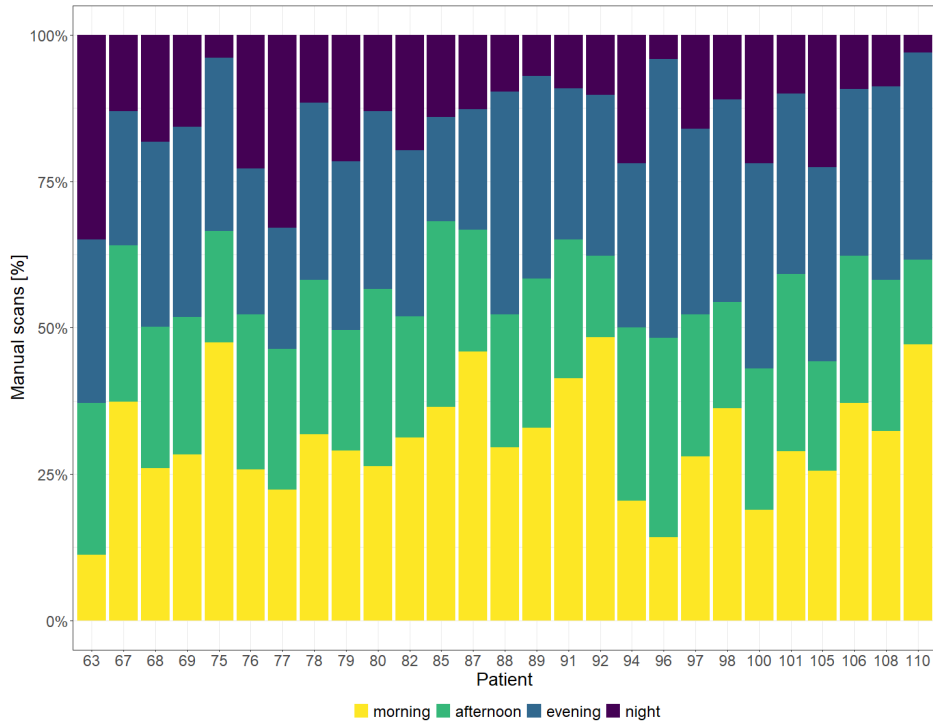


Figure 4.5: Stacked bar plot of manually detected blood glucose (BG) manual measurements grouped by daily period in the pediatric dataset.

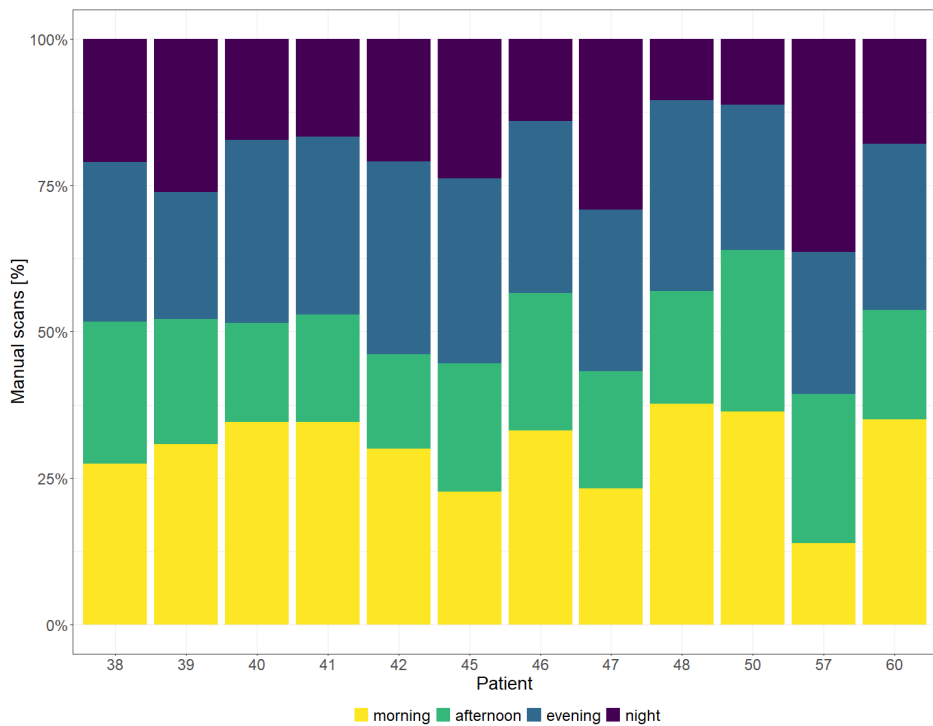


Figure 4.6: Stacked bar plot of manually detected blood glucose (BG) manual measurements grouped by daily period in the adult dataset.

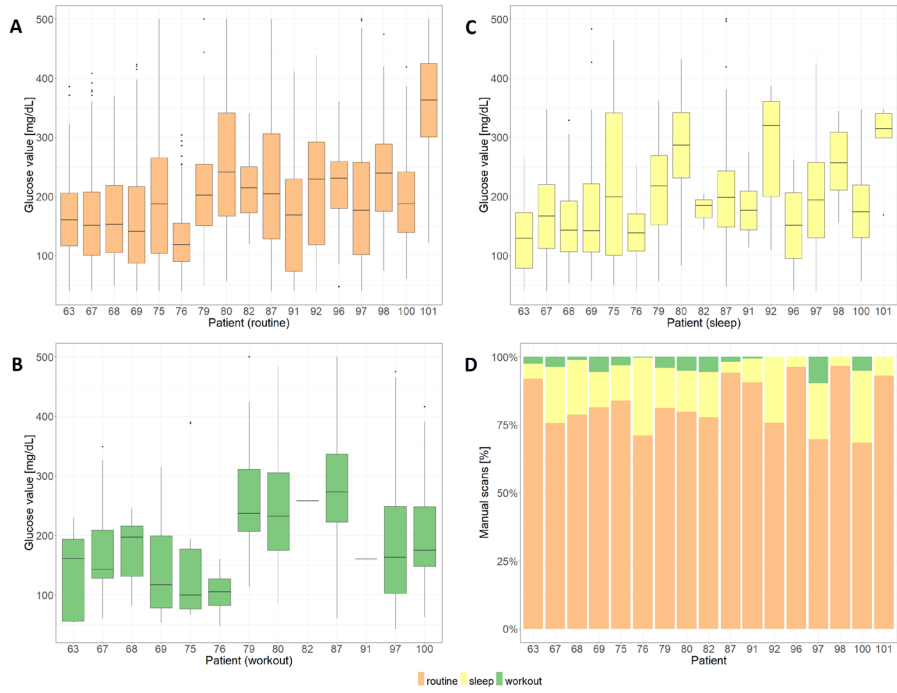


Figure 4.7: Manually detected blood glucose (BG) measurements grouped by Fitbit tag in the pediatric dataset: (A) boxplot of BG measurements in routine; (B) boxplot of BG measurements in sleep; (C) boxplot of BG measurements in workout; (D) stacked bar plot of manual scans per tag.

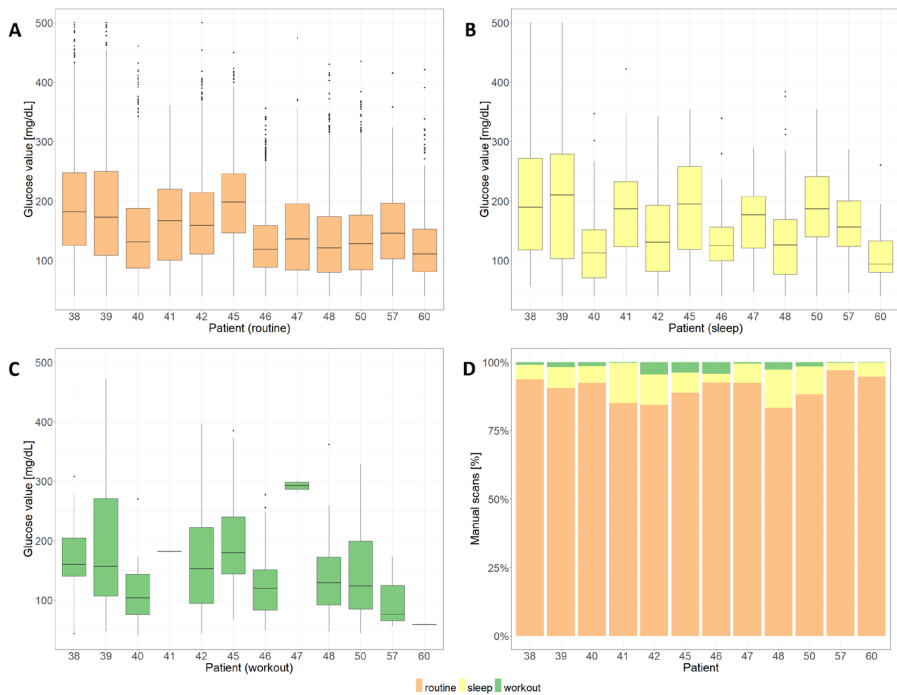


Figure 4.8: Manually detected blood glucose (BG) measurements grouped by Fitbit tag in the adult dataset: (A) boxplot of BG measurements in routine; (B) boxplot of BG measurements in sleep; (C) boxplot of BG measurements in workout; (D) stacked bar plot of manual scans per tag.

4.2. Glucose data analytics results

4.2.1. Glycated hemoglobin and time in ranges

Considering the pediatric dataset, four patients were discarded during the preprocessing phase for not meeting the 70%-data availability requirement with any window width, as shown in Table 4.2. Not surprisingly, the number of accepted windows and the number of considered patients decreased when the window width increased. Anyway, there was no significant difference (based on the results of a non-parametric Kruskal-Wallis test with significant threshold set to 0.05) between the median HbA1c values, which were 7.35, 7.30, and 7.25 in NGSP units, considering the accepted windows of 30, 60, and 90 days. Also the stacked bars in Figure 4.9 show that the average percent partition of time spent below, within, and above range was comparable in windows of 30, 60, and 90 days without statistically significant differences (based on the results of a Shapiro test with significant threshold set to 0.05).

Additionally, it is possible to notice that all median HbA1c values are higher than the recommended ISPAD target [21], as discussed in Section 2.1.2, and average TIR values, which resulted between 48.89% in 30-days windows and 54.02% in 90-days windows, are lower than the ATTD consensus recommendations [23], as described in Section 2.1.3.

Table 4.2: Number of monitoring windows with different widths in the pediatric dataset.

Windows width	Number of windows accepted	Number of windows discarded	Number of patients	HbA1c (%)
30 days	42	35	23	7.35 [6.93-8.48]
60 days	37	40	21	7.30 [6.90-8.50]
90 days	28	49	18	7.25 [6.85-8.10]

HbA1c: glycated hemoglobin in National Glycohemoglobin Standardization Program (NGSP) units, presented as median [1st quartile-3rd quartile].

After the preprocessing phase, time in ranges metrics were used to develop separate linear mixed model for HbA1c prediction. Table 4.3 presents the variables that resulted significant HbA1c predictors considering all window widths. Particularly, there was no significant relationship between TBR_Lev2 and HbA1c with any window widths, while TBR resulted a significant predictor only in the case of windows of 30 and 60 days ($R^2=0.89$).

The variance explained by each linear mixed models was always above 0.85 except for TAR_Lev2 in 90-days windows, characterized by a R^2 equal to 0.76. TIR and TIT showed a strong negative linear relationship with

HbA1c ($R^2>0.88$), while TAR and TAR_Lev2 revealed a positive linear relationship with HbA1c ($R^2>0.75$).

The Target column in Table 4.3 indicates the threshold values of each variable required for a safe glycemc control ($HbA1c \leq 7\%$), based on each linear mixed model using the overall estimated intercept, which is presented as fixed effect value \pm the random effect within-patient SD. Considering TIR and TIT, therefore, the target represents the minimum percentage of time spent within a specific range able to maintain $HbA1c \leq 7\%$, while for TAR and TAR_Lev2 the target is the maximum percentage of time spent above a specific range able to maintain $HbA1c \leq 7\%$.

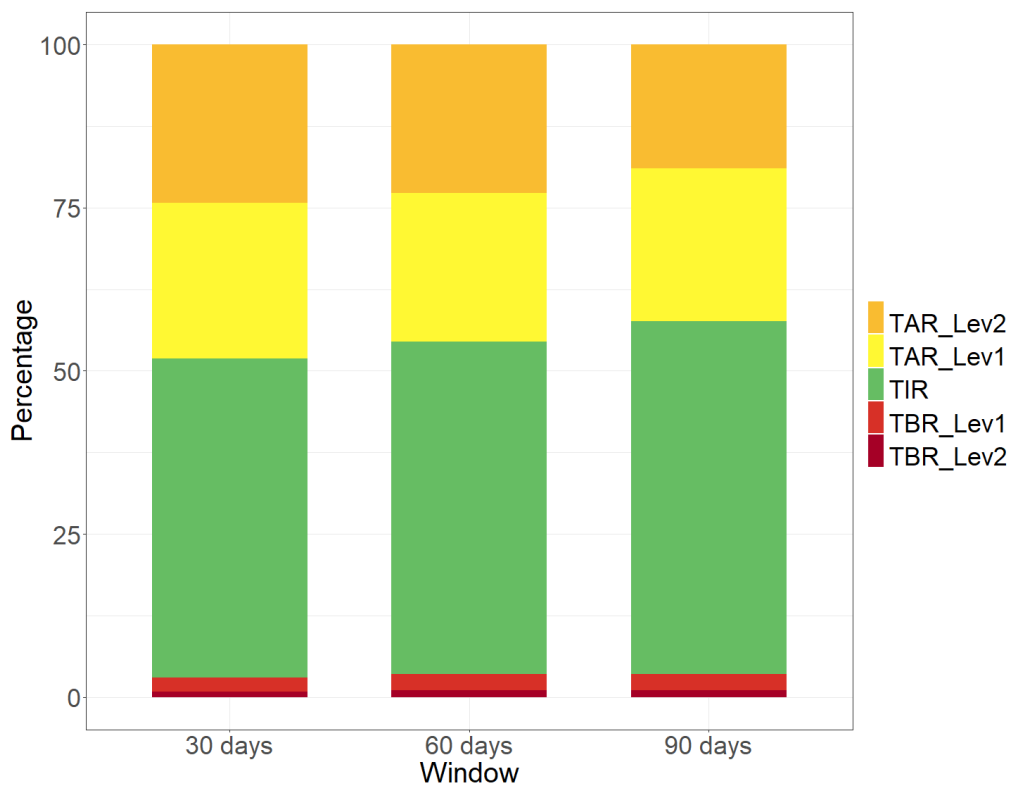


Figure 4.9: Stacked bar plot of average time in ranges using windows of 30, 60, and 90 days in the pediatric dataset. TAR_Lev2: Time severely Above Range; TAR_Lev1: Time slightly Above Range; TIR: Time in Range; TBR_Lev1: Time slightly Below Range, TBR_Lev2: Time severely Below Range.

Table 4.3: Separate linear mixed model predictor variables with different window widths in the pediatric dataset. Predictor coefficients are presented as value (lower 95% confidence limit; upper 95% confidence limit) while intercept coefficients are presented as fixed effect value \pm random effect within-patient standard deviation.

Windows width	Predictor		Intercept	R ²	Target
	Variable	Coefficient			
30 days	TIR	-0.0482 (-0.0598; -0.0366)	10.1678 \pm 0.5413	0.90	65.72%
	TIT	-0.0500 (-0.0653; -0.0348)	9.4176 \pm 0.6927	0.89	48.27%
	TAR	+0.0449 (0.0340; 0.0558)	5.6673 \pm 0.5572	0.90	29.68%
	TAR_Lev2	+0.0522 (+0.0414; +0.0631)	6.5325 \pm 0.4171	0.87	8.95%
60 days	TIR	-0.0591 (-0.0708; -0.0475)	10.6973 \pm 0.4726	0.95	62.52%
	TIT	-0.0650 (-0.0801; -0.0499)	9.8788 \pm 0.5828	0.94	44.30%
	TAR	+0.0549 (+0.0439; +0.0659)	5.2025 \pm 0.4921	0.95	32.76%
	TAR_Lev2	+0.0561 (+0.0443; +0.0679)	6.4403 \pm 0.4097	0.89	9.98%
90 days	TIR	-0.0598 (-0.0734; -0.0463)	10.7226 \pm 0.3894	0.92	62.24%
	TIT	-0.0641 (-0.0811; -0.0471)	9.7751 \pm 0.4961	0.91	43.29%
	TAR	+0.0544 (+0.0418; +0.0671)	5.2163 \pm 0.3608	0.89	32.78%
	TAR_Lev2	+0.0650 (+0.0491; +0.0809)	6.2934 \pm 0.7015	0.76	10.87%

TIR: Time in Range; TIT: Time in Target Range; TAR_Lev2: Time severely Above Range; SD: standard deviation.

Random intercepts estimated for each patient, taking into account the relationship between HbA1c and TIR in 30-days windows, are presented in Table 4.4. In this case, TIR targets are subject-specific and represent the minimum percentage of time spent in the euglycemic range required for a safe glycemic control. Instead, Figure 4.10 illustrates the negative relationship between TIR and HbA1c adopting the overall estimated intercept to draw the regression line, defined as:

$$HbA1c = 10.1678 - 0.0482 \cdot TIR$$

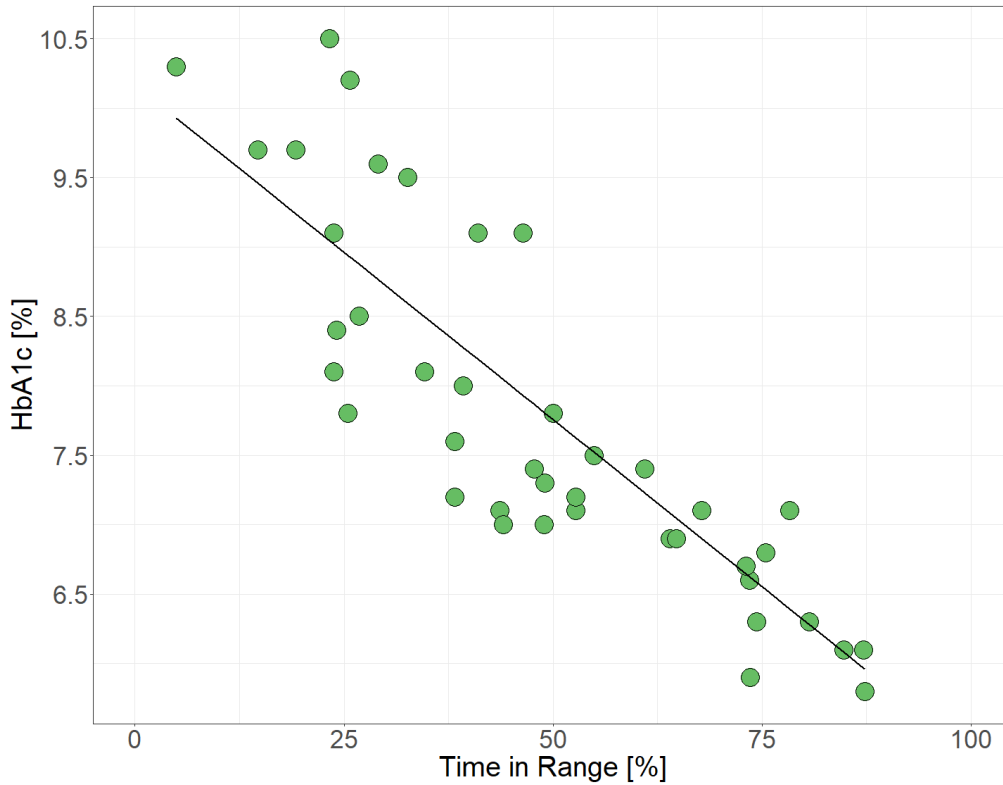


Figure 4.10: Linear relationship between glycated hemoglobin (HbA1c) and Time in Range using the overall estimated intercept with 30-days windows in the adult dataset. HbA1c is expressed in National Glycohemoglobin Standardization Program (NGSP) units.

Table 4.4: Estimated random intercepts and corresponding Time in Range (TIR) target values for maintaining glycated hemoglobin (HbA1c) $\leq 7\%$ in National Glycohemoglobin Standardization Program (NGSP) units, using 30-days windows in the pediatric dataset.

Patient	Average HbA1c	Average TIR	Intercept	TIR target
69	7.25	42.70	9.4129	50.06
79	7.40	41.41	9.5164	52.20
98	8.10	23.77	9.5749	53.42
78	7.10	48.40	9.5926	53.79
67	7.30	49.03	9.8435	58.99
63	7.00	58.38	9.8911	59.98
80	8.50	26.77	9.9252	60.69
75	8.00	39.24	9.9902	62.03
76	6.35	74.51	9.9909	62.05
68	7.20	59.81	10.1016	64.35
108	6.23	80.72	10.1309	64.95
94	8.67	30.48	10.1409	65.16

105	6.10	84.76	10.1793	65.96
91	7.80	50.00	10.1950	66.28
88	9.40	19.24	10.2927	68.31
85	7.10	67.83	10.2976	68.41
89	6.72	74.64	10.3030	68.52
101	10.30	4.94	10.4060	70.66
82	9.70	19.27	10.4644	71.87
110	9.60	29.06	10.7034	76.83
97	9.10	41.01	10.7522	77.84
100	9.10	46.42	10.9199	81.32
87	10.35	24.51	11.2353	87.86

Also in the adult dataset two patients were discarded during the preprocessing phase for not meeting the 70%-data availability requirement with any window width, as shown in Table 4.5. Anyway, when considering long monitoring windows, the number of accepted windows remained almost the same and the number of patients with valid data did not change. Consequently, there was no significant difference (based on the results of a non-parametric Kruskal-Wallis test with significant threshold set to 0.05) between the median HbA1c values using different windows widths. As displayed in Figure 4.11, there was no significant difference (based on the results of a Shapiro test with significant threshold set to 0.05) even in the average percent partition of time spent below, within, and above range in windows of 30, 60, and 90 days.

In terms of glycemic control monitoring, median HbA1c values are higher than the ADA recommendations [5], as discussed in Section 2.1.2, and average TIR values, which resulted between 54.59% in 30-days windows and 56.20% in 90-days windows, are lower than the ATTD consensus recommendations explained in Section 2.1.3 [23], although more elevated than those found in the pediatric dataset.

Table 4.5: Number of monitoring windows with different widths in the adult dataset.

Windows width	Number of windows accepted	Number of windows discarded	Number of patients	HbA1c (%)
30 days	23	18	10	7.50 [7.00-7.87]
60 days	22	19	10	7.60 [7.10-7.95]
90 days	21	20	10	7.50 [7.10-7.73]

HbA1c: glycated hemoglobin in National Glycohemoglobin Standardization Program (NGSP) units, presented as median [1st quartile-3rd quartile].

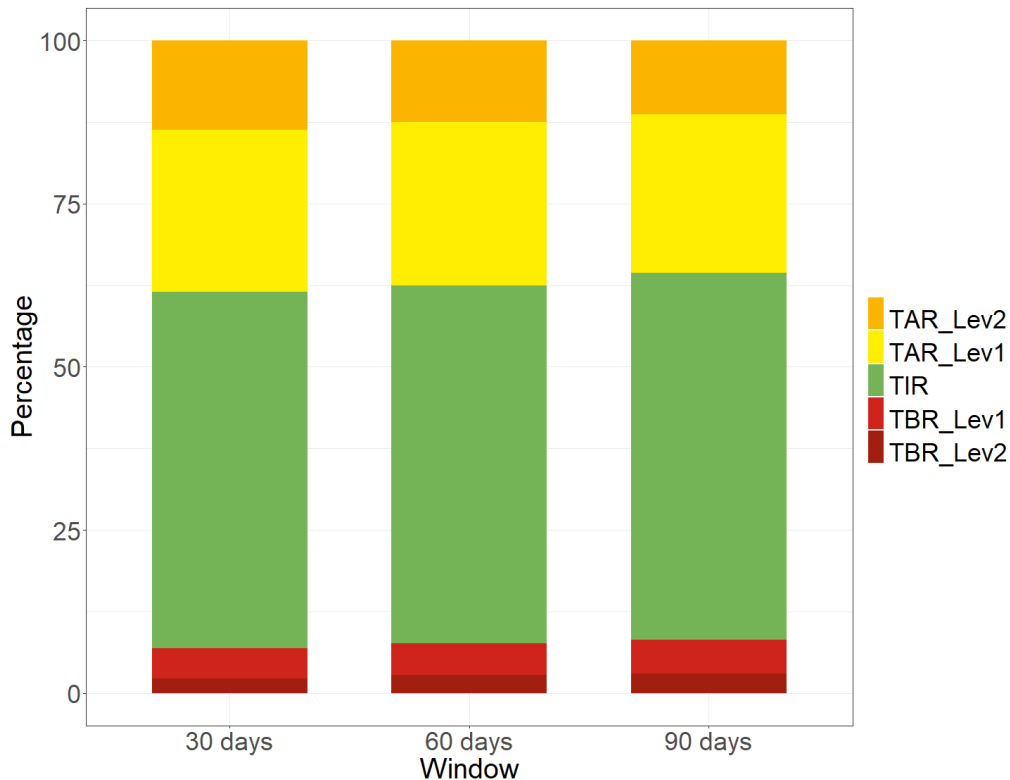


Figure 4.11: Stacked bar plot of average time in ranges using windows of 30, 60, and 90 days in the adult dataset. TAR_Lev2: Time severely Above Range; TAR_Lev1: Time slightly Above Range; TIR: Time in Range; TBR_Lev1: Time slightly Below Range, TBR_Lev2: Time severely Below Range.

Time in ranges metrics that resulted significant HbA1c predictors with all windows widths are presented in Table 4.6. As observed in the pediatric analysis, TIR and TIT showed a negative linear relationship with HbA1c, while TAR had a positive linear relationship with HbA1c, although in 30-days and 60-days windows the variance explained by these linear mixed models was not elevated. Moreover, TBR resulted a significant predictor only in the case of windows of 30 and 60 days ($R^2= 0.78$ and $R^2= 0.81$, respectively).

Anyway, it is possible to also underline some distinctions compared to the pediatric dataset. In particular, there was a significant relationship between TAR_Lev2 and HbA1c only in 30-days and 90-days windows with a modest variance explained by each model ($R^2=0.38$ and $R^2=0.63$, respectively). In addition, TBR_Lev2 resulted a significant HbA1c predictor in the case of 60-days windows ($R^2=0.74$).

Table 4.6: Separate linear mixed model predictor variables with different window widths in the adult dataset. Predictor coefficients are presented as value (lower 95% confidence limit; upper 95% confidence limit) while intercept coefficients are presented as fixed effect value \pm random effect within-patient standard deviation.

Windows width	Predictor		Intercept	R ²	Target
	Variable	Coefficient			
30 days	TIR	-0.0323 (-0.0535; -0.0110)	9.2778 \pm 0.2900	0.6102	70.58%
	TIT	-0.0423 (-0.0681; -0.0165)	8.9844 \pm 0.3208	0.6888	46.93%
	TAR	+0.0252 (+0.0080; +0.0424)	6.5426 \pm 0.2915	0.5834	18.18%
60 days	TIR	-0.0297 (-0.0543; -0.0050)	9.1760 \pm 0.3381	0.5894	73.38%
	TIT	-0.0381 (-0.0654; -0.0107)	8.8666 \pm 0.3612	0.6730	49.04%
	TAR	+0.0260 (+0.0073; +0.0446)	6.5756 \pm 0.3877	0.6951	16.36%
90 days	TIR	-0.0364 (-0.0628; -0.0100)	9.5426 \pm 0.4011	0.7416	69.89%
	TIT	-0.0434 (-0.0712; -0.0156)	9.0352 \pm 0.4388	0.8062	46.92%
	TAR	0.0319 (0.0126; 0.0512)	6.3479 \pm 0.4616	0.8291	20.45%

Table 4.7: Estimated random intercepts and corresponding Time in Range (TIR) target values for maintaining glycated hemoglobin (HbA1c) \leq 7% in National Glycohemoglobin Standardization Program (NGSP) units, using 30-days windows in the adult dataset.

Patient	Average HbA1c	Average TIR	Intercept	TIR target
42	7.18	49.68	8.9097	59.17
60	6.60	67.89	9.0986	65.02
48	7.36	54.10	9.1499	66.61
39	7.73	45.53	9.2490	69.68
45	7.85	43.61	9.2669	70.24
57	7.30	61.64	9.2821	70.71
46	6.88	77.58	9.3453	72.67
38	8.30	38.34	9.3735	73.54
40	8.00	50.93	9.5107	77.79
50	8.50	50.59	9.5928	80.34

Considering the relationship between HbA1c and TIR, Table 4.7 reports the random intercepts estimated for each patient in 30-days windows, while Figure 4.12 displays the negative relationship between TIR and HbA1c

adopting the overall estimated intercept to draw the regression line, defined as:

$$HbA1c = 9.2778 - 0.0323 \cdot TIR$$

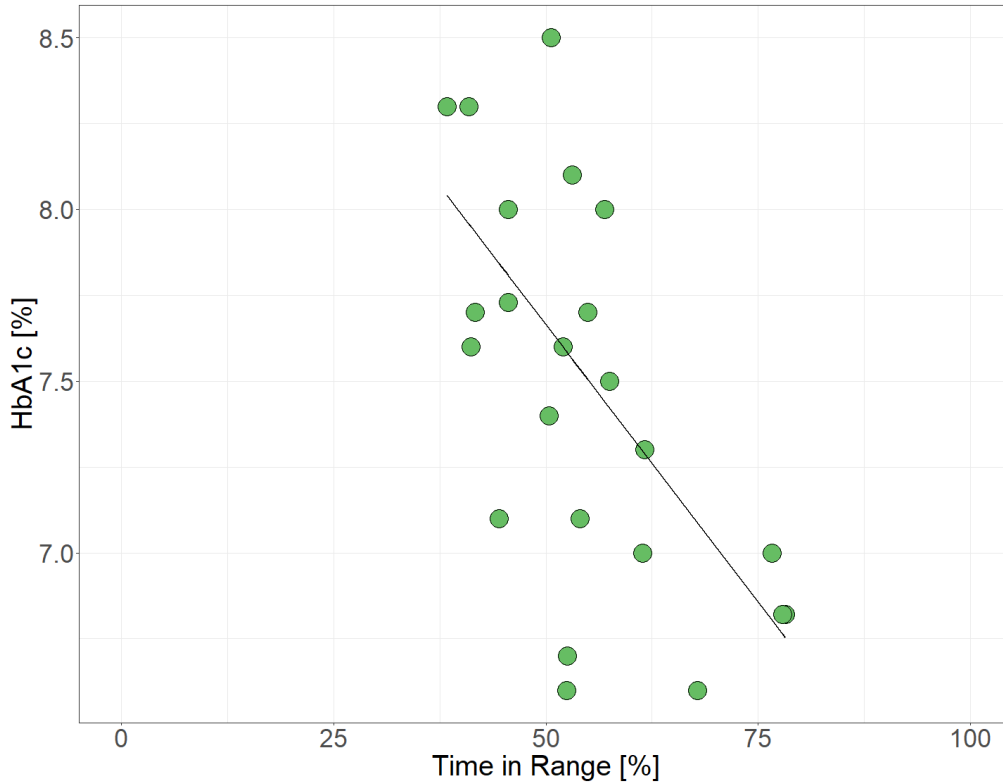


Figure 4.12: Linear relationship between glyated hemoglobin (HbA1c) and Time in Range using the overall estimated intercept with 30-days windows in the adult dataset. HbA1c is expressed in National Glycohemoglobin Standardization Program (NGSP) units.

The results obtained with windows of 30, 60, and 90 days, both in the pediatric and adult datasets as reported in Table 4.3 and Table 4.6, confirmed the relationship between HbA1c and time in ranges metrics. The targets found in our study using the overall intercepts estimated through LME models are comparable with the ATTD consensus recommendations for a safe glyceamic control [23], i.e. TIR >70%, TAR <25%, and TAR_Lev2 <10%. In addition, these findings are consistent even with other studies in literature. Beck et al. [93] analyzed through linear regression models the relationship between HbA1c and glyceamic metrics in T1DM adult patients across four RCT. Based on data at the beginning of the study, targets for a safe glyceamic control were set at 70% for TIR, at 46.73% for TIT, and at 24.89% for TAR, but based on data at the end of the study these targets were set at 64.63, 42.56, and 30%, which are almost similar to the targets identified in the pediatric dataset. Vigersky and McMahon [94] selected

paired HbA1c and TIR values from 18 studies, considering T1DM or T2DM patients, and they concluded that the TIR target should be set around 65%.

Furthermore, the proposed approach allows also investigating the question of individualized glycemic targets to meet the needs of each DM subject, as advised in the ATTD consensus report [23]. Consistently with a recent study on T1DM pediatric patients by Piona et al. [168], which reported that a four-week period is the optimal sampling window for reflecting a long-term glycemic control with CGM data, 30-days windows were used for exploring the inter-subject variability and identifying individualized CGM targets. This direction is suggested even by the JDRF CGM Study Group [54], which found that a substantial individual variability exists in the relationship between average glucose and HbA1c, and by Bergenstal et al. [169], who pointed out that people with the same average glucose could have different HbA1c value.

In Table 4.4 Table 4.7 it possible to observe a high variability between each patient's random effect with a more evident difference in the pediatric dataset compared to the adult dataset, since the patient-specific intercepts ranged in the interval [9.4129-11.2353] and in the interval [8.9097-9.5928], respectively. The differences between intercepts might be related to the individual biological variation in erythrocyte survival or glycation rates, as hypothesized by both the JDRF CGM Study Group [54] and Bergenstal. [169], although further studies on longer monitoring periods are needed to confirm this hypothesis. Such variability is reflected in the wide range of estimated TIR targets, which ranged in the interval [50.06 - 87.86] for pediatric patients and in the interval [59.17-80.34] for adult patients. Accordingly, some patients could maintain a lower TIR to preserve a safe glycemic control, while other patients need to stay in the range for a longer period to keep HbA1c $\leq 7\%$. This conclusion may be influenced by the difference between long-term average glucose from HbA1c and short-term average glucose during CGM [170], emphasizing the importance of individualized diabetes management also using the CGM-derived glycemic metrics, particularly in patients with suboptimally controlled DM [135].

4.2.2. Self-monitoring frequency and glycemic metrics

In the pediatric dataset, after the division of glucose data in 526 monitoring windows of 14-days, 218 windows were discarded because they contained less than 480 automatically stored readings. The 308 accepted windows were rank ordered by daily scan frequency, computed as the sum of the manual scans divided by the window length, and split into ten groups based on deciles. Within each group, which comprised 31 windows (except for the two highest groups that included 30 windows), average values of daily scan frequency and TIR were computed, as shown in Table 4.8.

Figure 4.13 allows a visual inspection of the relationship between daily scan frequency and TIR average values. The significant positive correlation (p -value <0.02) is confirmed through the Spearman coefficient computation,

with $\rho=0.75$. Based on the results of the non-parametric Dunn's test, the average TIR value in the highest scan frequency group was significantly different ($p\text{-value} < 10^{-3}$) from the average TIR in all but the ninth group. Indeed, average TIR decreased from 58.85% in the in the highest scan frequency group (30.02 scans/day) to 22.68% in the lowest scan frequency group (2.88 scans/day).

Table 4.8: Daily scan frequency and Time in Range (TIR) average values \pm standard deviation for each group, based on the daily scan frequency ranking in the pediatric dataset.

Group	Daily scan frequency	TIR
1	2.88 \pm 0.72	22.68 \pm 16.14
2	4.62 \pm 0.39	30.50 \pm 22.81
3	6.05 \pm 0.34	43.63 \pm 23.95
4	6.83 \pm 0.23	47.50 \pm 23.67
5	7.97 \pm 0.48	47.52 \pm 22.51
6	9.31 \pm 0.41	51.46 \pm 18.07
7	11.34 \pm 0.72	44.34 \pm 16.16
8	15.44 \pm 1.66	42.34 \pm 22.08
9	20.63 \pm 1.22	55.67 \pm 15.05
10	30.02 \pm 5.91	58.85 \pm 23.50

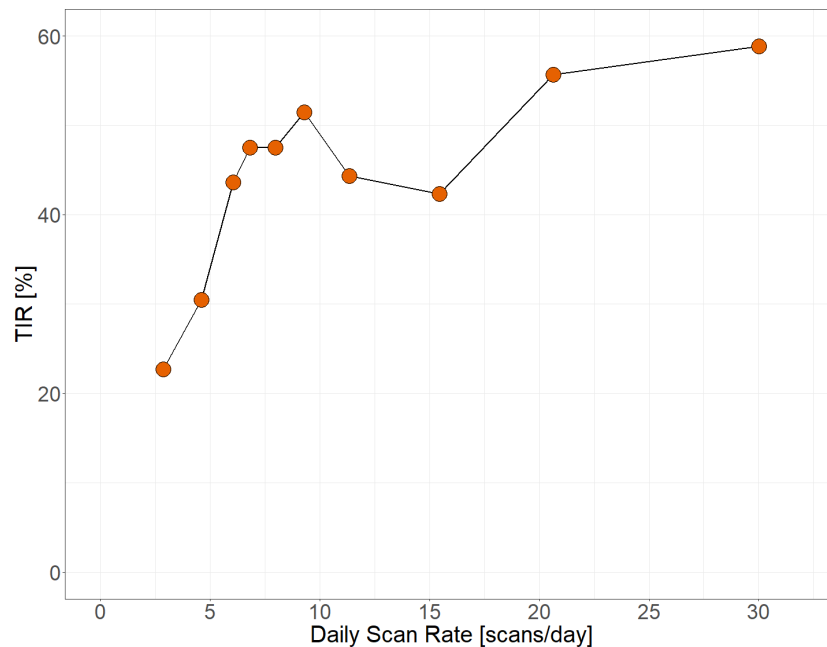


Figure 4.13: Scatter plot of daily scan frequency and Time in Range (TIR) average values, based on the daily scan frequency ranking in the pediatric dataset.

Afterwards, the 308 accepted windows were ranked ordered also by SD, CONGA_1 , and ADRR in separate analyses and split into ten groups based on deciles. Similarly, average values of TIR and the corresponding ranking variable were computed in every group. According to Dunn's tests, TIR resulted significantly higher in groups with the lowest variability, and a strong negative correlation ($p\text{-value} < 10^{-5}$) was found between each of the selected glycemic metrics, as illustrated in Figure 4.14. In particular, ρ was equal to -0.98 considering SD and equal to -0.99 considering CONGA_1 and ADRR.

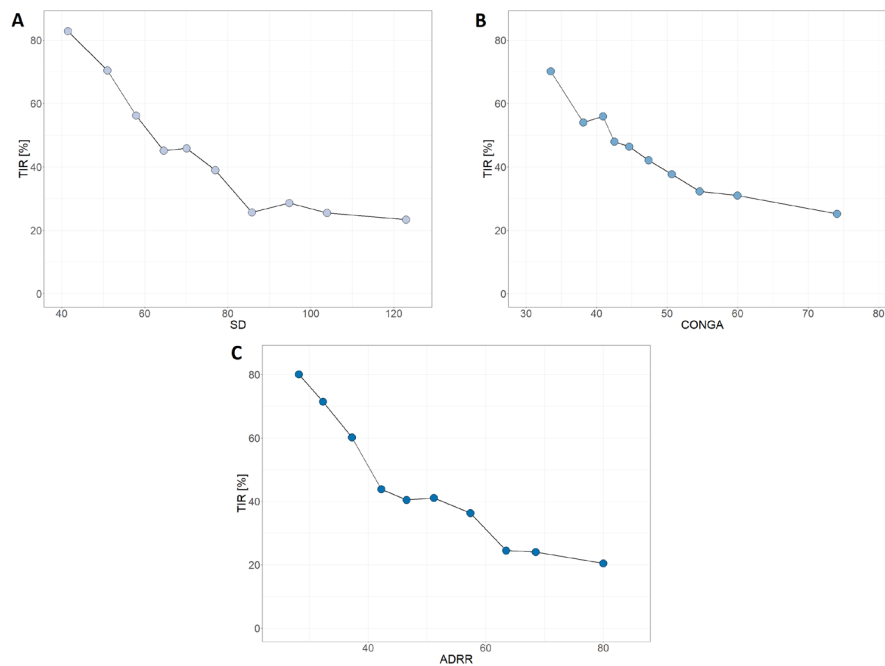


Figure 4.14: Scatter plots of average values of Time in Range (TIR) and Standard Deviations (SD) in part A, TIR and Continuous Overlapping Net Glycemic Action at 1-hour (CONGA_1) in part B, and of TIR and Average Daily Risk Range (ADRR) in part C, based on the respective ranking variable in the pediatric dataset.

Therefore, a high daily scan frequency through the FreeStyle Libre system and a reduction in glycemic variability are associated with high time spent in the euglycemic range in the pediatric dataset. The same positive correlation between elevated scanning frequency and improved glycemic control was observed in similar studies [139]–[142], although average daily scan frequency and TIR resulted lower in our T1DM pediatric population.

Considering the adult dataset, 320 monitoring windows were accepted after the preprocessing phase, while 96 windows were discarded because they contained less than 480 automatically stored readings. Anyway, there was not a significant positive correlation between daily scan frequency and TIR. In Table 4.9, indeed, it is possible to notice that average TIR values were almost the same among all groups, varying only in the 50%-60% range.

Instead, a strong negative correlation ($p\text{-value} < 10^{-3}$) was found between TIR and each of the selected glycemic metrics, as illustrated in Figure 4.15. In particular, ρ was equal to -0.99 considering SD, equal to -0.89 considering CONGA₁, and equal to -0.94 considering ADRR

Table 4.9: Daily scan frequency and Time in Range (TIR) average values \pm standard deviation for each group, based on the daily scan frequency ranking in the adult dataset.

Group	Daily scan frequency	TIR
1	3.16 \pm 0.44	54.03 \pm 13.04
2	4.08 \pm 0.25	54.58 \pm 14.74
3	5.01 \pm 0.35	54.86 \pm 13.65
4	5.84 \pm 0.15	55.83 \pm 10.04
5	6.66 \pm 0.26	54.68 \pm 11.14
6	7.35 \pm 0.20	52.47 \pm 8.26
7	8.12 \pm 0.28	50.82 \pm 9.29
8	9.20 \pm 0.30	51.88 \pm 11.00
9	10.34 \pm 0.42	64.95 \pm 14.25
10	12.08 \pm 0.80	58.68 \pm 15.42

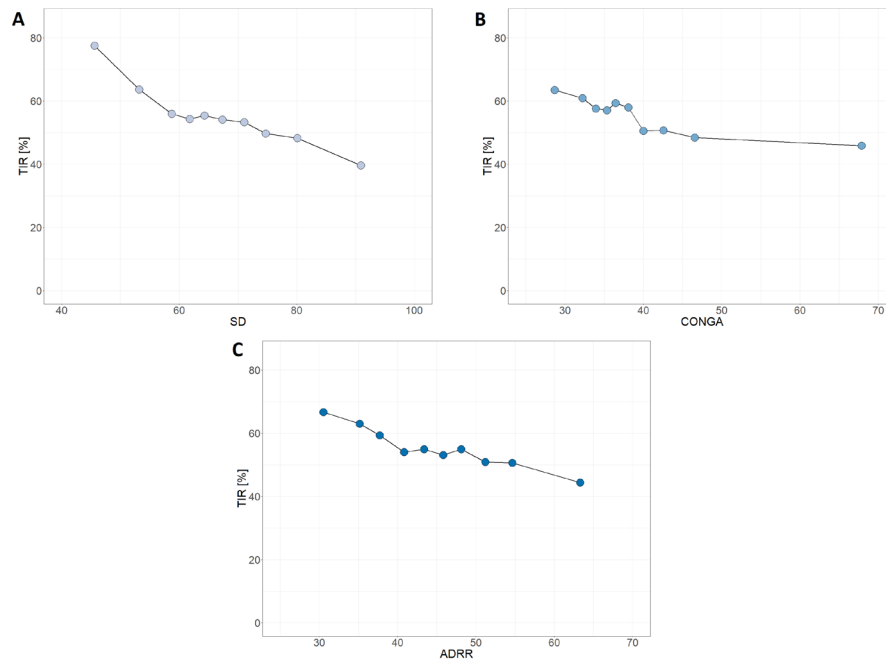


Figure 4.15: Scatter plots of average values of Time in Range (TIR) and Standard Deviations (SD) in part A, TIR and Continuous Overlapping Net Glycemic Action at 1-hour (CONGA₁) in part B, and of TIR and Average Daily Risk Range (ADRR) in part C, based on the respective ranking variable in the adult dataset.

The different relationship observed in the pediatric and the adult dataset between daily scan frequency and TIR might be related to the parental attitudes towards their children. In general, parents monitor child's glycemic levels through their CGM sensors on a regular basis, especially in case of young children who are unable to clearly express symptoms of hypoglycemia, and promptly manage potential hypoglycemic or hyperglycemic episodes in a short time; on the contrary, it is possible that some adults tend to delay their own self-care tasks.

4.3. Temporal data mining results

4.3.1. Pattern detection

Several workflows of diabetes-specific patterns have been included in the AID-GM platform. Through the GUI it was possible to select all the patterns of interest, along with patients and specific time periods, and visualize the results, i.e. time intervals in which the time-series assume behaviors of interest, presented in form of colored bars. For instance, Figure 4.16 shows all the hypoglycemic episodes occurred between the 1st of February 2018 and the 28th of February 2018 considering the adult dataset.

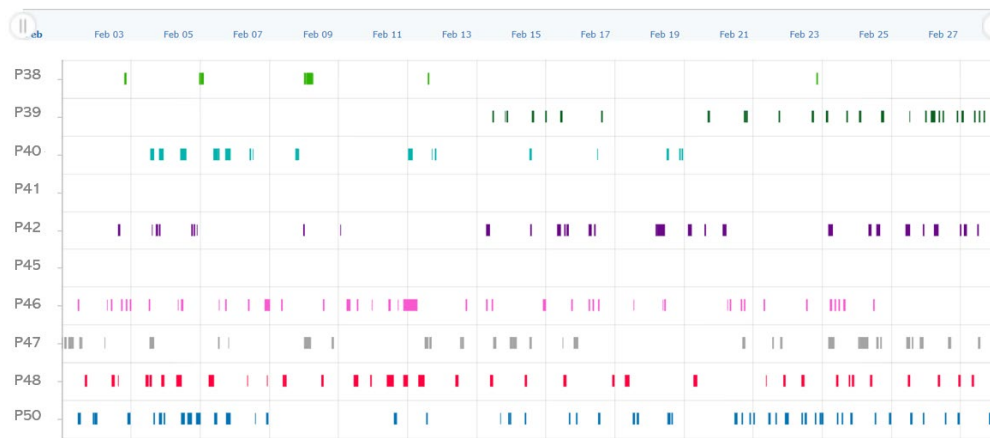


Figure 4.16: Hypoglycemia pattern visualization in the Advanced Intelligent Distant – Glucose Monitoring (AID-GM) platform, considering glucose monitoring data of adult patients between 1st February 2018 and 28th February 2018.

Figure 4.17, instead, presents a second kind of pattern visualization available in the AID-GM platform, providing various glycemic patterns of Patient 42 (from the adult dataset) in the same period of interest. Each colored bar links to a daily profiles chart, which is related to the time interval of the corresponding pattern occurrence, as for the hyperglycemic episode shown in Figure 4.18 occurred to Patient 42 on the 28th of February 2018.

Additionally, the daily profiles chart can be supplemented by information on the subject’s activities in that time interval, like the manually and automatically detected workouts in Figure 4.18, which may help the healthcare providers to evaluate the patient’s situation.

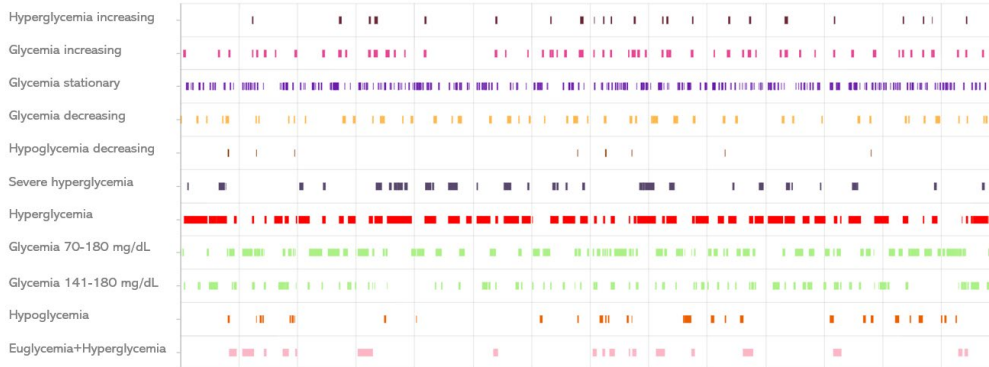


Figure 4.17: Glycemic pattern visualization in the Advanced Intelligent Distant – Glucose Monitoring (AID-GM) platform, considering glucose monitoring data of Patient 42 (adult dataset) between 1st February 2018 and 28th February 2018.

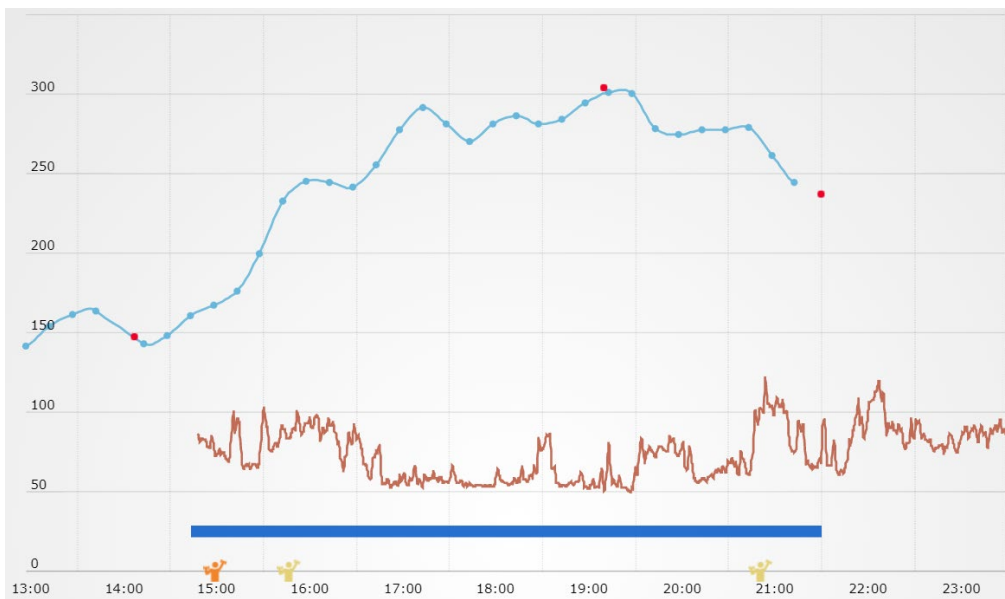


Figure 4.18: Pattern detection in the Advanced Intelligent Distant – Glucose Monitoring (AID-GM) platform, considering blood glucose (BG automatic: light blue line; BG manual: red dot) and heart rate (HR: dark orange line) data of Patient 46 in the adult dataset. On the timeline, the blue rectangle represents the time interval in which the selected pattern (in this case, hyperglycemia) occurred.

A summary of diabetes-specific patterns based on FreeStyle Libre system and Fitbit tracker monitoring data is presented in Table 4.10 and Table 4.11,

considering the pediatric and adult datasets, respectively. Moreover, such patterns can be further specified based on the Fitbit tag, as described in Section 3.3.2; all implementation details are provided in Appendix B. In particular, it is possible to note that both the count and the average duration of hypoglycemic episodes are higher in the adult dataset compared to the pediatric dataset, while the opposite consideration can be done for hyperglycemic episodes, which are longer and more frequent in children and adolescents compared to adults. Furthermore, 25 and 92 episodes of Dawn Effect were detected in the pediatric and adult dataset, showing an average duration of 339.56 minutes (± 141.57 SD) and 337.32 minutes (± 120.64 SD), respectively, along with multivariate patterns like Tachycardia precedes Hypoglycemia (146 versus 625 occurrences) or Hypoglycemia precedes Bradycardia during sleep periods (1 versus 39 occurrences).

Table 4.10: Summary of diabetes-specific patterns detected in the pediatric dataset; statistics are presented as frequencies or averages \pm standard deviations. Patterns durations are expressed in minutes.

Pattern	Episodes	Total duration	Average duration
BGDecDuringHypo	115	4,257	37.02 \pm 10.96
BGDecreasing	13,068	1115,536	85.36 \pm 45.72
BGIncreasing	13,434	1075,135	80.03 \pm 47.09
BGStationary	36,880	744,471	20.19 \pm 18.55
Bradycardia	2,913	64,020	21.98 \pm 31.00
DawnEffect	25	8,489	339.56 \pm 141.57
DecreasingHypo	900	23,470	26.08 \pm 17.99
Euglycemia	14,397	2720,661	188.97 \pm 213.74
HRDecreasing	10,437	79,950	7.66 \pm 2.55
HRIncreasing	9,404	72,052	7.66 \pm 2.88
HRStationary	16,618	170,960	10.29 \pm 6.29
Hyperglycemia	10,915	3083,652	282.52 \pm 338.56
Hyperglycemia_Lev1	15,254	1255,683	82.32 \pm 91.48
Hyperglycemia_Lev2	7,226	1610,693	222.9 \pm 249.20
HypoBeforeHyper	2	254	127 \pm 96,17
Hypoglycemia	2,991	162,012	54.17 \pm 65.25
Hypoglycemia_Lev1	2,646	83,246	31.46 \pm 27.85
Hypoglycemia_Lev2	866	50,081	57.83 \pm 65.88
HypoPrecBradyS	1	23	23.00
IncreasingHyper	4,880	298,202	61.11 \pm 49.83
Tachycardia	14,519	323,947	22.31 \pm 35.2
TachyPrecHypo	146	6,746	46.21 \pm 21.85

Table 4.11: Summary of diabetes-specific patterns detected in the adult dataset; statistics are presented as frequencies or averages \pm standard deviations. Patterns durations are expressed in minutes.

Pattern	Episodes	Total duration	Average duration
BGDecDuringHypo	268	10,024	37.40 \pm 10.79
BGDecreasing	8,251	688,626	83.46 \pm 43.96
BGIncreasing	9,650	728,245	75.47 \pm 39.63
BGStationary	37,333	779,361	20.88 \pm 15.49
Bradycardia	28,068	702,043	25.01 \pm 31.43
DawnEffect	92	31,033	337.32 \pm 120.64
DecreasingHypo	1,290	37,288	28.91 \pm 18.49
Euglycemia	14,078	2905,436	206.38 \pm 214.44
HRDecreasing	42,233	327,414	7.75 \pm 2.70
HRIncreasing	33,945	257,469	7.58 \pm 2.70
HRStationary	74,614	869,073	11.65 \pm 8.05
Hyperglycemia	8,608	1929,161	224.11 \pm 232.75
Hyperglycemia_Lev1	11,589	1166,613	100.67 \pm 104.43
Hyperglycemia_Lev2	4,281	627,212	146.51 \pm 148.42
HypoBeforeHyper	0	0	0
Hypoglycemia	4,617	366,464	79.37 \pm 77.74
Hypoglycemia_Lev1	4,448	182,279	40.98 \pm 35.87
Hypoglycemia_Lev2	1,943	126,231	64.97 \pm 64.23
HypoPrecBrady_Sleep	39	2,102	53.90 \pm 25.08
IncreasingHyper	3,666	198,194	54.06 \pm 40.82
Tachycardia	63,018	1530,833	24.29 \pm 38.17
TachyPrecHypo	625	40,279	64.45 \pm 31.30

4.3.2. Hypoglycemia analysis

The search for hypoglycemic patterns can be further refined based on the activity information provided to the AID-GM platform when the Fitbit tracker is worn by patients. In particular, Table 4.12 and Table 4.13 outline the episodes of hypoglycemia during routine, sleep, and workout periods in the pediatric and adult datasets, respectively. In particular, it is possible to notice a difference between the number of Hypoglycemia, as presented in Table 4.10 and Table 4.11, and the sum of HypoglycemiaR, HypoglycemiaS, and HypoglycemiaW episodes, equal to 452 occurrences for pediatric patients and to 2,701 for adult patients. The discrepancy, which is more evident in the pediatric dataset, is due to the fact that patients have used the Fitbit tracker for a shorter period compared to the FreeStyle Libre system.

Table 4.12: Summary of hypoglycemic patterns based on the Fitbit tag, detected in the pediatric dataset; statistics are presented as frequencies or averages \pm standard deviations. Patterns durations are expressed in minutes.

Pattern	Episodes	Total duration	Average duration
Hypoglycemia_R	312	11,573	37.09 \pm 34.64
Hypoglycemia_S	123	10,167	82.66 \pm 68.00
Hypoglycemia_W	17	362	21.29 \pm 11.06
Hypoglycemia_Lev1R	249	6,479	26.02 \pm 17.38
Hypoglycemia_Lev1S	113	4,307	38.12 \pm 33.11
Hypoglycemia_Lev1W	12	226	18.83 \pm 9.59
Hypoglycemia_Lev2R	69	2,669	38.68 \pm 31.80
Hypoglycemia_Lev2S	60	4,234	70.57 \pm 65.38
Hypoglycemia_Lev2W	2	30	15 \pm 0

Table 4.13: Summary of hypoglycemic patterns based on the Fitbit tag, detected in the adult dataset; statistics are presented as frequencies or averages \pm standard deviations. Patterns durations are expressed in minutes.

Pattern	Episodes	Total duration	Average duration
Hypoglycemia_R	2,071	125,454	60.58 \pm 54.33
Hypoglycemia_S	578	56,95	98.53 \pm 85.35
Hypoglycemia_W	52	1,326	25.5 \pm 16.81
Hypoglycemia_Lev1R	1,786	68,236	38.21 \pm 31.61
Hypoglycemia_Lev1S	543	25,024	46.08 \pm 38.72
Hypoglycemia_Lev1W	27	630	23.33 \pm 15.19
Hypoglycemia_Lev2R	757	34,883	46.08 \pm 42.85
Hypoglycemia_Lev2S	317	24,93	78.64 \pm 74.40
Hypoglycemia_Lev2W	15	316	21.07 \pm 15.81

Moreover, the importance of contextualizing glycaemic patterns within the day can be highlighted also in the comparison between the hypoglycemic patterns detected using the Profile tag or the Fitbit tag. Indeed, the frequency of hypoglycemia during sleep is a key information in diabetes monitoring, especially for children, and it is essential to quickly identify patients who are experiencing such pattern more frequently than others for apposite therapy adjustments. Considering the habitual bedtime and awakening-time for each patient, 266 episodes of HypoglycemiaS were detected in the pediatric dataset and 1,188 episodes in the adult dataset. Nevertheless, the search for HypoglycemiaS patterns using the Fitbit tag provided only 123 and 578 effective occurrences, respectively. In particular, the intersection between the HypoglycemiaS patterns detected based on Fitbit tag and Profile tag was

limited to 104 episodes for children and 457 episodes for adults, as shown in Figure 4.19 and Figure 4.20, respectively.

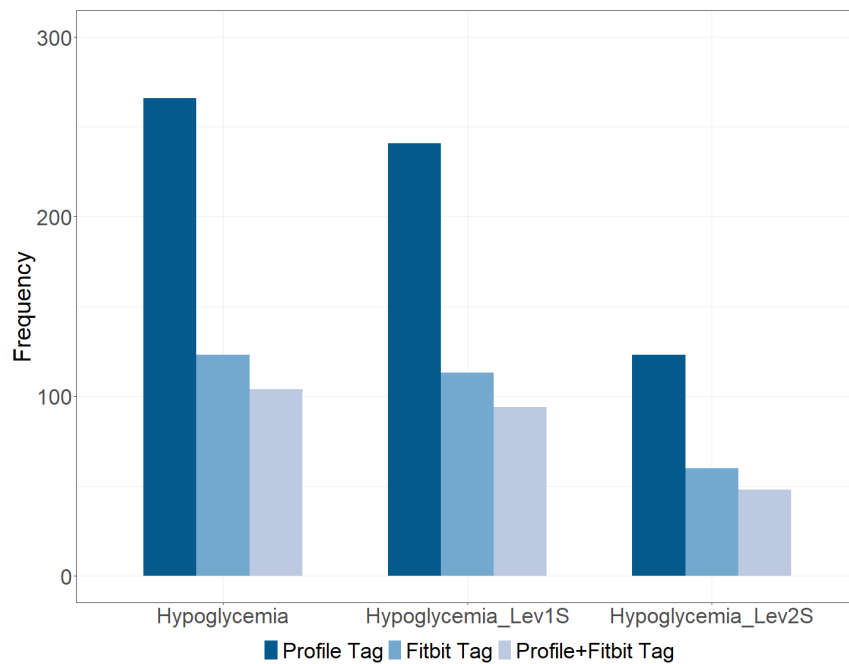


Figure 4.19: Count of hypoglycemic patterns during sleep detected using either the Profile tag, the Fitbit tag, or the intersection between the two tags in the pediatric dataset.

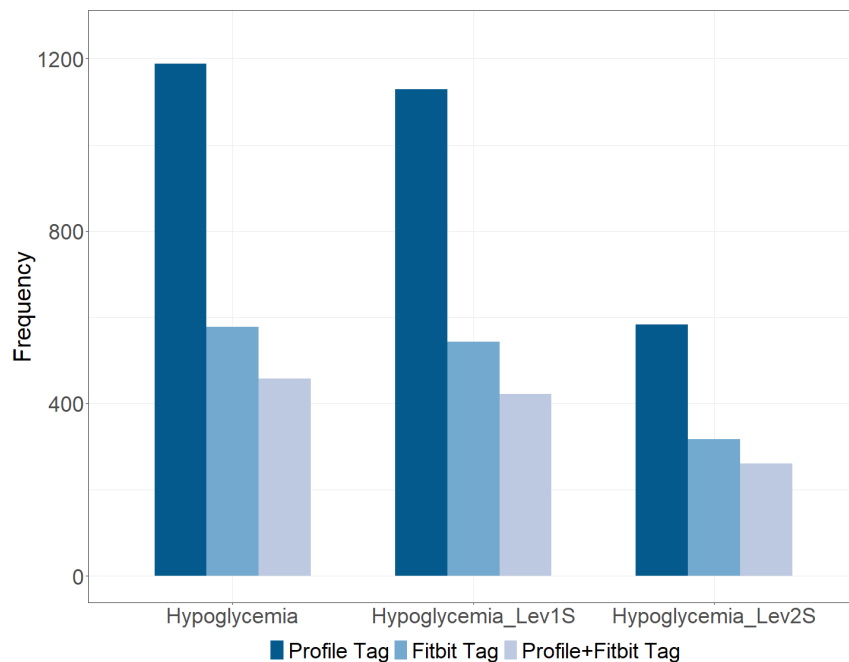


Figure 4.20: Count of hypoglycemic patterns during sleep detected using either the Profile tag, the Fitbit tag, or the intersection between the two tags in the adult dataset.

Furthermore, HR time-series related to HypoglycemiaS episodes were investigated among children and adolescent, as described in Section 3.3.3. Overall, 15,392 hours of simultaneous FreeStyle Libre system and Fitbit tracker monitoring were recorded in the pediatric dataset. A total of 773 sleep intervals were detected, including 170 hours of BG recordings during sleep in the hypoglycemic range, and the median duration of HypoglycemiaS episodes for each subject was 57 minutes (\pm IQR of 43 minutes).

Eight of the 17 patients equipped with the Fitbit tracker patients were excluded since they experienced less than three episodes of HypoglycemiaS. Therefore, a total of nine patients and 516 valid sleep intervals remained after the preprocessing phase, split into 68 intervals (13%) with the occurrence of hypoglycemic episodes and 448 intervals (87%) without hypoglycemic episodes. For each of the nine selected patient, the distribution of HR values in the before-hypoglycemia dataset was compared to the distribution of HR values in the no-hypoglycemia dataset, as shown in Figure 4.21. Based on the results of the non-parametric Mann-Whitney U test, a statistically significant difference (p -value $<10^{-2}$) between the before-hypoglycemia HR distribution and the no-hypoglycemia HR distribution was found in six of nine patients, such as Patient 67, 68, 69, 75, 76, and 87. In all these six cases the HR median values of the no-hypoglycemia dataset were higher than the HR median values of the before-hypoglycemia dataset. Examining the other three patients, instead, it was possible to observe that also Patient 63 showed a higher HR median value before HypoglycemiaS episodes compared to sleep intervals without hypoglycemia, but the difference was not statistically significant, while for Subjects 97 and 100 the HR median values were comparable. Additionally, a comparison between after-hypoglycemia and no-hypoglycemia HR distributions was presented in Figure 4.22. After the end of the hypoglycemic episode the HR values remained higher in all cases but one (Patient 97) compared to those collected in the no-hypoglycemia sleep intervals, with a statistically significant difference in six cases.

This analysis confirms that symptomatic or asymptomatic hypoglycemia repeatedly occur in children and adolescents with T1DM during sleep, suggesting that cardiac rhythm disturbances may represent a key element in the prevention of nighttime hypoglycemia. The presence of higher HR values in the before-hypoglycemia dataset compared to the no-hypoglycemia dataset, indeed, supports the sympathetic response to hypoglycemia [171], while a persistent increase in HR could be implicated in hypoglycemia-induced cardiac arrhythmias. Increased HR followed by an incorrect adjustment of repolarization, with inhomogeneous prolongation of the action potential duration, can lead to the dispersion of ventricle repolarization and fatal arrhythmias [171]; in T1DM individuals, the additional role of renin-angiotensin system activity in the magnitude of the adrenaline response to hypoglycemia could also be considered [172]. A subsequent increase of the parasympathetic activity to defend the organism cannot be excluded, leading to a risk for fatal heart rhythm problems in individuals with autonomic failure [150].

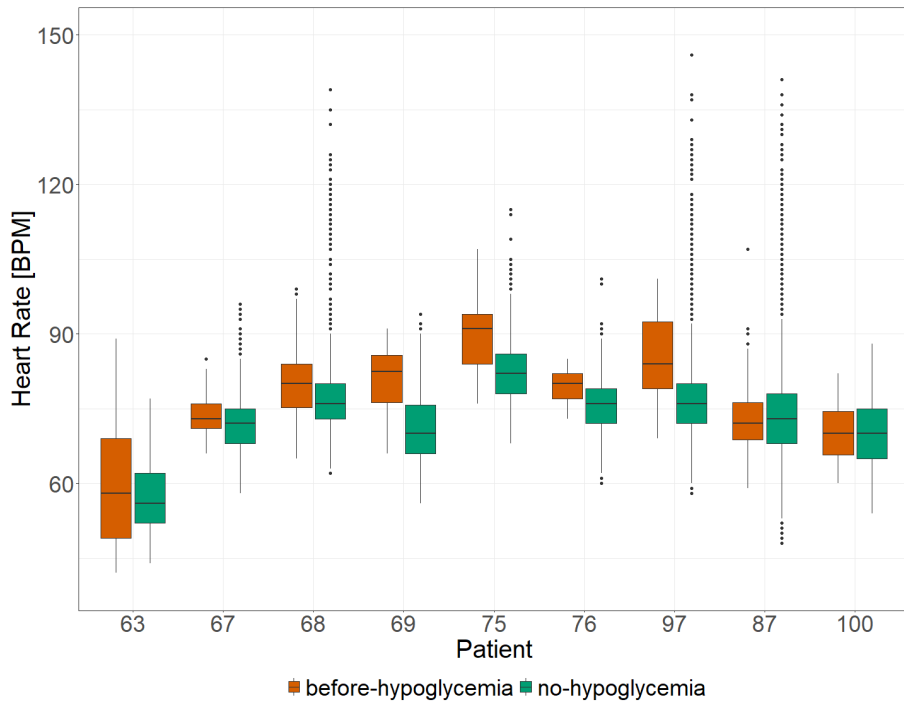


Figure 4.21: Comparison between the heart rate values collected in the hour before a hypoglycemic episode (in red) and in sleep intervals without hypoglycemic episodes (in green) in the pediatric dataset.

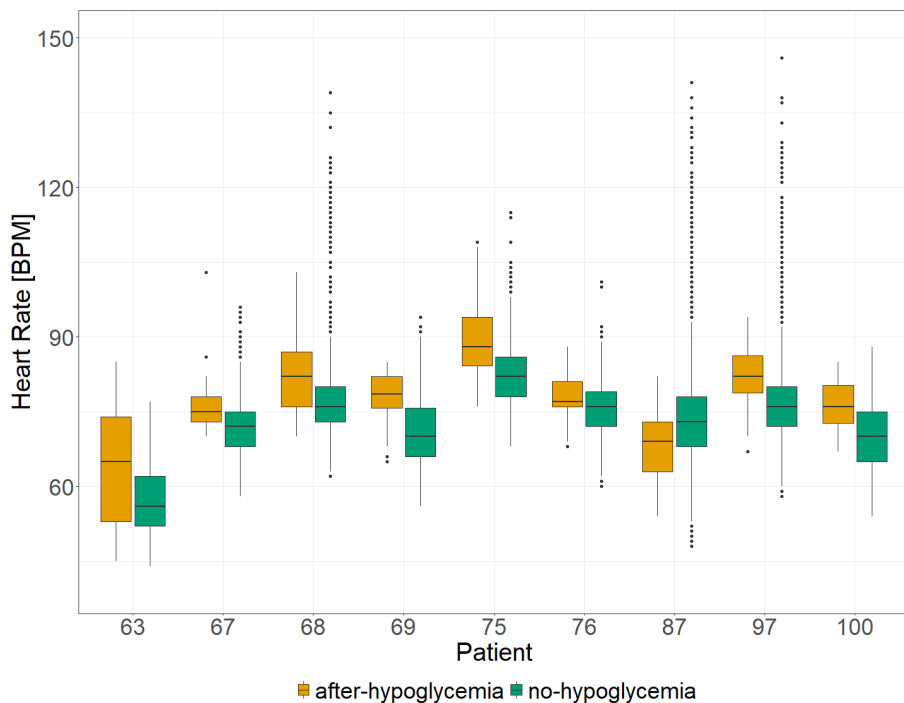


Figure 4.22: Comparison between the heart rate values collected in the hour after a hypoglycemic episode (in orange) and in sleep intervals without hypoglycemic episodes (in green) in the pediatric dataset.

4.4. Generalized deep learning model results

4.4.1. Results on the pediatric dataset

Table 4.14 allows to compare the average prediction errors of the proposed deep learning models based on pediatric patients, considering sliding windows with different widths and a 15-minutes PH. The “Model” column indicates the specific scenario, like the univariate scenario with only BG time-series (sBG), the multivariate scenario with BG and HR time-series (sBG-HR), and the multivariate scenario with a combination of BG, HR, and activities time-series (sBG-HR-Activity).

Models performances are almost comparable between different scenarios using a short sliding window of 15 minutes. Anyway, it is possible to notice that increasing the volume of historical data consented to obtain more accurate predictions, and with longer sliding windows of 45 minutes the multivariate sBG-HR-Activity scenario provided on average a lower prediction error compared to sBG and sBG-HR scenarios. Time windows larger than 45 minutes were considered as well (60, 75, and 90 minutes) to evaluate the behavior of RMSE on longer PHs. We noticed that, although RMSE continued to decrease, the relative improvement was not as strong as before. Thus, considering that widening the time windows increases the possibility of losing some information, we decided to use a maximum width of 45 minutes to show results. In addition, such values are comparable to those obtained by other generalized models in literature trained in similar conditions [118], [120].

Table 4.14: Overall analytical evaluation of pediatric multi-patient models by window width using the root mean square error (RMSE). RMSE values are presented as mean \pm standard deviation and expressed in mg/dL.

Model	Window width		
	15 min	30 min	45 min
sBG	15.67 \pm 1.63	11.10 \pm 1.16	10.55 \pm 1.12
sBG-HR	15.64 \pm 1.65	11.05 \pm 1.09	10.45 \pm 1.14
sBG-HR-Activity	15.67 \pm 1.64	11.09 \pm 1.20	10.35 \pm 1.15

The overall clinical evaluation of the proposed models through the CEGA is reported in Table 4.15. As emerged in the analytical assessment, the use of longer sliding windows allowed to achieve better results also in terms of severity of the potential harm caused by prediction errors. Indeed, in all scenarios the average percentages of points in zone A tended to rise as the windows width increased. In parallel, using 45-minutes windows the average percentages of points in a dangerous zone like the zone D decreased to 0.15% (\pm 0.11% SD) in the sBG scenario, to 0.17% (\pm 0.09% SD) in the sBG-HR scenario, and to 0.20% (\pm 0.07% SD) in the sBG-HR-Activity, while the

average percentages of points in the other dangerous zones such as zone C and zone E were very nearly to zero. Figure 4.23 displays an example of the resulting grid on Patient 98 using the sBG-HR-Fitbit model with 45-minutes sliding windows. Out of 1581 testing points, 1578 were in zone A with just three points in zone B and no points in dangerous areas.

Table 4.15: Overall clinical evaluation of pediatric multi-patient models by window width using the Clarke Error Grid analysis. Values are presented as mean \pm standard deviation and expressed in percentages.

Model	Window width	Clarke Error Grid zones				
		A	B	C	D	E
sBG	15 min	93.57 \pm 1.34	5.97 \pm 1.27	$\approx 0 \pm \approx 0$	0.46 \pm 0.18	0 \pm 0
	30 min	97.05 \pm 0.79	2.74 \pm 0.79	0 \pm 0	0.21 \pm 0.09	0 \pm 0
	45 min	97.66 \pm 0.87	2.19 \pm 0.80	0 \pm 0	0.15 \pm 0.11	0 \pm 0
sBG HR	15 min	93.60 \pm 1.48	5.80 \pm 1.27	$\approx 0 \pm \approx 0$	0.60 \pm 0.37	0 \pm 0
	30 min	97.11 \pm 0.77	2.62 \pm 0.77	0 \pm 0	0.27 \pm 0.10	0 \pm 0
	45 min	97.72 \pm 0.61	2.11 \pm 0.59	0 \pm 0	0.17 \pm 0.09	0 \pm 0
sBG HR Activity	15 min	93.79 \pm 1.40	5.68 \pm 1.28	$\approx 0 \pm \approx 0$	0.53 \pm 0.19	0 \pm 0
	30 min	97.06 \pm 0.80	2.67 \pm 0.78	0 \pm 0	0.27 \pm 0.11	0 \pm 0
	45 min	97.82 \pm 0.57	1.98 \pm 0.55	0 \pm 0	0.20 \pm 0.07	0 \pm 0

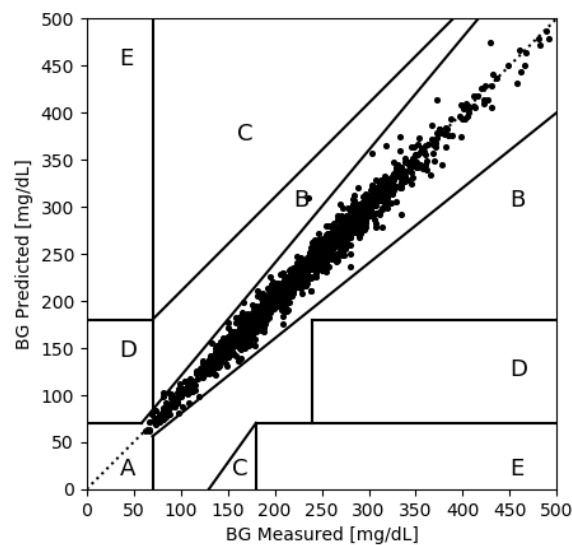


Figure 4.23: Clarke Error Grid for a pediatric test patient (Patient 98) using the BG-HR-Fitbit model with a 45-minutes window size.

Furthermore, multi-patient and multivariate models developed on the adult training sets were tested on the pediatric test patients, demonstrating high generalization capabilities. Indeed, using 45-minutes windows the

average prediction errors were lower compared with those obtained by models developed on pediatric patients in all scenarios. The highest improvements were found in the sBG scenario, with an average RMSE of 10.33 mg/dL (± 1.17 SD), and in the sBG-HR scenario, with an average RMSE of 10.30 mg/dL (± 1.17 SD), while in the sBG-HR-Activity scenario the average RMSE of 10.32 mg/dL (± 1.18 SD) was comparable with the average prediction accuracy achieved by models developed on pediatric patients.

4.4.2. Results on the adult dataset

Table 4.16 presents the average prediction errors of the proposed deep learning models based on adult patients, considering sliding windows of different widths and a 15-minutes PH. Overall, models that relied only on BG time-series performed slightly better than the other scenarios, even if the average prediction errors were comparable, especially considering 30-minutes and 45-minutes windows.

Table 4.16: Overall analytical evaluation of adult multi-patient models by window width using the root mean square error (RMSE). RMSE values are presented as mean \pm standard deviation and expressed in mg/dL.

Model	Window width		
	15 min	30 min	45 min
BG	14.16 \pm 2.37	9.31 \pm 1.33	8.60 \pm 1.10
BG-HR	14.22 \pm 2.40	9.33 \pm 1.35	8.62 \pm 1.11
BG-HR-Activity	14.22 \pm 2.37	9.31 \pm 1.29	8.63 \pm 1.08

Table 4.17: Overall clinical evaluation of adult multi-patient models by window width using the Clarke Error Grid analysis. Values are presented as mean \pm standard deviation and expressed in percentages.

Model	Window width	Clarke Error Grid zones				
		A	B	C	D	E
BG	15 min	94.72 \pm 2.82	4.94 \pm 2.67	0.01 \pm 0.02	0.33 \pm 0.15	0 \pm 0
	30 min	98.07 \pm 1.10	1.82 \pm 1.09	\approx 0 \pm \approx 0	0.11 \pm 0.06	0 \pm 0
	45 min	98.62 \pm 0.78	1.26 \pm 0.75	\approx 0 \pm \approx 0	0.12 \pm 0.04	0 \pm 0
BG HR	15 min	94.66 \pm 2.84	4.99 \pm 2.68	0.02 \pm 0.03	0.34 \pm 0.18	0 \pm 0
	30 min	98.04 \pm 1.18	1.84 \pm 1.17	\approx 0 \pm \approx 0	0.12 \pm 0.06	0 \pm 0
	45 min	98.64 \pm 0.76	1.23 \pm 0.73	\approx 0 \pm \approx 0	0.12 \pm 0.06	0 \pm 0
BG HR Activity	15 min	94.66 \pm 2.82	4.95 \pm 2.64	0.01 \pm 0.02	0.38 \pm 0.19	0 \pm 0
	30 min	98.10 \pm 1.12	1.77 \pm 1.11	\approx 0 \pm \approx 0	0.12 \pm 0.07	0 \pm 0
	45 min	98.62 \pm 0.81	1.26 \pm 0.78	\approx 0 \pm \approx 0	0.11 \pm 0.06	0 \pm 0

As observed in the pediatric models, a greater volume of historical data allowed to obtain more accurate predictions, both in analytical and clinical terms. In fact, Table 4.17 shows that the average percentage of points in zone A achieved 98.62% ($\pm 0.78\%$ SD) in the sBG scenario, 98.64% ($\pm 0.76\%$ SD) in the sBG-HR scenario, and 98.62% ($\pm 0.81\%$ SD) in the sBG-HR-Activity scenario, revealing better performances in terms of correct clinical decisions than pediatric models.

In addition, multi-patient and multivariate models developed on the pediatric training sets were tested on the adult test patients using 45-minutes windows. The differences in terms of average prediction errors between the pediatric models tested on adult patients and adult models were modest, always less than 0.4 mg/dL. Indeed, the average RMSE was equal to 8.96 mg/dL (± 1.13 SD) in the sBG scenario, to 8.99 mg/dL (± 1.17 SD) in the sBG-HR scenario, and to 8.95 mg/dL (± 0.99 SD) in the sBG-HR-Activity, revealing good generalization capabilities.

Chapter 5

Conclusions

Since DM is a lifelong condition that can lead to life-threatening health problems, early diagnosis, medication availability, life-style education, and constant monitoring represent crucial aspects for preventing acute events and reducing the risk of long-term complications.

The AID-GM web application allowed patients to share with their diabetologists both glucose data from FreeStyle Libre isCGM systems and activity information from Fitbit fitness trackers. Long-term remote monitoring was supported by the implementation of several temporal analytics functionalities in the platform, making available to clinicians a qualitative and quantitative overview of each patient's conditions. Fitbit information was used to contextualize BG measurements within the day and provide information about the actual lifestyle of a patient, identifying eventual irregularities in daily habits that can help clinicians in the interpretation of unusual metabolic responses.

The data collected in the two evaluation studies of the platform allowed building a research dataset that was used for the development of several temporal data analytics strategies to gain deeper insight in the data and to enhance critical events prediction.

The availability of considerable amount of BG data made it possible to investigate the relation between a set of summary indicators computed on CGM time series and HbA1c. HbA1c test represents the gold standard indirect measure of long-term glycemic control, since it can estimate the glycemic exposure over the last two or three months before sampling, while CGM-derived time in range indicators have become popular metrics for glycemic control, as they were associated with the risk of development of microvascular complications [92]. In this thesis, the relationship between HbA1c values and time in ranges metrics was investigated through the innovative adoption of LME models. TIR, TIT, and TAR resulted significant HbA1c predictors considering both pediatric and adult patients. As expected, TIR and TIT confirmed a negative linear relationship with HbA1c, while

TAR showed a positive linear relationship with HbA1c, as reported in previous studies. Thanks to the use of LME models, it was possible to assess the time in ranges targets for a safe glyceic control ($HbA1c \leq 7\%$), which were found to be comparable with the ATTD consensus recommendations for CGM-derived glyceic targets [23] and also with other findings in literature [93], [94]. Finally, the adoption of LME models consented also to explore the inter-subject variability and identify, even though on a small cohort of patients, individualized glyceic targets for maintaining a near-normal glyceic control.

Thanks to the available data, it was possible to explore a second analysis scenario, related to the relationships between self-monitoring frequency and glyceic metrics. In the pediatric dataset, we found a significant correlation between a high daily scan frequency through the FreeStyle Libre system and a reduction in glyceic variability with high time spent in the euglyceic range. Interestingly, this result was not confirmed in the adult dataset.

When considering BG time series, there exists a number of qualitative patterns that diabetologists used to look for in the data to identify specific patterns of interest. To extract such patterns from large time series datasets, TAs are a suitable solution. Thanks to the use of the JTSA tool, several workflows of diabetes-specific patterns, both univariate and multivariate, were formalized in collaboration with the diabetologists from the Fondazione IRCCS Policlinico San Matteo hospital and the IRCCS Istituti Clinici Scientifici Maugeri and have been included in the AID-GM platform. This allows clinicians to easily detect patterns of interest and possibly stratify the population in sub-groups, identifying the individuals who need apposite therapy adjustments. In this context, a particularly relevant analysis scenario has involved the investigation of the nighttime hypoglyceic pattern, especially for young patients, since it has been associated with the “dead-in-bed” syndrome. Analyzing pediatric patients, it was possible to notice that HR modifications occur in nighttime hypoglyceic episodes, suggesting that cardiac rhythm disturbances may represent a key element in the prevention of hypoglycemia during sleep. However, this explorative analysis presented several limitations, such as the relatively small number of number of participants, and the lack of data about morphological changes in electrocardiographic repolarization and/or the QTc prolongation, which could be useful to study the pathogenetic mechanisms of cardiac arrhythmias.

Given the importance of preventing acute glyceic events especially in specific contexts (e.g. sleep or exercise), as a final analytics application we developed a multi-patient and multivariate deep learning model for glucose prediction considering both the pediatric and adult datasets. The core of the model was represented by a LSTM layer, surrounded by a set of hidden layers. Analytical and clinical evaluations suggested that a general model with good prediction performance can be obtained from a population of patients. Additionally, increasing the volume of historical values and combining HR and lifestyle monitoring signals to contextualize the BG measures can help to improve BG prediction. Increasing the PH by

considering time windows of different lengths allowed lowering RMSE. Although several PH were taken into account, a decision was made to present results only for 15, 30, and 45-minutes windows, as the relative improvement with longer windows started to decrease afterwards.

Overall, this thesis presented an extensive analysis on BG monitoring time-series coupled with HR and lifestyle data. Thanks to the application of several advanced temporal analytics techniques, it was possible to evaluate different scenarios to exploit the data at its best. We took advantage of the possibility of contextualizing BG data with activities to study specific events during different moments of the day, and of TAs to easily identify such events in a large volume of time-series data. We had the possibility of comparing the results in two different populations, and we were able to highlight the diversities between the extracted results, which in some cases are due to the different management of the disease in different age classes. Future studies will be aimed at refining the models on a higher number of patients and validating the findings of the presented research scenarios on larger datasets.

Appendix A

Impaired glucose-insulin metabolism in Multisystem Inflammatory Syndrome related to SARS-CoV-2 in children

TA techniques presented in Section 3.3.1 were used also to evaluate the presence of glucose disorders in young patients affected by multisystem inflammatory syndrome in children (MIS-C), a critical health condition associated with the severe acute respiratory syndrome coronavirus 2 (SARS-CoV-2). Data was provided by the Vittore Buzzi Children's Hospital in Milan, Italy, during the coronavirus disease 2019 (COVID-19) pandemic [173].

As stated by the Center of Diseases Control and Prevention (CDC), the definition of MIS-C requires patients to be less than 21 years and to have evidence of either recent/current SARS-CoV-2 infection or exposure within the four weeks prior to the onset of symptoms, the presence of documented fever, elevated markers of inflammation, at least two signs of multisystem involvement, and finally, lack of an alternative diagnosis (e.g., bacterial sepsis, toxic shock syndrome) [174].

Between November 2020 and January 2021, a group of 30 children and adolescents (7 females and 23 males, aged on average 10.68 years \pm 7.25 SD) were admitted to the Pediatric Department of Vittore Buzzi Children's Hospital for MIS-C, defined according to the CDC classification [174]. Exclusion criteria included a history of DM and/or insulin resistance, assumption of steroid/drug inducing hyperglycemia at admission, and suspected or proven inborn errors of metabolism.

On admission, patients were asked to wear the FreeStyle Libre isCGM system, a clinical and biochemical assessment was recorded, and the metabolic profile including total and HDL cholesterol, FPG, fasting plasma insulin (FPI) and triglycerides (FTy) was analyzed (a blood sample was obtained in fasting state between 8:30 a.m. and 9:00 a.m.).

Two indexes were used as a surrogate of insulin resistance (IR), such as the homeostasis model analysis-insulin resistance (HOMA-IR) index [175], and the Triglyceride–glucose (TyG) index [176], [177], defined as in the following:

$$HOMA - IR = \frac{FPI (mU/L) \cdot FPG (mg/dL)}{405}$$

$$TyG = \ln \left(\frac{FTy(mg/dL) \cdot FPI(mg/dL)}{2} \right)$$

The cutoff point for pathological HOMA-IR index was set at the 97.5th percentile of the HOMA-IR distribution in a representative group of Italian healthy children and adolescents grouped by sex and pubertal stage [178], while the cutoff point for pathological TyG index was set at 7.88 [179], [180].

Due to some missing FPI data, it was possible to calculate the HOMA-IR index for only 18 patients (60%). Among these, 17 (94%) revealed a pathological HOMA-IR value. Instead, the TyG index was computed for all patients and pathological values were detected in all cases.

The Spearman coefficient ρ was used to estimate the correlation between each IR index and clinical and biochemical parameters. As shown Figure A.1, sodium had a significant correlation (p -value = 0.02) with HOMA-IR, while alanine transaminase (ALT), total cholesterol, gamma-glutamyl transferase (GGT), thyroid-stimulating hormone (TSH), and albumin revealed a significant correlation (p -value \leq 0.02) with TyG index, as displayed in Figure A.2. This may support the predominance of catabolic condition and the impairment of glucose homeostasis within the body.

Finally, Figure A.3 shows the average percent partition of time spent within different glucose ranges. It is possible to notice that time spent outside the euglycemic range was highly asymmetrical: average TBR was 5.67% (\pm 10.19% SD), while average TAR was 0.57% (\pm 1.20% SD). Additionally, four patients revealed glycemic fluctuation above the 180 mg/dL threshold of hyperglycemia, as illustrated in Figure A.4.

In conclusion, IR and glycemic fluctuations were detected in normal weight children and adolescent without previous glycemic disorders. The high prevalence of pathological values in HOMA-IR and TyG indexes supported a both hepatic and peripheral impaired insulin action, while the correlation between IR markers and lipids, hepatic parameters, thyroid values, electrolytes, and albumin may support the predominance of catabolic condition and the impairment of glucose homeostasis within the body. To the best of our knowledge, this was the first study describing glucose-insulin metabolic disorders in a pediatric population affected by MIS-C [173].

Impaired glucose-insulin metabolism in Multisystem Inflammatory Syndrome related to SARS-CoV-2 in children

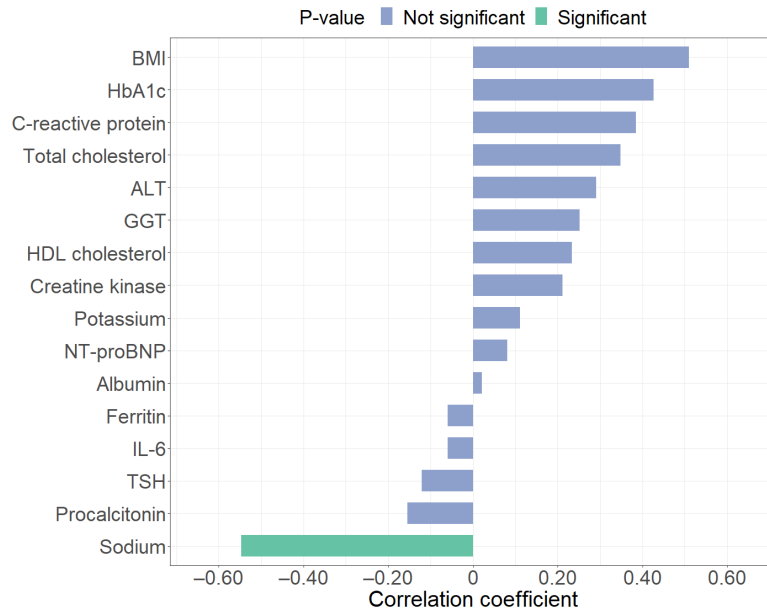


Figure A.1: Spearman correlation coefficients between clinical and biochemical parameters and homeostasis model analysis-insulin resistance (HOMA-IR) index. BMI: Body Mass Index; HbA1c: glycated hemoglobin; ALT: alanine transaminase; GGT: gamma-glutamyl transferase; NT-proBNP: N-Terminal pro-Brain Natriuretic Peptide; IL-6: interleukin-6; TSH: thyroid-stimulating hormone.

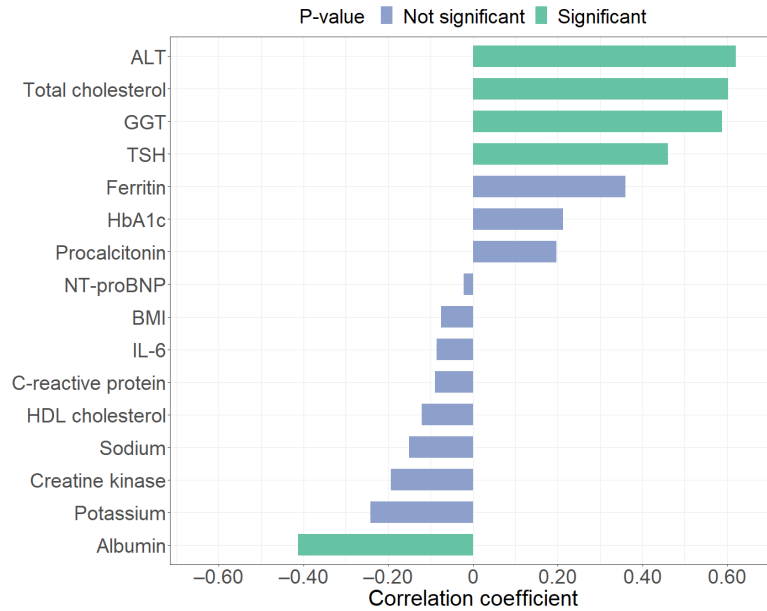


Figure A.2: Spearman correlation coefficients between clinical and biochemical parameters and homeostasis model analysis-insulin resistance (HOMA-IR) index. BMI: Body Mass Index; HbA1c: glycated hemoglobin; ALT: alanine transaminase; GGT: gamma-glutamyl transferase; NT-proBNP: N-Terminal pro-Brain Natriuretic Peptide; IL-6: interleukin-6; TSH: thyroid-stimulating hormone.

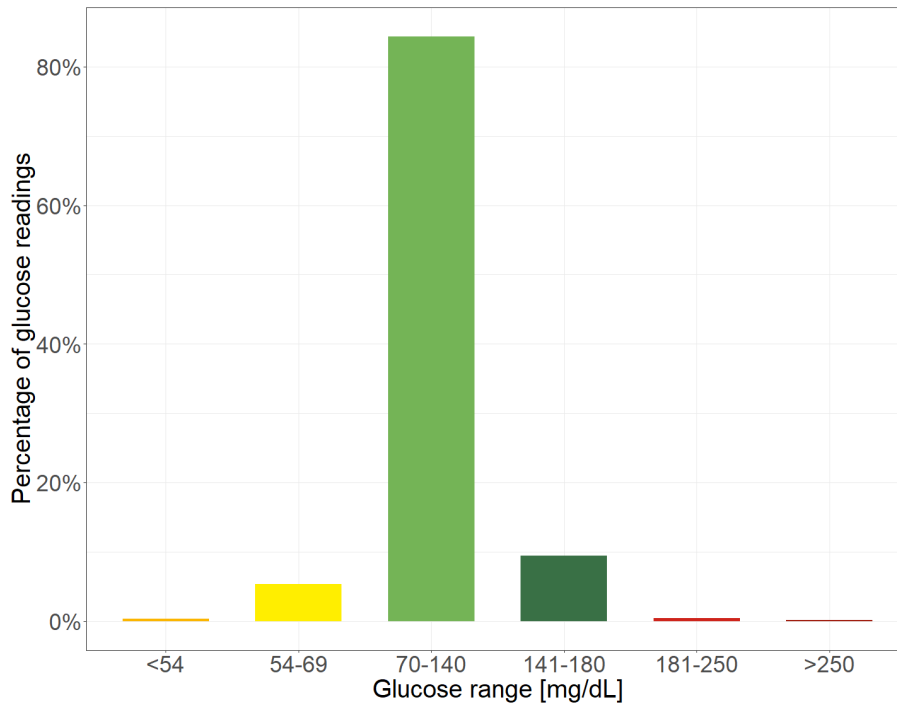


Figure A.3: Bar representation of average time in ranges.

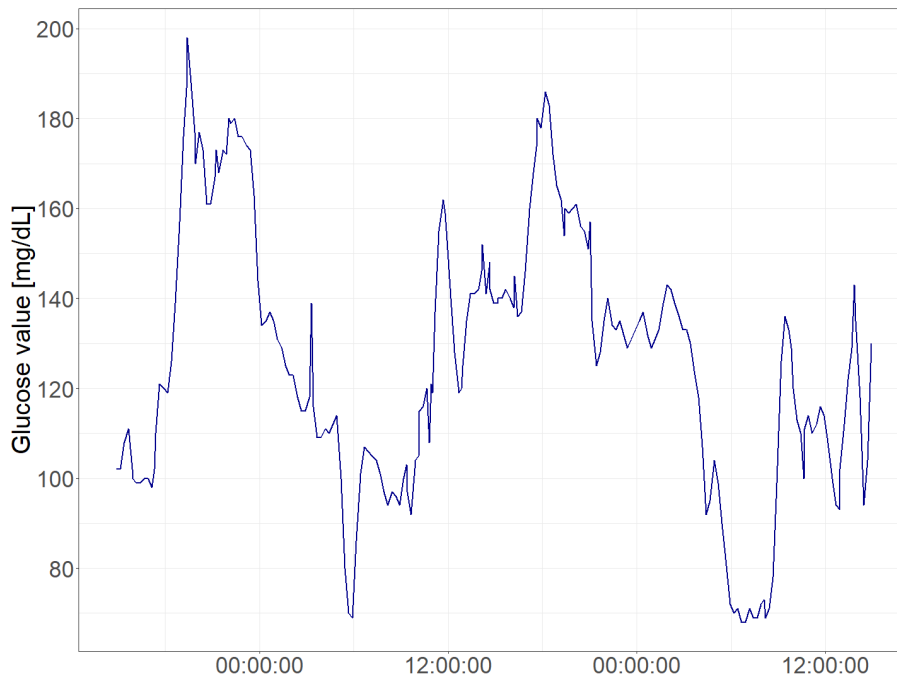


Figure A.4: Glycemic fluctuations in a patient 48-hours monitoring window.

Appendix B

Temporal abstractions workflows

Table B.1 presents the implementation details of XML workflows included in the AID-GM platform for detecting diabetes-specific patterns, based on basic, aggregation, and complex temporal abstraction, as described in Section 3.3.2. Each pattern can be searched either considering all the monitoring data or contextualizing the search based on the Fitbit tag. In particular, the suffix “S” indicates that the corresponding pattern is based on sleep intervals, the suffix “W” specifies that the search is restricted to workout intervals, while the suffix “R” is used when the search excludes both sleep and training periods. Instead, Table B.2 describes the parameters used in pattern definition for making the relational operators more or less restrictive.

Table B.1: Workflows parameters of the implemented patterns.

Filename	ID	Data Input	Step			Relational Operator	Combiner
			parameters	type	subtype		
BGDecDuringHypo	BGDec	BG	BGSlowDec	BASIC	BASIC_TRENDSLIDINGWINDOW	-	-
	Hypo	BG	qualitativeGlycemiaHighLevelAgg_Hypo	BASIC_AGGREGATION	BASIC_QUALITATIVE_AGGREGATION_HIGHLEVEL	-	-
	BGDecHypo	BGDecHypo	DURING	-	-	DURING	FirstInSeries
BGDecreasing	BGDec	BG	BGDec	BASIC	BASIC_TRENDSLIDINGWINDOW	-	-
BGIncreasing	BGInc	BG	BGInc	BASIC	BASIC_TRENDSLIDINGWINDOW	-	-
BGSlowDecreasing	BGDec	BG	BGSlowDec	BASIC	BASIC_TRENDSLIDINGWINDOW	-	-
BGStationary	BGStat	BG	BGStat	BASIC	BASIC_TRENDSLIDINGWINDOW	-	-
Bradycardia	Brady	HR	qualitativeHR	BASIC	BASIC_QUALITATIVE	-	-

			HighLevelAgg_Brady	AGGREGATION	AGGREGATION_HIGHLEVEL		
BradyPrecNormo	Brady	HR	qualitativeHR HighLevelAgg_Brady	BASIC AGGREGATION	BASIC_QUALITATIVE AGGREGATION_HIGHLEVEL	-	-
	Normo	HR	qualitativeHR HighLevelAgg_NormoHR	BASIC AGGREGATION	BASIC_QUALITATIVE AGGREGATION_HIGHLEVEL	-	-
	BradyPrecNormo	BradyNormo	PRECEDES_BradyNormo	-	-	PRECEDES	LastInSeries
DawnEffect	NormoSleep	BGSleep	qualitativeGlycemia HighLevelAgg_NormoDawn	BASIC AGGREGATION	BASIC_QUALITATIVE AGGREGATION_HIGHLEVEL	-	-
	HyperMorning	BGRoutine	qualitativeGlycemia HighLevelAgg_IperAlba	BASIC AGGREGATION	BASIC_QUALITATIVE AGGREGATION_HIGHLEVEL	-	-
	DawnEffect	NormoSleepHyperMorning	BEFORE_Dawn	-	-	BEFORE	Union
DecreasingHypo	BGDec	BG	BGDec	BASIC	BASIC_TRENDSLIDINGWINDOW	-	-
	Hypo	BG	qualitativeGlycemia HighLevelAgg_Hypo	BASIC AGGREGATION	BASIC_QUALITATIVE AGGREGATION_HIGHLEVEL	-	-
	DecreasingHypo	BGDecHypo	OVERLAPS	-	-	OVERLAPS	Intersection
Euglycemia	Eu	BG	qualitativeGlycemia HighLevelAgg_NormoBG	BASIC AGGREGATION	BASIC_QUALITATIVE AGGREGATION_HIGHLEVEL	-	-
Glycemia_141_180	Normo	BG	qualitativeGlycemia _NormoLev HighLevelAgg_NormoBG	BASIC AGGREGATION	BASIC_QUALITATIVE AGGREGATION_HIGHLEVEL	-	-
HRDecreasing	HRDec	HR	HRDec	BASIC	BASIC_TRENDSLIDINGWINDOW	-	-
HRFastIncreasing	HRIncFast	HR	HRFastInc	BASIC	BASIC_TRENDSLIDINGWINDOW	-	-
HRIncreasing	HRInc	HR	HRInc	BASIC	BASIC_TRENDSLIDINGWINDOW	-	-
HRStationary	HRStat	HR	HRStat	BASIC	BASIC_TRENDSLIDINGWINDOW	-	-
Hyperglycemia	Hyper	BG	qualitativeGlycemia HighLevelAgg_Hyper	BASIC AGGREGATION	BASIC_QUALITATIVE AGGREGATION_HIGHLEVEL	-	-
Hyperglycemia_H2207	Hyper	BG_H2207	qualitativeGlycemia HighLevelAgg_Hyper	BASIC AGGREGATION	BASIC_QUALITATIVE AGGREGATION_HIGHLEVEL	-	-

Temporal abstractions workflows

Hyperglycemia_Lev1	Hyper	BG	qualitativeGlycemia HighLevelAgg_HyperLev1	BASIC AGGREGATION	BASIC_QUALITATIVE AGGREGATION_HIGLEVEL	-	-
Hyperglycemia_Lev1_2207	Hyper	BG_H2 207	qualitativeGlycemia HighLevelAgg_HyperLev1	BASIC AGGREGATION	BASIC_QUALITATIVE AGGREGATION_HIGLEVEL	-	-
Hyperglycemia_Lev2	Hyper	BG	qualitativeGlycemia HighLevelAgg_Hyperglycemia_Lev2	BASIC AGGREGATION	BASIC_QUALITATIVE AGGREGATION_HIGLEVEL	-	-
HypoBeforeHyper	Hypo	BG	qualitativeGlycemia HighLevelAgg_Hypo	BASIC AGGREGATION	BASIC_QUALITATIVE AGGREGATION_HIGLEVEL	-	-
	Hyper	BG	qualitativeGlycemia HighLevelAgg_Hyper	BASIC AGGREGATION	BASIC_QUALITATIVE AGGREGATION_HIGLEVEL	-	-
	HypoHyper	HypoHyper	BEFORE_HypoHyper	-	-	BEFORE	Union
HypoContainsTachy	Hypo	BG	qualitativeGlycemia HighLevelAgg_Hypo	BASIC AGGREGATION	BASIC_QUALITATIVE AGGREGATION_HIGLEVEL		
	Tachy	HR	qualitativeHR HighLevelAgg_Tachy	BASIC AGGREGATION	BASIC_QUALITATIVE AGGREGATION_HIGLEVEL		
	HypoContainsTachy	HypoTachi	CONTAINS_HypoTachy			CONTAINS	Union
Hypoglycemia	Hypo	BG	qualitativeGlycemia HighLevelAgg_Hypo	BASIC AGGREGATION	BASIC_QUALITATIVE AGGREGATION_HIGLEVEL	-	-
Hypoglycemia_H2207	Hypo	BG_H2 207	qualitativeGlycemia HighLevelAgg_Hypo	BASIC AGGREGATION	BASIC_QUALITATIVE AGGREGATION_HIGLEVEL	-	-
Hypoglycemia_Lev1	Hypo	BG	qualitativeGlycemia HighLevelAgg_HypoLev1	BASIC AGGREGATION	BASIC_QUALITATIVE AGGREGATION_HIGLEVEL	-	-
Hypoglycemia_Lev1_H2207	Hypo	BG_H2 207	qualitativeGlycemia HighLevelAgg_HypoLev1	BASIC AGGREGATION	BASIC_QUALITATIVE AGGREGATION_HIGLEVEL	-	-
Hypoglycemia_Lev2	Hypo	BG	qualitativeGlycemia HighLevelAgg_Hypoglycemia_Lev2	BASIC AGGREGATION	BASIC_QUALITATIVE AGGREGATION_HIGLEVEL	-	-
Hypoglycemia_Lev2_2207	Hypo	BG_H2 207	qualitativeGlycemia HighLevelAgg_Hypoglycemia_Lev2	BASIC AGGREGATION	BASIC_QUALITATIVE AGGREGATION_HIGLEVEL	-	-
HypoPrecBradly	Hypo	BG	qualitativeGlycemia HighLevelAgg_Hypo	BASIC AGGREGATION	BASIC_QUALITATIVE	-	-

					AGGREGATION_HIGHLEVEL		
	Brady	HR	qualitativeHR HighLevelAgg_Brady	BASIC AGGREGATION	BASIC_QUALITATIVE AGGREGATION_HIGHLEVEL	-	-
	HypoPrec Brady	Hypo Brady	PRECEDES_Tachy Hypo	-	-	PRECEDES	Union
HypoPrecTachy	Hypo	BG	qualitativeGlycemia HighLevelAgg_Hypo	BASIC AGGREGATION	BASIC_QUALITATIVE AGGREGATION_HIGHLEVEL	-	-
	Tachy	HR	qualitativeHR HighLevelAgg_Tachy	BASIC AGGREGATION	BASIC_QUALITATIVE AGGREGATION_HIGHLEVEL	-	-
	HypoPrec Tachy	Hypo Tachi	PRECEDES_Tachy Hypo	-	-	PRECEDES	Union
IncreasingHyper	BGInc	BG	BGInc	BASIC	BASIC_TRENDSLIDINGWINDOW	-	-
	Hyper	BG	qualitativeGlycemia HighLevelAgg_Hyper	BASIC AGGREGATION	BASIC_QUALITATIVE AGGREGATION_HIGHLEVEL	-	-
	Increasing Hyper	BGInc Hyper	OVERLAPS	X	X	OVERLAPS	Intersection
NormoBeforeHyper	Normo	BG	qualitativeGlycemia HighLevelAgg_NormoBG	BASIC AGGREGATION	BASIC_QUALITATIVE AGGREGATION_HIGHLEVEL	-	-
	Hyper	BG	qualitativeGlycemia HighLevelAgg_Hyper	BASIC AGGREGATION	BASIC_QUALITATIVE AGGREGATION_HIGHLEVEL	-	-
	NormoHyper	Normo Hyper	BEFORE_HypoHyper	-	-	BEFORE	Union
Normocardia	Normocardia	HR	qualitativeHR HighLevelAgg_NormoHR	BASIC AGGREGATION	BASIC_QUALITATIVE AGGREGATION_HIGHLEVEL	-	-
NormoPrecTachy	Normo	HR	qualitativeHR HighLevelAgg_NormoHR	BASIC AGGREGATION	BASIC_QUALITATIVE AGGREGATION_HIGHLEVEL	-	-
	Tachi	HR	qualitativeHR HighLevelAgg_Tachy	BASIC AGGREGATION	BASIC_QUALITATIVE AGGREGATION_HIGHLEVEL	-	-
	NormoPrecTachy	Normo Tachi	PRECEDES_NormoTachy	-	-	PRECEDES	LastInSeries
Tachycardia	Tachi	HR	qualitativeHR HighLevelAgg_Tachy	BASIC AGGREGATION	BASIC_QUALITATIVE AGGREGATION_HIGHLEVEL	-	-
TachyPrecDecr	Tachi	HR	qualitativeHR HighLevelAgg_Tachy	BASIC AGGREGATION	BASIC_QUALITATIVE AGGREGATION_HIGHLEVEL	-	-

Temporal abstractions workflows

	BGDec	BG	BGFastDec	BASIC	BASIC_TRENDSLIDINGWINDOW	-	-
	TachyPrecDecr	TachyBGDec	PRECEDES_TachyDec	-	-	PRECEDES	Union
TachyPrecHypo	Tachi	HR	qualitativeHRHighLevelAgg_Tachy	BASICAGGREGATION	BASIC_QUALITATIVEAGGREGATION_HIGHLEVEL	-	-
	Hypo	BG	qualitativeGlycemiaHighLevelAgg_Hypo	BASICAGGREGATION	BASIC_QUALITATIVEAGGREGATION_HIGHLEVEL	-	-
	TachyPrecHypo	TachyHypo	PRECEDES_TachyDec	-	-	PRECEDES	Union

Table B.2.: Parameters for making the relational operators more or less restrictive.

Relational operator	Parameters [in minutes]
BEFORE	<ul style="list-style-type: none"> • ls= 540 • rs= 120 • gap= 60
BEFORE_Dawn	<ul style="list-style-type: none"> • ls= 540 • rs= 240 • gap= 45
BEFORE_HR	<ul style="list-style-type: none"> • ls= 180 • rs= 180 • gap= 4
BEFORE_HypoHyper	<ul style="list-style-type: none"> • ls= 540 • rs= 240 • gap= 30
BGDec	<ul style="list-style-type: none"> • minLen= 35 • label= Decreasing • minSlope= -200 • maxSlope= -1 • gap= 30
BGFastDec	<ul style="list-style-type: none"> • minLen= 30 • label= Decreasing • minSlope= -200 • maxSlope= -1.5 • gap= 30
BGFastInc	<ul style="list-style-type: none"> • minLen= 30 • label= Increasing • minSlope= 1.5 • maxSlope= 200 • gap= 30
BGInc	<ul style="list-style-type: none"> • minLen= 35 • label= Increasing • minSlope= 1 • maxSlope= 200 • gap= 30
BGSlowDec	<ul style="list-style-type: none"> • minLen= 20 • label= Decreasing • minSlope= -300 • maxSlope= -0.3

	<ul style="list-style-type: none"> • gap= 30
BGSlowInc	<ul style="list-style-type: none"> • minLen= 20 • label= Increasing • minSlope= 300 • maxSlope= 0.3 • gap= 30
BGStat	<ul style="list-style-type: none"> • minLen= 10 • label= Stationary • minSlope= -0.1 • maxSlope= 0.1 • gap= 30
CONTAINS_HypoTachy	<ul style="list-style-type: none"> • ls= 40 • rs= -90 • gap= -150
DURING	<ul style="list-style-type: none"> • ls= -700 • rs= 800 • gap= 750
HighLevelAgg_Brady	<ul style="list-style-type: none"> • gap= 10 • minLen= 5 • label= Bradycardia • levels= bradycardia
HighLevelAgg_Hyper	<ul style="list-style-type: none"> • gap= 60 • minLen= 13 • label= Hyperglycemia • levels= hyperglycemia,hyperglycemia_Lev2
HighLevelAgg_Hyperglycemia_Lev2	<ul style="list-style-type: none"> • gap= 60 • minLen= 13 • label= Hyperglycemia_Lev2 • levels= hyperglycemia_Lev2
HighLevelAgg_HyperLev1	<ul style="list-style-type: none"> • gap= 60 • minLen= 13 • label= Hyperglycemia • levels= hyperglycemia
HighLevelAgg_Hypo	<ul style="list-style-type: none"> • gap= 60 • minLen= 13 • label= Hypoglycemia • levels= hypoglycemia, hypoglycemia_Lev2
HighLevelAgg_Hypoglycemia_Lev2	<ul style="list-style-type: none"> • gap= 60 • minLen= 13 • label= Hypoglycemia_Lev2 • levels= hypoglycemia_Lev2
HighLevelAgg_HypoLev1	<ul style="list-style-type: none"> • gap= 60 • minLen= 13 • label= Hypoglycemia • levels= hypoglycemia
HighLevelAgg_NormoBG	<ul style="list-style-type: none"> • gap= 60 • minLen= 13 • label= Euglycemia • levels= euglycemia
HighLevelAgg_NormoDawn	<ul style="list-style-type: none"> • gap= 60 • minLen= 60 • label= Euglycemia • levels= euglycemia
HighLevelAgg_NormoHR	<ul style="list-style-type: none"> • gap= 10 • minLen= 5 • label= Normocardia

Temporal abstractions workflows

	<ul style="list-style-type: none"> • levels= normocardia
HighLevelAgg_Tachy	<ul style="list-style-type: none"> • gap= 10 • minLen= 5 • label= Tachycardia • levels= tachycardia
HRDec	<ul style="list-style-type: none"> • minLen= 6 • label= Increasing • minSlope= -200 • maxSlope= -1.3 • gap= 30
HRFastInc	<ul style="list-style-type: none"> • minLen= 6 • label= Increasing • minSlope= 3.5 • maxSlope= 200 • gap= 30
HRInc	<ul style="list-style-type: none"> • minLen= 6 • label= Increasing • minSlope= 1.3 • maxSlope= 200 • gap= 30
HRStat	<ul style="list-style-type: none"> • minLen= 6 • label= Stationarity • minSlope= -1.6 • maxSlope= 1.6 • gap= 30
OVERLAPS	<ul style="list-style-type: none"> • ls= 540 • rs= 540 • gap= -480
PRECEDES	<ul style="list-style-type: none"> • ls= 540 • rs= 540 • gap= 45
PRECEDES_BradyNormo	<ul style="list-style-type: none"> • ls= 60 • rs= 60 • gap= 25
PRECEDES_HypoTachy	<ul style="list-style-type: none"> • ls= 30 • rs= 120 • gap= 20
PRECEDES_NormoTachy	<ul style="list-style-type: none"> • ls= 60 • rs= 60 • gap= 25
PRECEDES_TachyDec	<ul style="list-style-type: none"> • ls= 30 • rs= 120 • gap= 20
PRECEDES_TachyHypo	<ul style="list-style-type: none"> • ls= 40 • rs= 90 • gap= 0
qualitativeGlycemia*	<ul style="list-style-type: none"> • label= hypoglycemia_Lev2,hypoglycemia, euglycemia, hyperglycemia,hyperglycemia_Lev2 • th= 54,70,181,251
qualitativeHR*	<ul style="list-style-type: none"> • label= bradycardia,normocardia,tachycardia • th= 60,101

ls: left shift; rs: right shift, minLen: minimum length of a pattern; maxSlope: maximum slope allowed in the pattern; minSlope: minimum slope allowed in the pattern. The asterisk (*) indicates that it is possible to use either fixed or subject-specific thresholds.

Appendix C

Descriptive statistics using Fitbit activities information

Fitbit activity information have been used also to provide clinicians with visual overviews of patients' conditions. Figure C.1 and Figure C.2 present a boxplot representation of HR measurements per patient, whereas the daily activities distribution is shown in Figure C.3 and Figure C.4, considering the pediatric and adult datasets, respectively. Then, the average number and average duration of automatically detected workouts per week are shown in Figure C.5 and Figure C.7 for pediatric patients, while in Figure C.6 and C.8 for adult patients. Finally, sleep quality can be explored in Figure C.9 and Figure C.10.

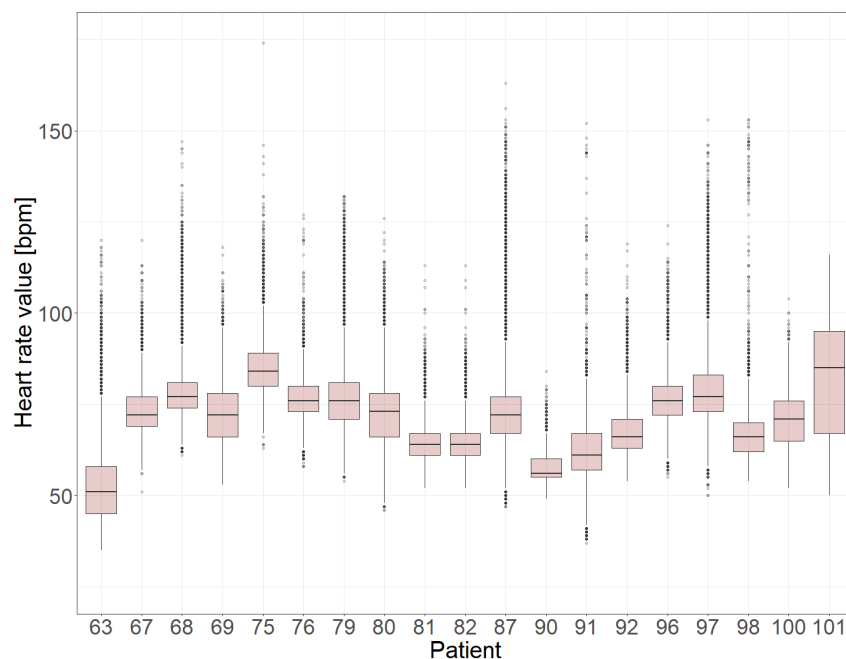


Figure C.1: Boxplot representation of heart rate (HR) measurements per patient in the pediatric dataset.

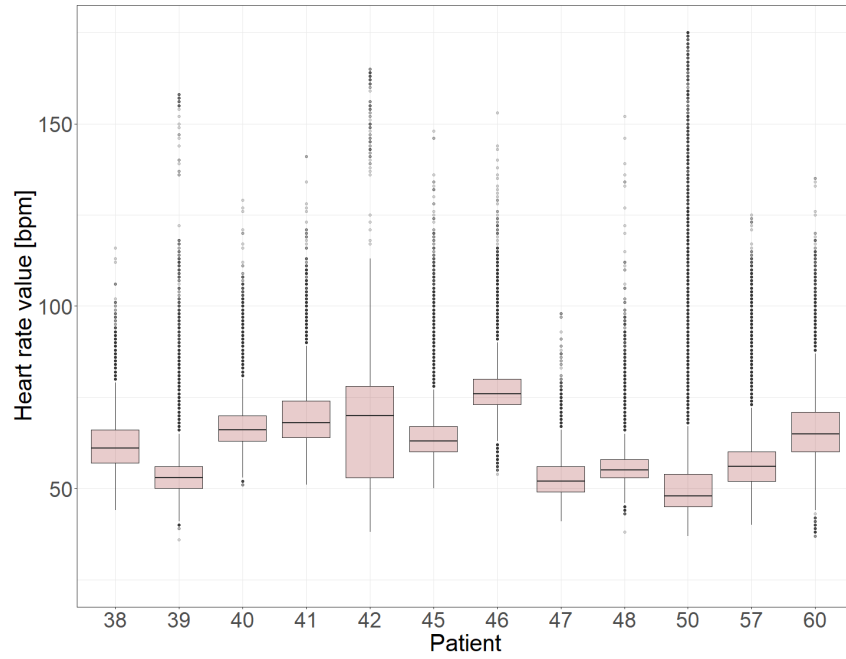


Figure C.2: Boxplot representation of heart rate (HR) measurements per patient in the adult dataset.

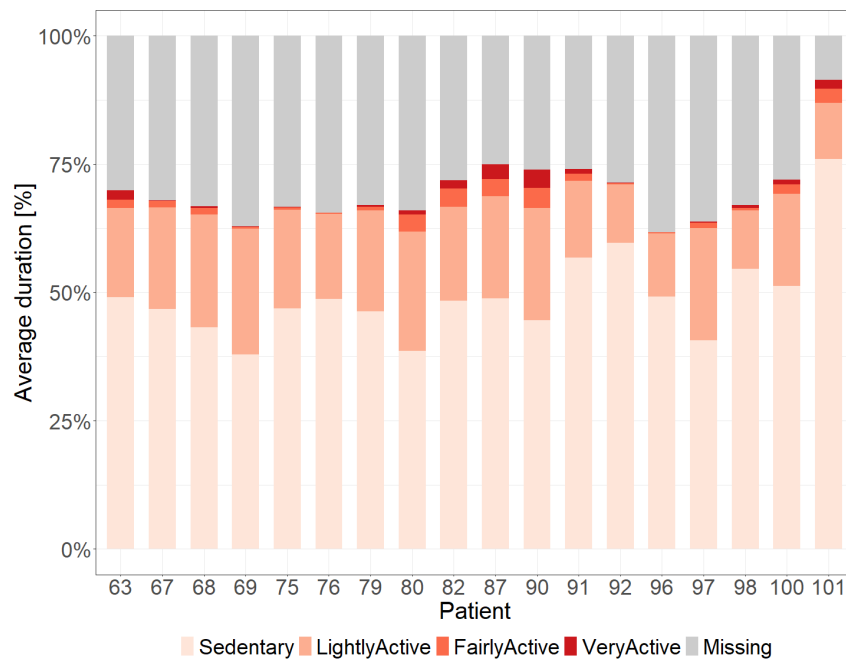


Figure C.3: Average duration of daily activities by intensity level in the pediatric dataset.

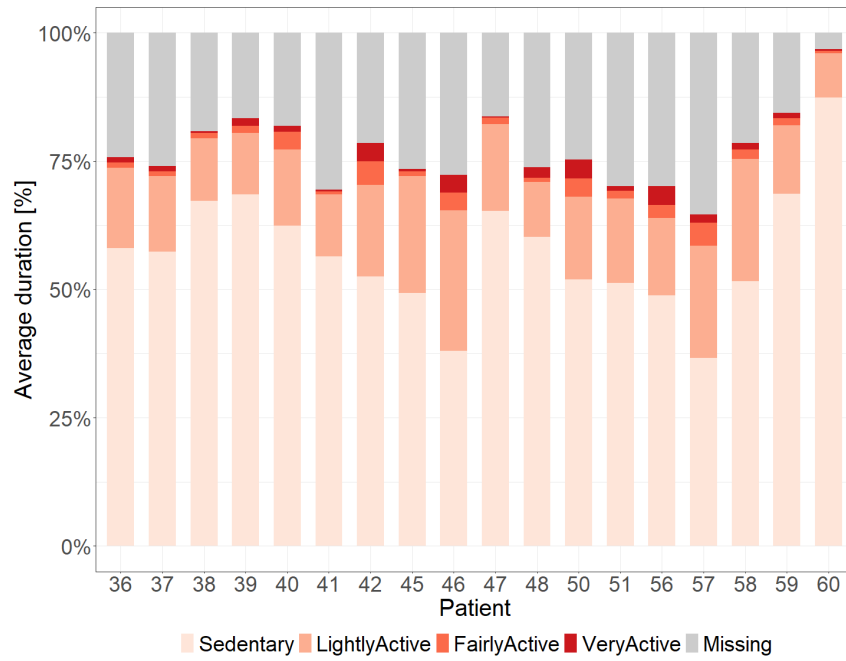


Figure C.4: Average duration of daily activities by intensity level in the adult dataset.

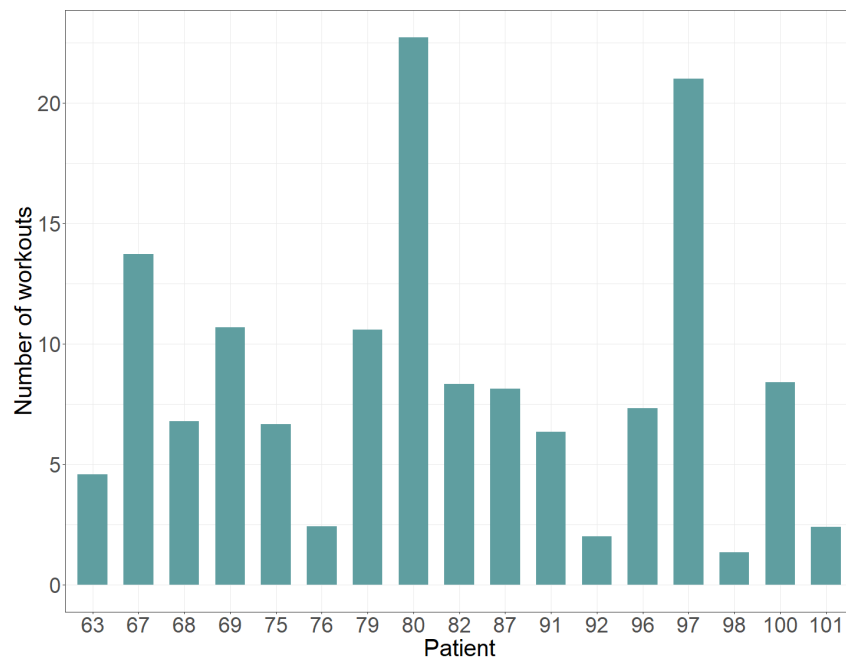


Figure C.5: Average number of automatically detected workouts per week in the pediatric dataset.

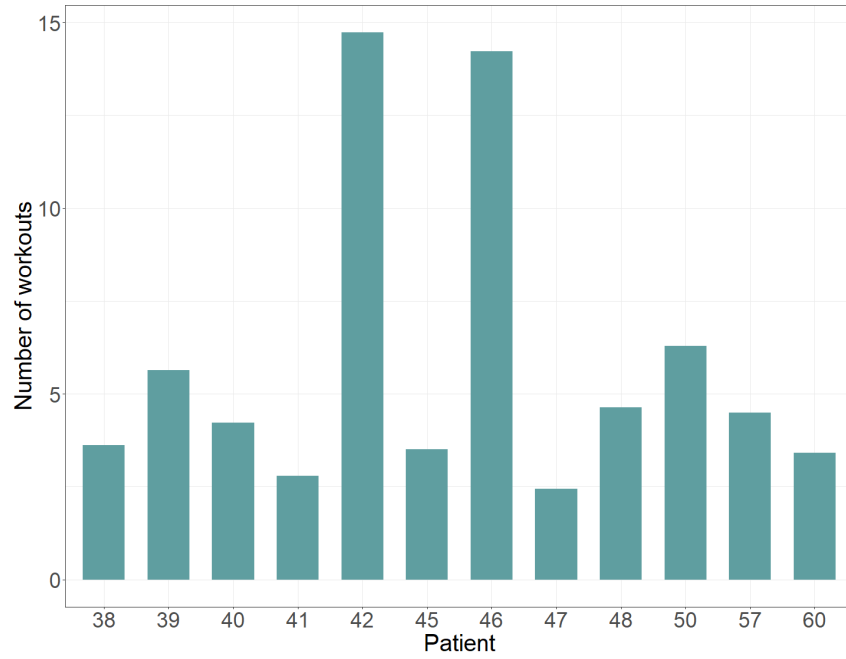


Figure C.6: Average number of automatically detected workouts per week in the adult dataset.

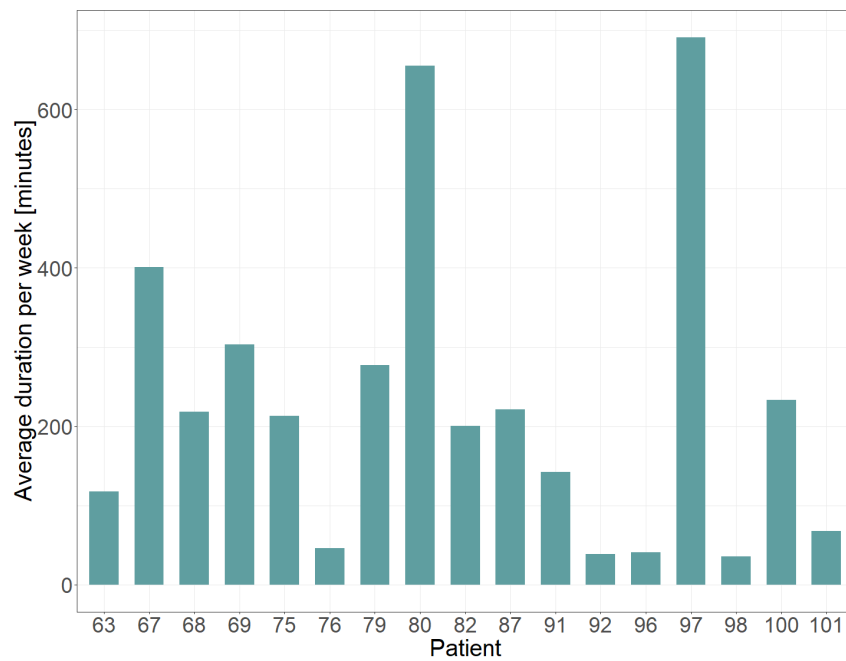


Figure C.7: Average duration of automatically detected workouts per week in the pediatric dataset.

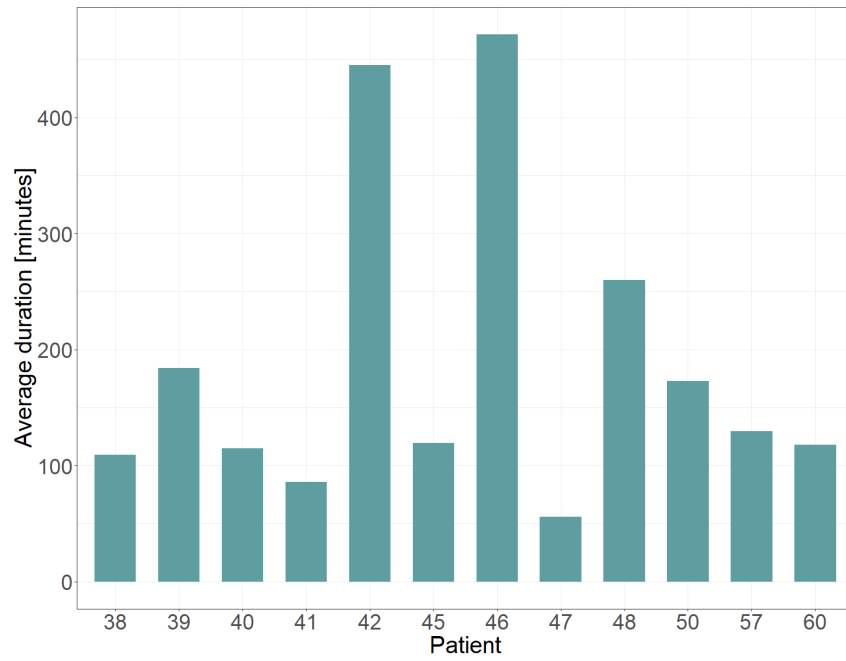


Figure C.8: Average duration of automatically detected workouts per week in the pediatric dataset.

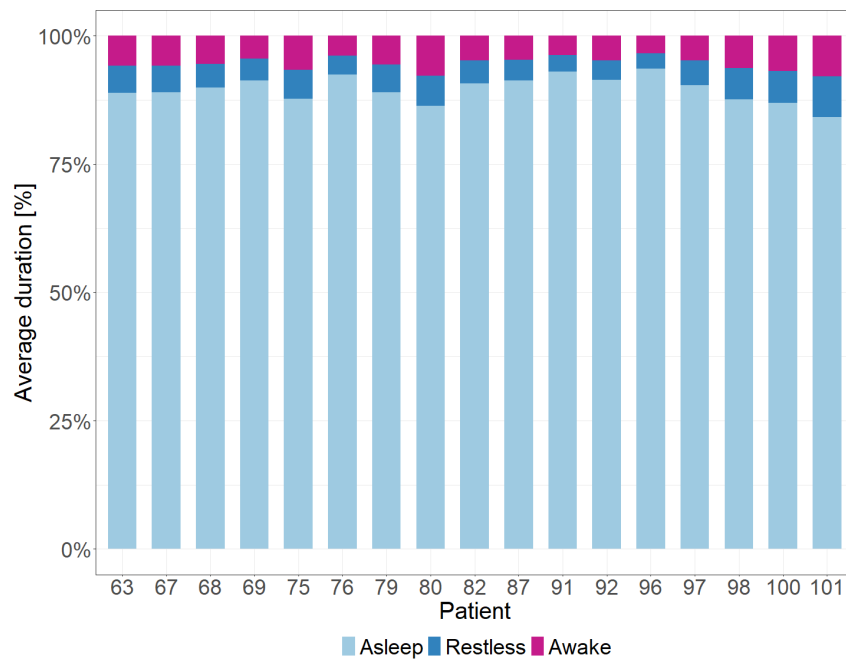


Figure C.9: Average main sleep duration by type in the pediatric dataset.

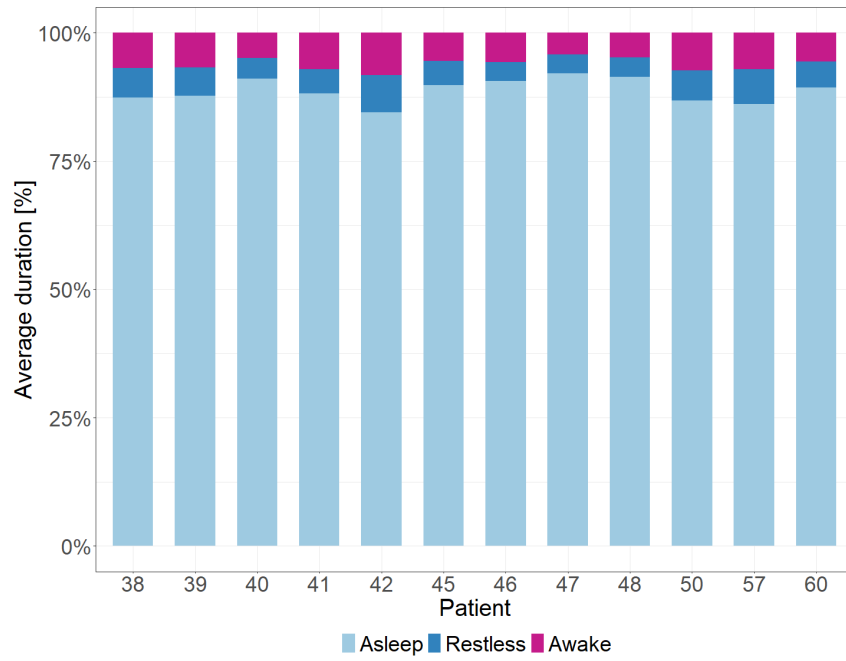


Figure C.10: Average duration of automatically detected workouts per week in the adult dataset.

References

- [1] World Health Organization, *Classification of diabetes mellitus - 2019*. Accessed: Aug. 02, 2021. [Online]. Available: <https://apps.who.int/iris/handle/10665/325182>
- [2] International Diabetes Federation, “IDF Diabetes Atlas 9th edition 2019.” <https://www.diabetesatlas.org/en/> (accessed Jul. 28, 2021).
- [3] American Diabetes Association, “1. Improving Care and Promoting Health in Populations: Standards of Medical Care in Diabetes-2021,” *Diabetes Care*, vol. 44, no. Suppl 1, pp. S7–S14, Jan. 2021, doi: 10.2337/dc21-S001.
- [4] A. Ramachandran, C. Snehalatha, and A. Nanditha, “Classification and Diagnosis of Diabetes,” in *Textbook of Diabetes*, John Wiley & Sons, Ltd, 2017, pp. 23–28. doi: 10.1002/9781118924853.ch2.
- [5] American Diabetes Association, “2. Classification and Diagnosis of Diabetes: Standards of Medical Care in Diabetes—2021,” *Diabetes Care*, vol. 44, no. Supplement 1, pp. S15–S33, Jan. 2021, doi: 10.2337/dc21-S002.
- [6] T. Tuomi, N. Santoro, S. Caprio, M. Cai, J. Weng, and L. Groop, “The many faces of diabetes: a disease with increasing heterogeneity,” *Lancet*, vol. 383, no. 9922, pp. 1084–1094, Mar. 2014, doi: 10.1016/S0140-6736(13)62219-9.
- [7] P. M. Jones and S. J. Persaud, “Islet Function and Insulin Secretion,” in *Textbook of Diabetes*, John Wiley & Sons, Ltd, 2017, pp. 87–102. doi: 10.1002/9781118924853.ch6.
- [8] S. Gough and P. Narendran, “Insulin and Insulin Treatment,” in *Textbook of Diabetes*, John Wiley & Sons, Ltd, 2017, pp. 399–413. doi: 10.1002/9781118924853.ch29.
- [9] P. E. Cryer, “The Barrier of Hypoglycemia in Diabetes,” *Diabetes*, vol. 57, no. 12, pp. 3169–3176, Dec. 2008, doi: 10.2337/db08-1084.
- [10] O. Sovik and H. Thordarson, “Dead-in-bed syndrome in young diabetic patients,” *Diabetes Care*, vol. 22 Suppl 2, pp. B40-42, Mar. 1999.

- [11] D. Koltin and D. Daneman, “Dead-in-bed syndrome - a diabetes nightmare,” *Pediatr Diabetes*, vol. 9, no. 5, pp. 504–507, Oct. 2008, doi: 10.1111/j.1399-5448.2008.00404.x.
- [12] S. Alshiekh, H. E. Larsson, S.-A. Ivarsson, and Å. Lernmark, “Autoimmune Type 1 Diabetes,” in *Textbook of Diabetes*, John Wiley & Sons, Ltd, 2017, pp. 143–153. doi: 10.1002/9781118924853.ch10.
- [13] M. J. Lenhard and G. D. Reeves, “Continuous Subcutaneous Insulin Infusion: A Comprehensive Review of Insulin Pump Therapy,” *Archives of Internal Medicine*, vol. 161, no. 19, pp. 2293–2300, Oct. 2001, doi: 10.1001/archinte.161.19.2293.
- [14] S. E. Inzucchi, “Diagnosis of diabetes,” *N Engl J Med*, vol. 368, no. 2, p. 193, Jan. 2013, doi: 10.1056/NEJMc1212738.
- [15] K. D. Barnard and R. I. G. Holt, “The Aims of Diabetes Care,” in *Textbook of Diabetes*, John Wiley & Sons, Ltd, 2017, pp. 314–325. doi: 10.1002/9781118924853.ch23.
- [16] A. Farmer, “Monitoring Diabetes,” in *Textbook of Diabetes*, John Wiley & Sons, Ltd, 2017, pp. 374–384. doi: 10.1002/9781118924853.ch27.
- [17] American Diabetes Association, “6. Glycemic Targets: Standards of Medical Care in Diabetes—2021,” *Diabetes Care*, vol. 44, no. Supplement 1, pp. S73–S84, Jan. 2021, doi: 10.2337/dc21-S006.
- [18] R. Hanas and G. John, “2010 Consensus Statement on the Worldwide Standardization of the Hemoglobin A1C Measurement,” *Diabetes Care*, vol. 33, no. 8, pp. 1903–1904, Aug. 2010, doi: 10.2337/dc10-0953.
- [19] “About the NGSP.” <http://www.ngsp.org/bgground.asp> (accessed Aug. 13, 2021).
- [20] S. I. Sherwani, H. A. Khan, A. Ekhzaimy, A. Masood, and M. K. Sakharkar, “Significance of HbA1c Test in Diagnosis and Prognosis of Diabetic Patients,” *Biomark Insights*, vol. 11, pp. 95–104, Jul. 2016, doi: 10.4137/BMI.S38440.
- [21] Linda A. DiMeglio *et al.*, “ISPAD Clinical Practice Consensus Guidelines 2018: Glycemic control targets and glucose monitoring for children, adolescents, and young adults with diabetes,” *Pediatric Diabetes*, vol. 19, no. S27, pp. 105–114, 2018, doi: 10.1111/pedi.12737.
- [22] R. Hanas and W. G. John, “2013 update on the worldwide standardization of the hemoglobin A1c measurement,” *Clinical Chemistry and Laboratory Medicine*, vol. 51, no. 5, pp. 1041–1042, May 2013, doi: 10.1515/cclm-2013-0161.

-
- [23] T. Battelino *et al.*, “Clinical Targets for Continuous Glucose Monitoring Data Interpretation: Recommendations From the International Consensus on Time in Range,” *Diabetes Care*, Jun. 2019, doi: 10.2337/dci19-0028.
- [24] G. Freckmann, S. Pleus, M. Grady, S. Setford, and B. Levy, “Measures of Accuracy for Continuous Glucose Monitoring and Blood Glucose Monitoring Devices,” *J Diabetes Sci Technol*, vol. 13, no. 3, pp. 575–583, Nov. 2018, doi: 10.1177/1932296818812062.
- [25] Y. Handelsman *et al.*, “American association of clinical endocrinologists and american college of endocrinology - clinical practice guidelines for developing a diabetes mellitus comprehensive care plan - 2015,” *Endocr Pract*, vol. 21 Suppl 1, pp. 1–87, Apr. 2015, doi: 10.4158/EP15672.GL.
- [26] K. M. Miller *et al.*, “Evidence of a Strong Association Between Frequency of Self-Monitoring of Blood Glucose and Hemoglobin A1c Levels in T1D Exchange Clinic Registry Participants,” *Diabetes Care*, vol. 36, no. 7, pp. 2009–2014, Jul. 2013, doi: 10.2337/dc12-1770.
- [27] R. Ziegler *et al.*, “Frequency of SMBG correlates with HbA1c and acute complications in children and adolescents with type 1 diabetes,” *Pediatr Diabetes*, vol. 12, no. 1, pp. 11–17, Feb. 2011, doi: 10.1111/j.1399-5448.2010.00650.x.
- [28] M. Schütt *et al.*, “Is the frequency of self-monitoring of blood glucose related to long-term metabolic control? Multicenter analysis including 24,500 patients from 191 centers in Germany and Austria,” *Exp Clin Endocrinol Diabetes*, vol. 114, no. 7, pp. 384–388, Jul. 2006, doi: 10.1055/s-2006-924152.
- [29] “ISO 15197:2013. In vitro diagnostic test systems - Requirements for blood-glucose monitoring systems for self-testing in managing diabetes mellitus.” <https://www.iso.org/cms/render/live/en/sites/isoorg/contents/data/standard/05/49/54976.html> (accessed Aug. 18, 2021).
- [30] “Self-Monitoring Blood Glucose Test Systems for Over-the-Counter Use.” <https://www.fda.gov/regulatory-information/search-fda-guidance-documents/self-monitoring-blood-glucose-test-systems-over-counter-use> (accessed Aug. 18, 2021).
- [31] American Diabetes Association, “7. Diabetes Technology: Standards of Medical Care in Diabetes—2021,” *Diabetes Care*, vol. 44, no. Supplement 1, pp. S85–S99, Jan. 2021, doi: 10.2337/dc21-S007.

- [32] G. Cappon, M. Vettoretti, G. Sparacino, and A. Facchinetti, “Continuous Glucose Monitoring Sensors for Diabetes Management: A Review of Technologies and Applications,” *Diabetes Metab J*, vol. 43, no. 4, pp. 383–397, Aug. 2019, doi: 10.4093/dmj.2019.0121.
- [33] G. Freckmann, “Basics and use of continuous glucose monitoring (CGM) in diabetes therapy,” *Journal of Laboratory Medicine*, vol. 44, no. 2, pp. 71–79, Apr. 2020, doi: 10.1515/labmed-2019-0189.
- [34] E. Cengiz and W. V. Tamborlane, “A Tale of Two Compartments: Interstitial Versus Blood Glucose Monitoring,” *Diabetes Technol Ther*, vol. 11, no. Suppl 1, p. S-11-S-16, Jun. 2009, doi: 10.1089/dia.2009.0002.
- [35] R. S. Mazze, D. Lucido, O. Langer, K. Hartmann, and D. Rodbard, “Ambulatory glucose profile: representation of verified self-monitored blood glucose data,” *Diabetes Care*, vol. 10, no. 1, pp. 111–117, Feb. 1987, doi: 10.2337/diacare.10.1.111.
- [36] R. M. Bergenstal *et al.*, “Recommendations for Standardizing Glucose Reporting and Analysis to Optimize Clinical Decision Making in Diabetes: The Ambulatory Glucose Profile (AGP),” *Diabetes Technology & Therapeutics*, vol. 15, no. 3, pp. 198–211, Mar. 2013, doi: 10.1089/dia.2013.0051.
- [37] D. Olczuk and R. Priefer, “A history of continuous glucose monitors (CGMs) in self-monitoring of diabetes mellitus,” *Diabetes Metab Syndr*, vol. 12, no. 2, pp. 181–187, Jun. 2018, doi: 10.1016/j.dsx.2017.09.005.
- [38] Dexcom, “Upcoming Obsolescence for the United States: Dexcom G4 Platinum/G5 Mobile CGM Systems.” <https://www.dexcom.com/obsolescence> (accessed Aug. 30, 2021).
- [39] Dexcom, “G6 CGM System.” <https://www.dexcom.com/g6-cgm-system> (accessed Aug. 27, 2021).
- [40] Medtronic, “Enlite CGM Sensor.” <https://www.medtronic.com/ca-en/diabetes/home/products/cgm-systems/enlite-sensor.html> (accessed Aug. 30, 2021).
- [41] Medtronic, “Guardian Sensor 3 CGM System.” <https://www.medtronic.com/us-en/healthcare-professionals/products/diabetes/continuous-glucose-monitoring-systems/guardian-sensor-3.html> (accessed Aug. 27, 2021).

-
- [42] Senseonics, “Eversense CGM System.” <https://www.ascensiadiabetes.com/eversense/eversense-cgm-system> (accessed Aug. 30, 2021).
- [43] Abbott, “FreeStyle Libre FGM System.” <https://www.freestyle.abbott/us-en/> (accessed Aug. 27, 2021).
- [44] J. Edge *et al.*, “An alternative sensor-based method for glucose monitoring in children and young people with diabetes,” *Archives of Disease in Childhood*, vol. 102, no. 6, pp. 543–549, Jun. 2017, doi: 10.1136/archdischild-2016-311530.
- [45] Abbott, “FreeStyle Libre 2 FGM System.” <https://www.freestyle.abbott/us-en/> (accessed Aug. 27, 2021).
- [46] Abbott, “FreeStyle Libre 2 iCGM cleared in U.S. for adults and children with diabetes, achieving highest level of accuracy and performance standards.” <https://abbott.mediaroom.com/2020-06-15-Abbotts-FreeStyle-R-Libre-2-iCGM-Cleared-in-U-S-for-Adults-and-Children-with-Diabetes-Achieving-Highest-Level-of-Accuracy-and-Performance-Standards> (accessed Sep. 03, 2021).
- [47] Dexcom, “FDA authorizes marketing of the new Dexcom G6 CGM eliminating the need for fingerstick blood testing for people with diabetes,” Mar. 27, 2018. <https://www.dexcom.com/news/fda-authorizes-dexcom-g6> (accessed Sep. 03, 2021).
- [48] R. Longo and S. Sperling, “Personal Versus Professional Continuous Glucose Monitoring: When to Use Which on Whom,” *Diabetes Spectrum*, vol. 32, no. 3, pp. 183–193, Aug. 2019, doi: 10.2337/ds18-0093.
- [49] R. Vigersky and M. Shrivastav, “Role of continuous glucose monitoring for type 2 in diabetes management and research,” *Journal of Diabetes and its Complications*, vol. 31, no. 1, pp. 280–287, Jan. 2017, doi: 10.1016/j.jdiacomp.2016.10.007.
- [50] Abbott, “FreeStyle Libre Pro FGM System.” <https://www.freestyle.abbott/in-en/products/freestyle-libre-pro.html> (accessed Aug. 23, 2021).
- [51] Medtronic, “iPro2 Professional CGM System.” <https://www.medtronic.com/ca-en/diabetes/home/products/cgm-systems/ipro2-professional.html> (accessed Aug. 23, 2021).
- [52] Dexcom, “G6 Pro CGM System.” <https://www.dexcompro.com/> (accessed Aug. 23, 2021).

- [53] I. B. Hirsch and E. E. Wright, “Using Flash Continuous Glucose Monitoring in Primary Practice,” *Clinical Diabetes*, vol. 37, no. 2, pp. 150–161, Apr. 2019, doi: 10.2337/cd18-0054.
- [54] The Juvenile Diabetes Research Foundation Continuous Glucose Monitoring Study Group, “Continuous Glucose Monitoring and Intensive Treatment of Type 1 Diabetes.” <https://www.nejm.org/doi/10.1056/NEJMoa0805017> (accessed Sep. 06, 2021).
- [55] M. Lind *et al.*, “Continuous Glucose Monitoring vs Conventional Therapy for Glycemic Control in Adults With Type 1 Diabetes Treated With Multiple Daily Insulin Injections: The GOLD Randomized Clinical Trial,” *JAMA*, vol. 317, no. 4, pp. 379–387, Jan. 2017, doi: 10.1001/jama.2016.19976.
- [56] R. W. Beck *et al.*, “Effect of Continuous Glucose Monitoring on Glycemic Control in Adults With Type 1 Diabetes Using Insulin Injections: The DIAMOND Randomized Clinical Trial,” *JAMA*, vol. 317, no. 4, pp. 371–378, Jan. 2017, doi: 10.1001/jama.2016.19975.
- [57] G. Aleppo *et al.*, “REPLACE-BG: A Randomized Trial Comparing Continuous Glucose Monitoring With and Without Routine Blood Glucose Monitoring in Adults With Well-Controlled Type 1 Diabetes,” *Diabetes Care*, vol. 40, no. 4, pp. 538–545, Apr. 2017, doi: 10.2337/dc16-2482.
- [58] L. Heinemann *et al.*, “Real-time continuous glucose monitoring in adults with type 1 diabetes and impaired hypoglycaemia awareness or severe hypoglycaemia treated with multiple daily insulin injections (HypoDE): a multicentre, randomised controlled trial,” *Lancet*, vol. 391, no. 10128, pp. 1367–1377, Apr. 2018, doi: 10.1016/S0140-6736(18)30297-6.
- [59] C. A. J. van Beers *et al.*, “Continuous glucose monitoring for patients with type 1 diabetes and impaired awareness of hypoglycaemia (IN CONTROL): a randomised, open-label, crossover trial,” *Lancet Diabetes Endocrinol*, vol. 4, no. 11, pp. 893–902, Nov. 2016, doi: 10.1016/S2213-8587(16)30193-0.
- [60] J. Bolinder, R. Antuna, P. Geelhoed-Duijvestijn, J. Kröger, and R. Weitgasser, “Novel glucose-sensing technology and hypoglycaemia in type 1 diabetes: a multicentre, non-masked, randomised controlled trial,” *The Lancet*, vol. 388, no. 10057, pp. 2254–2263, Nov. 2016, doi: 10.1016/S0140-6736(16)31535-5.
- [61] R. M. Bergenstal *et al.*, “Effectiveness of sensor-augmented insulin-pump therapy in type 1 diabetes,” *N Engl J Med*, vol.

-
- 363, no. 4, pp. 311–320, Jul. 2010, doi: 10.1056/NEJMoa1002853.
- [62] R. W. Beck *et al.*, “Continuous Glucose Monitoring Versus Usual Care in Patients With Type 2 Diabetes Receiving Multiple Daily Insulin Injections,” *Annals of Internal Medicine*, Aug. 2017, Accessed: Sep. 07, 2021. [Online]. Available: <https://www.acpjournals.org/doi/abs/10.7326/M16-2855>
- [63] S. Suh and J. H. Kim, “Glycemic Variability: How Do We Measure It and Why Is It Important?,” *Diabetes Metab J*, vol. 39, no. 4, pp. 273–282, Aug. 2015, doi: 10.4093/dmj.2015.39.4.273.
- [64] A. Nusca *et al.*, “Glycemic variability in the development of cardiovascular complications in diabetes,” *Diabetes Metab Res Rev*, vol. 34, no. 8, p. e3047, Nov. 2018, doi: 10.1002/dmrr.3047.
- [65] Z. Zhou, B. Sun, S. Huang, C. Zhu, and M. Bian, “Glycemic variability: adverse clinical outcomes and how to improve it?,” *Cardiovasc Diabetol*, vol. 19, p. 102, Jul. 2020, doi: 10.1186/s12933-020-01085-6.
- [66] D. Rodbard, “Optimizing display, analysis, interpretation and utility of self-monitoring of blood glucose (SMBG) data for management of patients with diabetes,” *J Diabetes Sci Technol*, vol. 1, no. 1, pp. 62–71, Jan. 2007, doi: 10.1177/193229680700100111.
- [67] D. Rodbard, “New and improved methods to characterize glycemic variability using continuous glucose monitoring,” *Diabetes Technol Ther*, vol. 11, no. 9, pp. 551–565, Sep. 2009, doi: 10.1089/dia.2009.0015.
- [68] J. Schlichtkrull, O. Munck, and M. Jersild, “The M-Value, an Index of Blood-sugar Control in Diabetics,” *Acta Medica Scandinavica*, vol. 177, no. 1, pp. 95–102, 1965, doi: 10.1111/j.0954-6820.1965.tb01810.x.
- [69] J. M. Wójcicki, “Mathematical descriptions of the glucose control in diabetes therapy. Analysis of the Schlichtkrull ‘M’-value,” *Horm Metab Res*, vol. 27, no. 1, pp. 1–5, Jan. 1995, doi: 10.1055/s-2007-979895.
- [70] F. J. Service, “Glucose Variability,” *Diabetes*, vol. 62, no. 5, pp. 1398–1404, May 2013, doi: 10.2337/db12-1396.
- [71] F. J. Service and R. L. Nelson, “Characteristics of Glycemic Stability,” *Diabetes Care*, vol. 3, no. 1, pp. 58–62, Jan. 1980, doi: 10.2337/diacare.3.1.58.

- [72] J. M. Wójcicki, “‘J’-Index. A New Proposition of the Assessment of Current Glucose Control in Diabetic Patients,” *Horm Metab Res*, vol. 27, no. 1, pp. 41–42, Jan. 1995, doi: 10.1055/s-2007-979906.
- [73] C. M. McDonnell, S. M. Donath, S. I. Vidmar, G. A. Werther, and F. J. Cameron, “A novel approach to continuous glucose analysis utilizing glycemic variation,” *Diabetes Technol Ther*, vol. 7, no. 2, pp. 253–263, Apr. 2005, doi: 10.1089/dia.2005.7.253.
- [74] G. D. Molnar, W. F. Taylor, and M. M. Ho, “Day-to-day variation of continuously monitored glycaemia: a further measure of diabetic instability,” *Diabetologia*, vol. 8, no. 5, pp. 342–348, Nov. 1972, doi: 10.1007/BF01218495.
- [75] G. Agiostratidou *et al.*, “Standardizing Clinically Meaningful Outcome Measures Beyond HbA1c for Type 1 Diabetes: A Consensus Report of the American Association of Clinical Endocrinologists, the American Association of Diabetes Educators, the American Diabetes Association, the Endocrine Society, JDRF International, The Leona M. and Harry B. Helmsley Charitable Trust, the Pediatric Endocrine Society, and the T1D Exchange,” *Diabetes Care*, vol. 40, no. 12, pp. 1622–1630, Dec. 2017, doi: 10.2337/dc17-1624.
- [76] B. P. Kovatchev, “Metrics for glycaemic control — from HbA1c to continuous glucose monitoring,” *Nat Rev Endocrinol*, vol. 13, no. 7, pp. 425–436, Jul. 2017, doi: 10.1038/nrendo.2017.3.
- [77] B. P. Kovatchev, D. J. Cox, L. A. Gonder-Frederick, and W. Clarke, “Symmetrization of the blood glucose measurement scale and its applications,” *Diabetes Care*, vol. 20, no. 11, pp. 1655–1658, Nov. 1997, doi: 10.2337/diacare.20.11.1655.
- [78] B. P. Kovatchev, D. J. Cox, A. Kumar, L. Gonder-Frederick, and W. L. Clarke, “Algorithmic evaluation of metabolic control and risk of severe hypoglycemia in type 1 and type 2 diabetes using self-monitoring blood glucose data,” *Diabetes Technol Ther*, vol. 5, no. 5, pp. 817–828, 2003, doi: 10.1089/152091503322527021.
- [79] B. P. Kovatchev, W. L. Clarke, M. Breton, K. Brayman, and A. McCall, “Quantifying Temporal Glucose Variability in Diabetes via Continuous Glucose Monitoring: Mathematical Methods and Clinical Application,” *Diabetes Technology & Therapeutics*, vol. 7, no. 6, pp. 849–862, Dec. 2005, doi: 10.1089/dia.2005.7.849.

-
- [80] B. P. Kovatchev, E. Otto, D. Cox, L. Gonder-Frederick, and W. Clarke, "Evaluation of a new measure of blood glucose variability in diabetes," *Diabetes Care*, vol. 29, no. 11, pp. 2433–2438, Nov. 2006, doi: 10.2337/dc06-1085.
- [81] N. R. Hill, P. C. Hindmarsh, R. J. Stevens, I. M. Stratton, J. C. Levy, and D. R. Matthews, "A method for assessing quality of control from glucose profiles," *Diabet Med*, vol. 24, no. 7, pp. 753–758, Jul. 2007, doi: 10.1111/j.1464-5491.2007.02119.x.
- [82] D. Rodbard, "Interpretation of continuous glucose monitoring data: glycemic variability and quality of glycemic control," *Diabetes Technol Ther*, vol. 11 Suppl 1, pp. S55-67, Jun. 2009, doi: 10.1089/dia.2008.0132.
- [83] F. J. Service, G. D. Molnar, J. W. Rosevear, E. Ackerman, L. C. Gatewood, and W. F. Taylor, "Mean Amplitude of Glycemic Excursions, a Measure of Diabetic Instability," *Diabetes*, vol. 19, no. 9, pp. 644–655, Sep. 1970, doi: 10.2337/diab.19.9.644.
- [84] D. Czerwoniuk, W. Fendler, L. Walenciak, and W. Mlynarski, "GlyCulator: A Glycemic Variability Calculation Tool for Continuous Glucose Monitoring Data," *J Diabetes Sci Technol*, vol. 5, no. 2, pp. 447–451, Mar. 2011.
- [85] N. R. Hill, N. S. Oliver, P. Choudhary, J. C. Levy, P. Hindmarsh, and D. R. Matthews, "Normal Reference Range for Mean Tissue Glucose and Glycemic Variability Derived from Continuous Glucose Monitoring for Subjects Without Diabetes in Different Ethnic Groups," *Diabetes Technol Ther*, vol. 13, no. 9, pp. 921–928, Sep. 2011, doi: 10.1089/dia.2010.0247.
- [86] G. Fritzsche, K.-D. Kohnert, P. Heinke, L. Vogt, and E. Salzsieder, "The use of a computer program to calculate the mean amplitude of glycemic excursions," *Diabetes Technol Ther*, vol. 13, no. 3, pp. 319–325, Mar. 2011, doi: 10.1089/dia.2010.0108.
- [87] P. A. Baghurst, "Calculating the mean amplitude of glycemic excursion from continuous glucose monitoring data: an automated algorithm," *Diabetes Technol Ther*, vol. 13, no. 3, pp. 296–302, Mar. 2011, doi: 10.1089/dia.2010.0090.
- [88] M. K. Sechterberger, Y. M. Luijf, and J. H. Devries, "Poor agreement of computerized calculators for mean amplitude of glycemic excursions," *Diabetes Technol Ther*, vol. 16, no. 2, pp. 72–75, Feb. 2014, doi: 10.1089/dia.2013.0138.
- [89] D. Rodbard, "Glucose Variability: A Review of Clinical Applications and Research Developments," *Diabetes*

- Technology & Therapeutics*, vol. 20, no. S2, pp. S2-5, Jun. 2018, doi: 10.1089/dia.2018.0092.
- [90] S. Garg and L. Jovanovic, “Relationship of Fasting and Hourly Blood Glucose Levels to HbA1c Values: Safety, accuracy, and improvements in glucose profiles obtained using a 7-day continuous glucose sensor,” *Diabetes Care*, vol. 29, no. 12, pp. 2644–2649, Dec. 2006, doi: 10.2337/dc06-1361.
- [91] S. Garg *et al.*, “Improvement in glycemic excursions with a transcutaneous, real-time continuous glucose sensor: a randomized controlled trial,” *Diabetes Care*, vol. 29, no. 1, pp. 44–50, Jan. 2006, doi: 10.2337/diacare.29.01.06.dc05-1686.
- [92] R. W. Beck *et al.*, “Validation of Time in Range as an Outcome Measure for Diabetes Clinical Trials,” *Diabetes Care*, vol. 42, no. 3, pp. 400–405, Mar. 2019, doi: 10.2337/dc18-1444.
- [93] R. W. Beck *et al.*, “The Relationships Between Time in Range, Hyperglycemia Metrics, and HbA1c:,” *Journal of Diabetes Science and Technology*, Jan. 2019, doi: 10.1177/1932296818822496.
- [94] R. A. Vigersky and C. McMahon, “The Relationship of Hemoglobin A1C to Time-in-Range in Patients with Diabetes,” *Diabetes Technology & Therapeutics*, vol. 21, no. 2, pp. 81–85, Dec. 2018, doi: 10.1089/dia.2018.0310.
- [95] P. J. Brockwell and R. A. Davis, “Introduction,” in *Introduction to Time Series and Forecasting*, P. J. Brockwell and R. A. Davis, Eds. Cham: Springer International Publishing, 2016, pp. 1–37. doi: 10.1007/978-3-319-29854-2_1.
- [96] I. Rodríguez-Rodríguez, I. Chatzigiannakis, J.-V. Rodríguez, M. Maranghi, M. Gentili, and M.-Á. Zamora-Izquierdo, “Utility of Big Data in Predicting Short-Term Blood Glucose Levels in Type 1 Diabetes Mellitus Through Machine Learning Techniques,” *Sensors (Basel)*, vol. 19, no. 20, p. E4482, Oct. 2019, doi: 10.3390/s19204482.
- [97] S. Oviedo, J. Vehí, R. Calm, and J. Armengol, “A review of personalized blood glucose prediction strategies for T1DM patients,” *Int J Numer Method Biomed Eng*, vol. 33, no. 6, Jun. 2017, doi: 10.1002/cnm.2833.
- [98] J. Reifman, S. Rajaraman, A. Gribok, and W. K. Ward, “Predictive Monitoring for Improved Management of Glucose Levels,” *J Diabetes Sci Technol*, vol. 1, no. 4, pp. 478–486, Jul. 2007.
- [99] G. Sparacino, F. Zanderigo, S. Corazza, A. Maran, A. Facchinetti, and C. Cobelli, “Glucose concentration can be

-
- predicted ahead in time from continuous glucose monitoring sensor time-series,” *IEEE Trans Biomed Eng*, vol. 54, no. 5, pp. 931–937, May 2007, doi: 10.1109/TBME.2006.889774.
- [100] A. Maran *et al.*, “Continuous subcutaneous glucose monitoring in diabetic patients: a multicenter analysis,” *Diabetes Care*, vol. 25, no. 2, pp. 347–352, Feb. 2002, doi: 10.2337/diacare.25.2.347.
- [101] M. Eren-Oruklu, A. Cinar, L. Quinn, and D. Smith, “Estimation of Future Glucose Concentrations with Subject-Specific Recursive Linear Models,” *Diabetes Technology & Therapeutics*, vol. 11, no. 4, pp. 243–253, Apr. 2009, doi: 10.1089/dia.2008.0065.
- [102] T. Hamdi, J. Ben Ali, V. Di Costanzo, F. Fnaiech, E. Moreau, and J.-M. Ginoux, “Accurate prediction of continuous blood glucose based on support vector regression and differential evolution algorithm,” *Biocybernetics and Biomedical Engineering*, vol. 38, no. 2, pp. 362–372, Jan. 2018, doi: 10.1016/j.bbe.2018.02.005.
- [103] C. Pérez-Gandía *et al.*, “Artificial neural network algorithm for online glucose prediction from continuous glucose monitoring,” *Diabetes Technol Ther*, vol. 12, no. 1, pp. 81–88, Jan. 2010, doi: 10.1089/dia.2009.0076.
- [104] J. Martinsson, A. Schliep, B. Eliasson, and O. Mogren, “Blood Glucose Prediction with Variance Estimation Using Recurrent Neural Networks,” *J Healthc Inform Res*, vol. 4, no. 1, pp. 1–18, Mar. 2020, doi: 10.1007/s41666-019-00059-y.
- [105] C. Marling and R. Bunescu, “The OhioT1DM Dataset for Blood Glucose Level Prediction: Update 2020,” *CEUR Workshop Proc*, vol. 2675, pp. 71–74, Sep. 2020.
- [106] Y. Wang, X. Wu, and X. Mo, “A Novel Adaptive-Weighted-Average Framework for Blood Glucose Prediction,” *Diabetes Technol Ther*, vol. 15, no. 10, pp. 792–801, Oct. 2013, doi: 10.1089/dia.2013.0104.
- [107] C. Zecchin, A. Facchinetti, G. Sparacino, and C. Cobelli, “Jump neural network for online short-time prediction of blood glucose from continuous monitoring sensors and meal information,” *Computer Methods and Programs in Biomedicine*, vol. 113, no. 1, pp. 144–152, Jan. 2014, doi: 10.1016/j.cmpb.2013.09.016.
- [108] D. A. Finan *et al.*, “Experimental Evaluation of a Recursive Model Identification Technique for Type 1 Diabetes,” *J Diabetes Sci Technol*, vol. 3, no. 5, pp. 1192–1202, Sep. 2009.

- [109] K. Turksoy, E. S. Bayrak, L. Quinn, E. Littlejohn, D. Rollins, and A. Cinar, “Hypoglycemia Early Alarm Systems Based On Multivariable Models,” *Ind Eng Chem Res*, vol. 52, no. 35, p. 10.1021/ie3034015, Sep. 2013, doi: 10.1021/ie3034015.
- [110] “BodyMedia Homepage.” <https://bodymedia.com/> (accessed Nov. 02, 2021).
- [111] C. Zhao, E. Dassau, L. Jovanovič, H. C. Zisser, F. J. Doyle, and D. E. Seborg, “Predicting Subcutaneous Glucose Concentration Using a Latent-Variable-Based Statistical Method for Type 1 Diabetes Mellitus,” *J Diabetes Sci Technol*, vol. 6, no. 3, pp. 617–633, May 2012.
- [112] C. D. Man, F. Micheletto, D. Lv, M. Breton, B. Kovatchev, and C. Cobelli, “The UVA/PADOVA Type 1 Diabetes Simulator,” *J Diabetes Sci Technol*, vol. 8, no. 1, pp. 26–34, Jan. 2014, doi: 10.1177/1932296813514502.
- [113] E. I. Georga *et al.*, “Multivariate prediction of subcutaneous glucose concentration in type 1 diabetes patients based on support vector regression,” *IEEE J Biomed Health Inform*, vol. 17, no. 1, pp. 71–81, Jan. 2013, doi: 10.1109/TITB.2012.2219876.
- [114] E. D. Lehmann and T. Deutsch, “A physiological model of glucose-insulin interaction in type 1 diabetes mellitus,” *J Biomed Eng*, vol. 14, no. 3, pp. 235–242, May 1992, doi: 10.1016/0141-5425(92)90058-s.
- [115] “METABO EU Project.” <https://cordis.europa.eu/project/id/216270> (accessed Nov. 03, 2021).
- [116] C. Zecchin, A. Facchinetti, G. Sparacino, G. De Nicolao, and C. Cobelli, “A new neural network approach for short-term glucose prediction using continuous glucose monitoring time-series and meal information,” *Annu Int Conf IEEE Eng Med Biol Soc*, vol. 2011, pp. 5653–5656, 2011, doi: 10.1109/IEMBS.2011.6091368.
- [117] “DIAdvisor EU Project.” <https://cordis.europa.eu/project/id/216592> (accessed Nov. 03, 2021).
- [118] “GluNet: A Deep Learning Framework for Accurate Glucose Forecasting | IEEE Journals & Magazine | IEEE Xplore.” <https://ieeexplore.ieee.org/document/8779644> (accessed Nov. 03, 2021).
- [119] M. Reddy *et al.*, “Clinical Safety and Feasibility of the Advanced Bolus Calculator for Type 1 Diabetes Based on Case-

-
- Based Reasoning: A 6-Week Nonrandomized Single-Arm Pilot Study,” *Diabetes Technol Ther*, vol. 18, no. 8, pp. 487–493, Aug. 2016, doi: 10.1089/dia.2015.0413.
- [120] A. Aliberti *et al.*, “A Multi-Patient Data-Driven Approach to Blood Glucose Prediction,” *IEEE Access*, vol. 7, pp. 69311–69325, 2019, doi: 10.1109/ACCESS.2019.2919184.
- [121] E. Salvi *et al.*, “Patient-Generated Health Data Integration and Advanced Analytics for Diabetes Management: The AID-GM Platform,” *Sensors*, vol. 20, no. 1, p. 128, Jan. 2020, doi: 10.3390/s20010128.
- [122] “JavaServer Faces Technology Overview.” <https://www.oracle.com/java/technologies/javaserverfaces.html> (accessed Oct. 11, 2021).
- [123] “Hibernate Home.” <https://hibernate.org/> (accessed Oct. 11, 2021).
- [124] “MySQL Home.” <https://www.mysql.com/> (accessed Oct. 11, 2021).
- [125] “Apache HttpClient Overview.” <https://hc.apache.org/httpcomponents-client-5.1.x/> (accessed Oct. 08, 2021).
- [126] “JSON Home.” <https://www.json.org/json-en.html> (accessed Oct. 08, 2021).
- [127] E. Salvi *et al.*, “Patient-Generated Health Data Integration and Advanced Analytics for Diabetes Management: The AID-GM Platform,” *Sensors*, vol. 20, no. 1, Art. no. 1, Jan. 2020, doi: 10.3390/s20010128.
- [128] Fitbit, “Fitbit Activity Trackers.” <https://www.fitbit.com/global/us/home> (accessed Oct. 05, 2021).
- [129] T. Somboon, M. M. Grigg-Damberger, and N. Foldvary-Schaefer, “Night Stepping: Fitbit Cracks the Case,” *J Clin Sleep Med*, vol. 15, no. 2, pp. 355–357, Feb. 2019, doi: 10.5664/jcsm.7646.
- [130] W. A. Marshall and J. M. Tanner, “Variations in pattern of pubertal changes in girls.,” *Arch Dis Child*, vol. 44, no. 235, pp. 291–303, Jun. 1969.
- [131] W. A. Marshall and J. M. Tanner, “Variations in the Pattern of Pubertal Changes in Boys,” *Arch Dis Child*, vol. 45, no. 239, pp. 13–23, Feb. 1970.
- [132] “The R software for statistical computing.” <https://www.r-project.org/> (accessed Nov. 11, 2021).

- [133] N. M. Laird and J. H. Ware, “Random-Effects Models for Longitudinal Data,” *Biometrics*, vol. 38, no. 4, pp. 963–974, 1982, doi: 10.2307/2529876.
- [134] “Linear Mixed-Effects Models function | R Documentation.” <https://www.rdocumentation.org/packages/nlme/versions/3.1-148/topics/lme> (accessed Sep. 29, 2021).
- [135] P. Bosoni *et al.*, “Exploring the inter-subject variability in the relationship between glucose monitoring metrics and glycated hemoglobin for pediatric patients with type 1 diabetes,” *Journal of Pediatric Endocrinology and Metabolism*, vol. 34, no. 5, pp. 619–625, May 2021, doi: 10.1515/jpem-2020-0725.
- [136] “Shapiro-Wilk’s test | R Documentation.” <https://www.rdocumentation.org/packages/stats/versions/3.6.2/topics/shapiro.test> (accessed Nov. 12, 2021).
- [137] S. Nakagawa and H. Schielzeth, “A general and simple method for obtaining R² from generalized linear mixed-effects models,” *Methods in Ecology and Evolution*, vol. 4, no. 2, pp. 133–142, 2013, doi: 10.1111/j.2041-210x.2012.00261.x.
- [138] “Multi-Model Inference package | R Documentation.” <https://www.rdocumentation.org/packages/MuMIn/versions/1.43.17> (accessed Sep. 29, 2021).
- [139] T. C. Dunn, Y. Xu, G. Hayter, and R. A. Ajjan, “Real-world flash glucose monitoring patterns and associations between self-monitoring frequency and glycaemic measures: A European analysis of over 60 million glucose tests,” *Diabetes Res Clin Pract*, vol. 137, pp. 37–46, Mar. 2018, doi: 10.1016/j.diabres.2017.12.015.
- [140] F. Gomez-Peralta, T. Dunn, K. Landuyt, Y. Xu, and J. F. Merino-Torres, “Flash glucose monitoring reduces glycemic variability and hypoglycemia: real-world data from Spain,” *BMJ Open Diabetes Res Care*, vol. 8, no. 1, p. e001052, Mar. 2020, doi: 10.1136/bmjdr-2019-001052.
- [141] L. E. P. Calliari *et al.*, “Real-world flash glucose monitoring in Brazil: can sensors make a difference in diabetes management in developing countries?,” *Diabetol Metab Syndr*, vol. 12, p. 3, 2020, doi: 10.1186/s13098-019-0513-z.
- [142] A. Lameijer *et al.*, “Flash Glucose Monitoring in the Netherlands: Increased monitoring frequency is associated with improvement of glycemic parameters,” *Diabetes Res Clin Pract*, vol. 177, p. 108897, Jul. 2021, doi: 10.1016/j.diabres.2021.108897.

-
- [143] “dunnTest function | RDocumentation.”
<https://www.rdocumentation.org/packages/FSA/versions/0.8.20/topics/dunnTest> (accessed Nov. 16, 2021).
- [144] “Spearman correlation function | R Documentation.”
<https://www.rdocumentation.org/packages/Hmisc/versions/4.6-0/topics/rcorr> (accessed Nov. 12, 2021).
- [145] L. Sacchi, C. Larizza, C. Combi, and R. Bellazzi, “Data mining with Temporal Abstractions: learning rules from time series,” *Data Min Knowl Disc*, vol. 15, no. 2, pp. 217–247, Oct. 2007, doi: 10.1007/s10618-007-0077-7.
- [146] Y. Shahar, “A framework for knowledge-based temporal abstraction,” *Artificial Intelligence*, vol. 90, no. 1, pp. 79–133, Feb. 1997, doi: 10.1016/S0004-3702(96)00025-2.
- [147] L. Sacchi, D. Capozzi, R. Bellazzi, and C. Larizza, “JTSA: An open source framework for time series abstractions,” *Computer Methods and Programs in Biomedicine*, vol. 121, no. 3, pp. 175–188, Oct. 2015, doi: 10.1016/j.cmpb.2015.05.006.
- [148] J. F. Allen, “Towards a general theory of action and time,” *Artificial Intelligence*, vol. 23, no. 2, pp. 123–154, Jul. 1984, doi: 10.1016/0004-3702(84)90008-0.
- [149] M. I. Schmidt, A. Hadji-Georgopoulos, M. Rendell, S. Margolis, and A. Kowarski, “The dawn phenomenon, an early morning glucose rise: implications for diabetic intraday blood glucose variation,” *Diabetes Care*, vol. 4, no. 6, pp. 579–585, Dec. 1981, doi: 10.2337/diacare.4.6.579.
- [150] V. Calcaterra *et al.*, “Continuous Glucose and Heart Rate Monitoring in Young People with Type 1 Diabetes: An Exploratory Study about Perspectives in Nocturnal Hypoglycemia Detection,” *Metabolites*, vol. 11, no. 1, Art. no. 1, Jan. 2021, doi: 10.3390/metabo11010005.
- [151] “wilcox.test function | R Documentation.”
<https://www.rdocumentation.org/packages/stats/versions/3.6.2/topics/wilcox.test/> (accessed Oct. 25, 2021).
- [152] S. Hochreiter and J. Schmidhuber, “Long Short-Term Memory,” *Neural Computation*, vol. 9, no. 8, pp. 1735–1780, Nov. 1997, doi: 10.1162/neco.1997.9.8.1735.
- [153] Y. Bengio, P. Simard, and P. Frasconi, “Learning long-term dependencies with gradient descent is difficult,” *IEEE Transactions on Neural Networks*, vol. 5, no. 2, pp. 157–166, Mar. 1994, doi: 10.1109/72.279181.
- [154] R. Pascanu, T. Mikolov, and Y. Bengio, “On the difficulty of training recurrent neural networks,” in *Proceedings of the 30th*

- International Conference on Machine Learning*, May 2013, pp. 1310–1318. Accessed: Nov. 17, 2021. [Online]. Available: <https://proceedings.mlr.press/v28/pascanu13.html>
- [155] Christopher Olah, “Understanding LSTM Networks.” <https://colah.github.io/posts/2015-08-Understanding-LSTMs/> (accessed Nov. 17, 2021).
- [156] S. Yan, “Understanding LSTM and its diagrams,” *Medium*, Nov. 15, 2017. <https://blog.mlreview.com/understanding-lstm-and-its-diagrams-37e2f46f1714> (accessed Nov. 17, 2021).
- [157] “PyCharm: the Python IDE for Professional Developers by JetBrains.” <https://www.jetbrains.com/pycharm/> (accessed Nov. 17, 2021).
- [158] “Keras: the Python deep learning API.” <https://keras.io/> (accessed Nov. 17, 2021).
- [159] “TensorFlow Core.” https://www.tensorflow.org/guide/keras/sequential_model (accessed Nov. 17, 2021).
- [160] “Reshape function - NumPy Manual.” <https://numpy.org/doc/stable/reference/generated/numpy.reshape.html> (accessed Nov. 19, 2021).
- [161] P. Bosoni, M. Meccariello, V. Calcaterra, C. Larizza, L. Sacchi, and R. Bellazzi, “Deep Learning Applied to Blood Glucose Prediction from Flash Glucose Monitoring and Fitbit Data,” in *Artificial Intelligence in Medicine*, Cham, 2020, pp. 59–63. doi: 10.1007/978-3-030-59137-3_6.
- [162] “Keras activation ReLU | TensorFlow Documentation.” https://www.tensorflow.org/api_docs/python/tf/keras/activations/relu (accessed Nov. 20, 2021).
- [163] X. Glorot, A. Bordes, and Y. Bengio, “Deep Sparse Rectifier Neural Networks,” in *Proceedings of the Fourteenth International Conference on Artificial Intelligence and Statistics*, Jun. 2011, pp. 315–323. Accessed: Nov. 20, 2021. [Online]. Available: <https://proceedings.mlr.press/v15/glorot11a.html>
- [164] P. J. Werbos, “Backpropagation through time: what it does and how to do it,” *Proceedings of the IEEE*, vol. 78, no. 10, pp. 1550–1560, Oct. 1990, doi: 10.1109/5.58337.
- [165] D. P. Kingma and J. Ba, “Adam: A Method for Stochastic Optimization,” *arXiv:1412.6980 [cs]*, Jan. 2017, Accessed: Nov. 20, 2021. [Online]. Available: <http://arxiv.org/abs/1412.6980>

-
- [166] “Keras callback EarlyStopping | TensorFlow Documentation.”
https://www.tensorflow.org/api_docs/python/tf/keras/callbacks/EarlyStopping (accessed Nov. 19, 2021).
- [167] W. L. Clarke, D. Cox, L. A. Gonder-Frederick, W. Carter, and S. L. Pohl, “Evaluating clinical accuracy of systems for self-monitoring of blood glucose,” *Diabetes Care*, vol. 10, no. 5, pp. 622–628, Oct. 1987, doi: 10.2337/diacare.10.5.622.
- [168] C. Piona *et al.*, “Long-term glycemic control and glucose variability assessed with continuous glucose monitoring in a pediatric population with type 1 diabetes: Determination of optimal sampling duration,” *Pediatr Diabetes*, vol. 21, no. 8, pp. 1485–1492, Dec. 2020, doi: 10.1111/pedi.13115.
- [169] R. M. Bergenstal *et al.*, “Glucose Management Indicator (GMI): A New Term for Estimating A1C From Continuous Glucose Monitoring,” *Diabetes Care*, vol. 41, no. 11, pp. 2275–2280, Nov. 2018, doi: 10.2337/dc18-1581.
- [170] I. B. Hirsch, J. B. Welsh, P. Calhoun, S. Puhr, T. C. Walker, and D. A. Price, “Associations between HbA1c and continuous glucose monitoring-derived glycaemic variables,” *Diabetic Medicine*, vol. 36, no. 12, pp. 1637–1642, 2019, doi: 10.1111/dme.14065.
- [171] C. M. Reno, D. Daphna-Iken, Y. S. Chen, J. VanderWeele, K. Jethi, and S. J. Fisher, “Severe hypoglycemia-induced lethal cardiac arrhythmias are mediated by sympathoadrenal activation,” *Diabetes*, vol. 62, no. 10, pp. 3570–3581, Oct. 2013, doi: 10.2337/db13-0216.
- [172] R. Due-Andersen *et al.*, “Cardiac repolarization during hypoglycaemia in type 1 diabetes: impact of basal renin-angiotensin system activity,” *Europace*, vol. 10, no. 7, pp. 860–867, May 2008, doi: 10.1093/europace/eun137.
- [173] V. Calcaterra *et al.*, “Impaired Glucose-Insulin Metabolism in Multisystem Inflammatory Syndrome Related to SARS-CoV-2 in Children,” *Children*, vol. 8, no. 5, Art. no. 5, May 2021, doi: 10.3390/children8050384.
- [174] CDC, “Multisystem Inflammatory Syndrome in Children (MIS-C),” *Centers for Disease Control and Prevention*, Feb. 11, 2020. <https://www.cdc.gov/mis-c/hcp/> (accessed Mar. 01, 2021).
- [175] D. R. Matthews, J. P. Hosker, A. S. Rudenski, B. A. Naylor, D. F. Treacher, and R. C. Turner, “Homeostasis model assessment: insulin resistance and β -cell function from fasting

- plasma glucose and insulin concentrations in man,” *Diabetologia*, vol. 28, no. 7, pp. 412–419, Jul. 1985, doi: 10.1007/BF00280883.
- [176] L. E. Simental-Mendía, M. Rodríguez-Morán, and F. Guerrero-Romero, “The Product of Fasting Glucose and Triglycerides As Surrogate for Identifying Insulin Resistance in Apparently Healthy Subjects,” *Metabolic Syndrome and Related Disorders*, vol. 6, no. 4, pp. 299–304, Dec. 2008, doi: 10.1089/met.2008.0034.
- [177] D. Navarro-González, L. Sánchez-Íñigo, J. Pastrana-Delgado, A. Fernández-Montero, and J. A. Martínez, “Triglyceride–glucose index (TyG index) in comparison with fasting plasma glucose improved diabetes prediction in patients with normal fasting glucose: The Vascular-Metabolic CUN cohort,” *Preventive Medicine*, vol. 86, pp. 99–105, May 2016, doi: 10.1016/j.ypmed.2016.01.022.
- [178] G. d’Annunzio *et al.*, “Insulin resistance and secretion indexes in healthy Italian children and adolescents: a multicentre study,” *Acta Biomed*, vol. 80, no. 1, pp. 21–28, Apr. 2009.
- [179] S. A. Vieira-Ribeiro *et al.*, “The TyG index cutoff point and its association with body adiposity and lifestyle in children,” *Jornal de Pediatria*, vol. 95, no. 2, pp. 217–223, Apr. 2019, doi: 10.1016/j.jped.2017.12.012.
- [180] V. Calcaterra *et al.*, “Triglyceride Glucose Index as a Surrogate Measure of Insulin Sensitivity in a Caucasian Pediatric Population,” *J Clin Res Pediatr Endocrinol*, May 2019, doi: 10.4274/jcrpe.galenos.2019.2019.0024.

List of publications

Journal papers:

- Salvi E, Bosoni P, Tibollo V, Kruijver L, Calcaterra V, Sacchi L, Bellazzi R, Larizza C (2020) Patient-Generated Health Data Integration and Advanced Analytics for Diabetes Management: The AID-GM Platform. *Sensors* 20:128. <https://doi.org/10.3390/s20010128>
- Calcaterra V, Bosoni P, Sacchi L, Zuccotti GV, Mannarino S, Bellazzi R, Larizza C (2021) Continuous Glucose and Heart Rate Monitoring in Young People with Type 1 Diabetes: An Exploratory Study about Perspectives in Nocturnal Hypoglycemia Detection. *Metabolites* 11:5. <https://doi.org/10.3390/metabo11010005>
- Bosoni P, Calcaterra V, Tibollo V, Malovini A, Zuccotti G, Mameli C, Sacchi L, Bellazzi R, Larizza C (2021) Exploring the inter-subject variability in the relationship between glucose monitoring metrics and glycosylated hemoglobin for pediatric patients with type 1 diabetes. *Journal of Pediatric Endocrinology and Metabolism* 34:619–625. <https://doi.org/10.1515/jpem-2020-0725>
- Calcaterra V, Bosoni P, Dilillo D, Mannarino S, Fiori L, Fabiano V, Carlucci P, Di Profio E, Verduci E, Mameli C, Pelizzo G, Zoia E, Sacchi L, Larizza C, Zuccotti G (2021) Impaired Glucose-Insulin Metabolism in Multisystem Inflammatory Syndrome Related to SARS-CoV-2 in Children. *Children* 8:384. <https://doi.org/10.3390/children8050384>

Indexed congress papers and abstracts:

- Bosoni P, Meccariello M, Calcaterra V, Larizza C, Sacchi L, Bellazzi R (2020) Blood glucose prediction from flash glucose monitoring and Fitbit data: a deep learning approach. In: Accardo A, Brun F, Marcegaglia S, Pedrizzetti G (eds) *Seventh National Congress of Bioengineering*. Pàtron Editore (accepted for publication)
- Bosoni P, Meccariello M, Calcaterra V, Larizza C, Sacchi L, Bellazzi R (2020) Deep Learning Applied to Blood Glucose Prediction from Flash Glucose Monitoring and Fitbit Data. In: Michalowski M, Moskovitch R (eds) *Artificial Intelligence in Medicine*. Springer International Publishing, Cham, pp 59–63
- Bosoni P, Sacchi L, Calcaterra V, Larizza C, Bellazzi R (2021) Relationship between Time in Range, Glycemic Variability Metrics and Daily Scan Rate in Children with Type 1 Diabetes. *J Diabetes Sci Technol, Diabetes Technology Meeting Abstracts* (accepted for publication)

List of abbreviations

ADA	American Diabetes Association
ADRR	Average Daily Risk Range
AGP	Ambulatory Glucose Profile
AID-GM	Advanced Intelligent Distant – Glucose Monitoring
ALT	Alanine Transaminase
API	Application Programming Interface
AR	AutoRegressive
ARMA	AutoRegressive Moving Average
ARMAX	AutoRegressive Moving Average with eXogenous inputs
ARX	AutoRegressive with eXogenous inputs
A-TS	Abstractions – Time-Series
ATTD	Advanced Technologies and Treatments for Diabetes
BG	Blood Glucose
BGRI	Blood Glucose Risk Index
BMI	Body Mass Index
BPM	Beats Per Minute
BPTT	Backward Propagation Trough Time
CA-TS	Complex Abstractions – Time-Series
CDC	Center of Diseases Control and Prevention
CEGA	Clarke Error Grid Analysis
CGM	Continuous Glucose Monitoring
CHO	Carbohydrate
CNN	Convolutional Neural Networks
CONGA	Continuous Overlapping Net Glycemic Action
COVID-19	Coronavirus Disease – 2019
CSII	Continuous Subcutaneous Insulin Infusion
CV	Coefficient of Variation
DCCT	Diabetes Control and Complications Trial
DM	Diabetes Mellitus
ESOD	Energy of the Second-Order Differences
E-TS	Events – Time-Series
FDA	Food and Drug Administration
FGM	Flash Glucose Monitoring
FPG	Fasting Plasma Glucose
FPI	Fasting Plasma Insulin
FTy	Fasting Triglycerides
GGT	Gamma-Glutamyl Transferase

GOD	Glucose Oxidase
GRADE	Glycemic Risk Assessment Diabetes Equation
GUI	Graphical User Interface
GV	Glycemic Variability
HbA1c	Glycated Hemoglobin
HBGI	High Blood Glucose Index
HOMA-IR	Homeostasis Model Analysis – Insulin Resistance
HR	Heart Rate
IDC	International Diabetes Center
IDF	International Diabetes Federation
IFCC	International Federation of Clinical Chemistry
IGC	Index of Glycemic Control
IGV	Ideal Glucose Value
IL-6	Interleukin – 6
IQR	Interquartile Range
IR	Insulin Resistance
isCGM	Intermittently scanned Continuous Glucose Monitoring
ISO	International Organization for Standardization
ISPAD	International Society for Pediatric and Adolescent Diabetes
JDRF	Juvenile Diabetes Research Foundation
JTSA	Java Time Series Abstractor
LBGi	Low Blood Glucose Index
LLTR	Lower Limit of Target Range
LME	Linear Mixed Effects
LS	Left Shift
LSTM	Long-Short Term Memory
LVX	Latent Variable with eXogenous input
MA	Moving Average
MAE	Mean Absolute Error
MAGE	Mean Amplitude of Glycemic Excursions
MARD	Mean Absolute Relative Difference
MDI	Multiple Daily Injection
MIS-C	Multisystem Inflammatory Syndrome – Children
MODD	Mean Of Daily Difference
MSPE	Mean Square Prediction Error
NA	Not-Available
NGSP	National Glycohemoglobin Standardization Program
NN	Neural Network
NT-proBNP	N-Terminal – pro-Brain Natriuretic Peptide
pCGM	Professional Continuous Glucose Monitoring
PFT	Personal Fitness Tracker
PGHD	Patient-Generated Health Data
PH	Prediction Horizon
PPG	Postprandial Glucose
Q-Q	Quantile – Quantile
RAD	Relative Absolute Deviation
RCT	Randomized Controlled Trial

ReLU	Rectified Linear Unit
RF	Random Forest
RMSE	Root Mean Square Error
RNN	Recurrent Neural Network
RS	Right Shift
rtCGM	Real-time Continuous Glucose Monitoring
SARS-CoV-2	Severe acute respiratory syndrome – coronavirus – 2
SD	Standard Deviation
SD_{dm}	Daily Means Standard Deviation
SD_w	Within-day Standard Deviation
SI	Système Internationale
SMBG	Self-Monitoring of Blood Glucose
SSGPE	Sum of Squares of the Glucose Prediction Error
SVR	Support Vector Regression
T1DM	Type 1 Diabetes Mellitus
T2DM	Type 2 Diabetes Mellitus
TA	Temporal Abstractions
TAR	Time Above Range
TAR_Lev1	Time slightly Above Range
TAR_Lev2	Time severely Above Range
TBR	Time Below Range
TBR_Lev1	Time slightly Below Range
TBR_Lev2	Time severely Below Range
TIR	Time In Range
TIT	Time in Target Range
TSH	Thyroid-Stimulating Hormone
TyG	Triglyceride-Glucose
ULTR	Upper Limit of Target Range
XML	eXtensible Markup Language
WHO	World Health Organization